รายงานวิจัยฉบับสมบูรณ์

การอธิบายคุณลักษณะทางสโตแคสติก ของอนุกรมเวลาอคูสติกของมหาสมุทร โดยใช้วิธีการกรองแบบเบเซียนอย่างเป็นลำดับ

โดย ผู้ช่วยศาสตราจารย์ ดร.ณัฐพล อุ่นศรี

กุมภาพันธ์ 2562

สัญญาเลขที่ MRG6080152

รายงานวิจัยฉบับสมบูรณ์

การอธิบายคุณลักษณะทางสโตแคสติก ของอนุกรมเวลาอคูสติกของมหาสมุทร โดยใช้วิธีการกรองแบบเบเชียนอย่างเป็นลำดับ

ผู้ช่วยศาสตราจารย์ ดร.ณัฐพล อุ่นศรี
มหาวิทยาลัยแม่ฟ้าหลวง

สนับสนุนโดยสำนักงานกองทุนสนับสนุนการวิจัย
และสำนักงานคณะกรรมการการอุดมศึกษา

บทคัดย่อ

รหัสโครงการ : **MRG6080152**

ชื่อโครงการ: การอธิบายคุณลักษณะทางสโตแคสติกของอนุกรมเวลาอคูสติกของมหาสมุทร โดยใช้วิธีการกรองแบบเบเชียนอย่างเป็นลำดับ

ชื่อนักวิจัย: ผู้ช่วยศาสตราจารย์ ดร. ณัฐพล อุ่นศรี

E-mail Address : nattapol.aun@mfu.ac.th

ระยะเวลาโครงการ : **2** ปี

Abstract

การสกัดข้อมูลที่ซ่อนอยู่ในสัญญาณอคูสติกที่เคลื่อนที่ผ่านช่องตัวกลางมีความสำคัญในการประมาณค่าพารามิเตอร์และการหาค่าต่าง ๆทางอคูสติกทางภูมิศาสตร์ ดังนั้นการหาค่าข้อมูลเหล่านี้อย่างถูกต้องสามารถนำไปสู่การหาค่าพารามิเตอร์ต่าง ๆที่สำคัญสำหรับการศึกษาเกี่ยวกับสิ่งแวดล้อม การเฝ้าระวังภูมิอากาศและการป้องกัน รูปแบบที่สำคัญที่สุดของข้อมูลความถี่ที่แปรตามเวลาแสดงถึงคุณลักษณะของเส้นโค้งการกระจายตัว (Dispersion curve) ซึ่งเป็นผลจากสภาพแวดล้อมแบบกระจายตัว (Dispersive environments) ปัจจุบันยังไม่มีแบบจำลองที่ถูกต้องที่อธิบายอนุกรมเวลาทางอคูสติกทำให้ไม่สามารถประมาณค่าเส้นโค้งการกระจายตัวได้แม่นยำ โครงการนี้จึงศึกษาคุณลักษณะทางสโตคาสติกของอนุกรมเวลาอคูสติกของมหาสมุทรโดยใช้วิธีการกรองแบบเบเชียนอย่างเป็นลำดับ การอธิบายทางคณิตศาสตร์และสถิติของสัญญาณอย่างแม่นยำได้ถูกพัฒนาขึ้นสำหรับเครื่องกรองซึ่งเป็นข้อมูลพื้นฐานสำหรับการติดตามการกระจายตัวต่อไป โครงการนี้ยังใช้กระบวนการสุ่มซ้ำแบบปรับตัวได้เพื่อเพิ่มประสิทธิภาพของระบบโดยรวมอีกทางด้วย ผลการทดลองแสดงให้เห็นว่าวิธีการที่นำเสนอเหนือกว่าวิธีดั้งเดิมที่ปรากฏในวรรณกรรม

คำหลัก: การกรองแบบเบเชียน; การประมาณค่าความถี่; การประมวลผลสัญญาณ; อนุกรมเวลา; อคูสติกของมหาสมุทร

Abstract

Project Code : MRG6080152

Project Title : Stochastic Characterization of Ocean Acoustics Time-Series for Dispersion Tracking Using Sequential Bayesian Filtering

Investigator : Assist. Prof. Nattapol Aunsri, Ph.D.

E-mail Address : nattapol.aun@mfu.ac.th

Project Period : 2 years.

Abstract

Extracting information that is embedded in the propagating acoustic signals is important in environmental parameter estimation and geoacoustic inversion. Accurately retrieving this information leads us to effectively estimate parameters that are of utmost importance in environmental studies, climate monitoring, and defense. The most important pattern of the frequency content with time exhibits in the dispersion characteristics of the waveguide resulting from the dispersive environments. Currently, there is no accurate stochastic model describing the ocean acoustics time-series available, consequently, the estimated dispersion curves are not precise. This project, hence, has investigated a stochastic characterization of ocean acoustics time-series for dispersion tracking with a sequential Bayesian filtering framework. An accurate mathematical and statistical description of the ocean acoustics signals was developed and it will serve as the foundation in dispersion tracking. In addition, the adaptive resampling scheme was implemented in the filtering system to further enhance the performance of tracking system. Simulation results shown the superiority of the proposed method to the conventional technique used in literature.

Keywords : Bayesian filtering; frequency estimation; signal processing; time-series, ocean acoustics

TABLE OF CONTENTS

TABLE OF CONTENTS
(Continued)

Chapter **Page**

LIST OF TABLES

Table **Page**

LIST OF FIGURES

LIST OF FIGURES
(Continued)

Figure **Page**

CHAPTER 1

EXECUTIVE SUMMARY

1.1 Introduction to the research problem and its significance

In the last few decades, there has been explosive growth in the research and development of numerical and statistical models used as tools in research involving underwater acoustics. The particular area of interest in underwater acoustics is the propagation of sound in a shallow ocean environment. The reason, in part, for such interest is the way that submarines are constructed today. Some submarines, such as those which transport navy seals, are much smaller than they were years ago. Their compact size nowadays allows the submarines to maneuver into more shallow water. Moreover, the submarines are actually designed to be very much quieter than they were in the past. This, as a result, makes them more difficult to be detected. The harder these sounds are to detect, the easier it is for these vessels to approach land, and therefore, travel into shallow water. These sounds, if detected, can be linked to a sound propagation model for the estimation of source location. Acoustic signals propagating in the ocean carry information about geometry and environmental parameters within the propagation medium. Effectively estimate parameters that are of utmost importance in environmental studies, climate monitoring, and defense just as described above, can be performed when accurate information from acoustic signals was extracted.

Motivated by the importance of environmental parameter estimation and geoacoustic inversion, the proposal focuses on the use of sequential Bayesian filtering to obtain accurate estimates of instantaneous frequencies within the acoustic field measured at an array of hydrophones. We use normal mode modeling for the propagation of broadband signals in this work. Group velocity is the most important quantity

describing pulse dispersion in a waveguide. Dispersion depends on the characteristics of the waveguide that we wish to extract. With this reason, when we obtain accurate dispersion characteristics, inversion of geoacoustic properties and bottom properties can be performed. Compressional wave speeds can also be estimated based on the dispersion behavior of broadband acoustic propagation.

This research project hence proposes a stochastic characterization of ocean acoustics Time-Series for tracking the dispersion pattern of the received signal. The goal is to obtain the robust characterization that mathematically and statistically describes the dispersion curve accurately.

The results from the proposed method show that the frequency estimates using the developed stochastic and mathematical models are better than the conventional method, resulting in enhancing the accuracy of the extracted dispersion curves.

1.2 Objective

To achieve accurate stochastic nature and dispersion curve of the ocean acoustic time-series using the sequential Bayesian filtering framework.

1.3 Research Methodology

The methodology of this work is described as the followings.

1.3.1 Review the literatures

The literature for this work includes parameter estimation in ocean acoustics, mathematical and stochastic models of the time-frequency representations of the ocean acoustic signals, and Bayesian filtering. To be specific, the statistical description of the signals and noise in the transformed domain must be studied, especially when the statistical independence property is broken. The closed-form chi-squared probability

distribution with DOF of two was found to be sufficient to represent the spectrogram of the ocean acoustic time-series.

1.3.2 Analyze and develop the stochastic models

After the literature reviews, we then developed the appropriate model and analyze their accuracy mathematically. To begin with, the simplest chi-squared probability distribution where the noise is considered to be statistically independent for both two components in the frequency domain will be developed. This model is the starting point for the investigation of the more accurate model where the noise assumption is relaxed. As described before, DOF may not be exactly two; we then derived the accurate model that fits or can capture the desired information where chi-squared with DOF of two is indeed reasonable. This is not trivial since the acoustic model for the signal propagating in the ocean must be incorporated with the statistical model in order to deliver all the required models setting for the PF implementation which will be discussed in the next step. We needed to be careful in the analysis before the PF implementation.

1.3.3 Validate the models by implementing the filtering framework

After careful and rigorous analysis from the previous step, a particle filtering framework was developed and used to test the performance of the models to the ocean acoustic time-series. We firstly implemented the chi-squared distribution model with DOF two for the PF and perform the filtering to acquire the tracking results which will be used to compare to the benchmark, conventional MAP estimates, and the recent results in [12]. Then, the next crucial step is devoted for PF implementation to achieve better accuracy in which the MSE is reduced compared to the recent works in literatures. Moreover, we investigated the validity of the model by presenting the slices of the spectrogram and the corresponding spectrums from resulting mathematical

model of the acoustic time-series and statistical noise model. If the both models are accurate, slices of the spectrogram and spectrums should be coincided; and this is for the validation of the accuracy of the models.

In addition to what we described above, simulations to test the analysis about the effects of the use of the various window functions has been performed.

The proposed models should be robust to the noise, i.e., we evaluated the performance of the models for different noise levels. This is what the PF is developed for; the estimates provided by the PF should still be accurate in low SNRs, and we performed this evaluation in this project. Finally, noise variance PDFs for different SNR levels as estimated from PF were displayed to present the tracking performance of the filter. This is one of the tests that can confirm the model validity and accuracy. Conventional MAP estimates, the benchmark of the estimation problem was used to compared to our results. We found that the results from this project were superior.

1.3.4 Analyze and discuss the results

The results from the previous step were analyzed and discussed. We discussed the performance of the filter where the simplest model is used. Then when the complicated statistical was implemented and performed, the comparison of the tracking results can be provided. The advantages, disadvantages, findings, or observations have been discussed.

1.3.5 Draw conclusions and suggestions

After the analysis and discussions, conclusions and suggestions was provided.

1.4 Outputs

The outputs from this project are listed as follows:

1. P. Taveeapiradeecharoen, K. Chamnongthai, and N. Aunsri, Bayesian Compressed Vector Autoregression for Financial Time-series Analysis and Forecasting, *IEEE ACCESS* 7:16777-16786, 2019.

2. N. Aunsri, Effect of Window Functions on the Sequential Bayesian Filtering Based Frequency Estimation, *The 21st International Symposium on Wireless Personal Multimedia Communications (WPMC- 2018)* pp. 411-415, 2018.

3. Sequential Bayesian Filtering with Stochastic Characterization of Ocean Acoustics Time-series for Frequency and Dispersion Estimation, submitted to Measurement, now *Under Review*

4. Particle Filtering with Adaptive Resampling Scheme for Modal Frequency Identification and Dispersion Curves Estimation in Ocean Acoustics, submitted to Applied Acoustics, *Under Review (minor revision)*

CHAPTER 2

BASIC THEORY

2.1 Introduction

A problem of frequency estimation has always been one of the most important task in science and engineering applications including physics, signal processing, communication, and ocean acoustics; see [6, 10, 30, 32, 33] for examples. Given a white Gaussian noise contaminated ocean acoustics time-series, we consider a time-frequency analysis of such time-series via a short-time Fourier transform (STFT). The goal of this work is to incorporate the statistical description of the signal in the frequency domain to a sequential frequency estimation framework, the particle filtering, in particular, to obtain the posterior PDF of the frequency and its corresponding quantities. The posterior PDF of these quantities play an important role in environmental inversion in which the geoacoustics properties of the ocean can be revealed [6, 24, 25].

Frequency estimation in ocean acoustics has been as of interest for decades as seen in literature [5, 6, 22, 35, 36]. The importance of this problem stems from the fact that most important pattern of the frequency content with time exhibits in the dispersion characteristics of the waveguide resulting from the dispersive environments. Therefore, retrieving this information could lead us to effectively estimate parameters that are of utmost importance in environmental studies [11, 20, 24, 27, 28]. This work implements a PF based on the incorporation of mathematical and statistical models of the ocean acoustics signal in the frequency domain to construct the likelihood function and the particle weight calculation for formulating the frequency PDF and, hence, the dispersion PDF of the signal. We derive an accurate statistical model to explain the stochastic property of the noisy ocean acoustics time-series and combine it with a modal representation of the signal in the frequency domain in order to obtain

more accurate frequency estimates and, therefore, a better dispersion estimates from the measured data.

2.2 Fundamental of modal mode technique in ocean acoustics

The evolution of the frequency content of an acoustic signal with time plays a key role as a "*footprint*" of the propagation medium. This is typically the case with broadband signals with frequencies of a few hundred Hz propagating from long distances in underwater environments. The frequency content with time exhibits the variation pattern as a result of dispersion characteristics of the waveguide, allowing the estimation of modal arrival times and amplitudes for various modes and frequencies within each mode.

The ocean acoustics model in the time-frequency space can be considered as a broadband acoustic signal received at a hydrophone. The acoustic signal received at a hydrophone in the ocean can be expressed as

$$p(r,z,z_r,t) = \frac{1}{2\pi}\sum_n \int_{-\infty}^{+\infty} \mu(\omega^{'}) G_n(r,z,z_r,\omega^{'}) exp\{i(\omega^{'}t - k_n r - \frac{\pi}{4})\} d\omega^{'}. \quad (2.1)$$

where r represents the distance between source and receiver, z and z_r are the source and receiver depths, respectively, k_n stands for the modal wave number, μ is the source spectrum, $\omega = 2\pi f$, where f is frequency in Hz and

$$G_n(r,z,z_r,\omega) = \frac{i\sqrt{\pi}}{\rho(z_r)\sqrt{2k_n r}} \Psi_n(z)\Psi_n(z_r), \quad (2.2)$$

where Ψ_n are orthogonal, normalized, depth-dependent functions, and $\rho(z_r)$ is the medium density. To simplify the analysis, we consider now only one mode. The frequency spectrum of a finite time segment of the signal is given by [22, 35]:

$$P_n(\omega,t) = \int_{t-\Delta t}^{t+\Delta t} p_n(r,z,z_r,t) e^{-i\omega\tau} d\tau, \quad (2.3)$$

whereas the segment starts and ends at $t - \Delta t$ and $t + \Delta t$, respectively. Substituting the nth term of Eq. (2.1) into Eq. (2.3) and performing integration, we then obtain

$$P_n(\omega, t) = \frac{e^{-i\omega t}}{\pi} \int_{\infty}^{\infty} \mu(\omega^{'}) G_n(r, z, z_r, \omega^{'}) \frac{\sin(\omega^{'} - \omega)\Delta t}{\omega^{'} - \omega} exp\{i(\omega^{'} t - k_n r - \frac{\pi}{4})\} d\omega^{'}. \tag{2.4}$$

We can approximate the above quantity by using stationary phase approximation technique as explained in [35], then the squared frequency spectrum of a finite time segment of the signal can be expressed as

$$|P_n(\omega, t)|^2 = \frac{\pi}{|k_n^{''}|^2} |\mu(\omega_n) G_n(r, z, z_r, \omega_n)|^2 \Big| \frac{\sin(\omega - \omega_n)\Delta t}{\omega - \omega_n} \Big|^2, \tag{2.5}$$

for $|\omega - \omega_n| < \frac{\pi}{\Delta t}$.

It can be clearly seen that the spectrum expressed in Eq. (2.5) has a peak at ω_n which is called a *modal frequency*. This observation allows us to formulate a PF framework for tracking the instantaneous power spectral peaks to identify the modal frequencies of the acoustic signal, which will be discussed in the next section.

2.3 Sequential Bayesian Filtering

Back to 1960 where the pioneer work in new filtering method named Kalman Filter (KF) was proposed as reported in [17]. The filter delivers an optimal estimator according to the minimum mean squared error metric. However, the limitation of the KF is that the evolution of the unknown parameters is assumed to be in the case of Gaussian and additive perturbations, the additive Gaussian noise model is considered in the observed data, and a linear function describing the measurements and state vector parameters.

It is not a case for most practical systems that the assumptions made for the KFs are always valid, most systems are nonlinear/non-Gaussian as well as non-additive noise structure. Variants of the KFs were developed to remedy these problems; the

extended KF (EKF), unscented Kalman filters (UKFs), and ensemble Kalman filter (EnKF) are examples of KF variants that were proposed in literature. Nevertheless, a system with highly nonlinear models and complex noise processes are not easily to deal with, it requires computational or numerical approaches to formulate the desired posterior PDFs, and the inferences on the state parameters have to be done numerically since the closed form PDFs may not be feasible to obtain, these approaches are particle filtering.

Particle filter (PF), a class of sequential Monte Carlo method, is used for the estimation of the underlying posterior PDFs of random variables, allowing the extraction of the desired information from complex noisy observation data becomes possible. PF, derived from the basic importance sampling (IS) concepts, is a numerical approach proposed to effectively handle nonlinear relations between unknown parameters and observations, complex noise processes, and unknown as well as the time-varying dynamical systems [2, 12, 13, 26, 29, 34].

2.4 Bayesian Filtering Framework and its conceptual solution

In this section, the fundamentals of sequential Bayesian filtering are recalled and a construction of particle filtering method is then provided.

2.4.1 State space model

Consider the following nonlinear system:

$$\mathbf{x}_n = \mathbf{f}_{n-1}(\mathbf{x}_{n-1}, \mathbf{v}_{n-1}) \tag{2.6}$$

$$\mathbf{y}_n = \mathbf{g}_n(\mathbf{x}_n, \mathbf{w}_n). \tag{2.7}$$

where n is time, $\mathbf{x} \subseteq \mathbb{R}^{n_x}$ is the n_x-dimensional state vector, $\mathbf{y} \subseteq \mathbb{R}^{n_y}$ is the n_y-dimensional observation vector, $\mathbf{v}_{n-1}$ denotes n_x-dimensional process noise vector, and $\mathbf{w}_n$ denotes n_y-dimensional measuring process noise vector.

The first state equation describes how the states evolve with time; and the transition of the states from the consecutive time is followed the nonlinear function first order process $\mathbf{f}_n$ as given in Eq. (2.6). The second equation is called the observation equation relating the observation data to the state vector through a nonlinear function $\mathbf{g}_n$ and this equation is given in Eq. (2.7). Both $\mathbf{f}_{n-1}$ and $\mathbf{g}_n$ are known in this work. The state and observation noise quantities are declared as $\mathbf{v}_n$ and $\mathbf{w}_n$, respectively. Functions $\mathbf{f}_{n-1}$ and $\mathbf{g}_n$ are typically nonlinear and assumed to be the known multivariate functions. The evolution of the state vector with time is done via a function $\mathbf{f}_{n-1}$ relating the changes of the state parameters from the previous time to the current time according to the process noise $\mathbf{v}_{n-1}$. The relationship between the state vector and the observation vector is described by the measurement or observation function $\mathbf{g}_n$ and the measuring process noise. Both process noises can by additive, multiplicative, or other forms depending on the problem at hands.

In general, let $\mathbf{X}_n = [\mathbf{x}_1, \mathbf{x}_2, \ldots, \mathbf{x}_n]$ be a sequence of the unknown state vectors up to time n, the aim of filtering is to recursively estimate the state vector $\mathbf{x}_n$ based on a set of available information from the measurements $\mathbf{Y}_n = [\mathbf{y}_1, \mathbf{y}_2, \ldots, \mathbf{y}_n]$. This problem can be addressed by computing the posterior PDF $p(\mathbf{x}_n|\mathbf{Y}_n)$. Assuming that the initial PDF of the state vector $p(\mathbf{x}_0|\mathbf{y}_0) = p(\mathbf{x}_0)$, the posterior PDF $p(\mathbf{x}_n|\mathbf{Y}_n)$ can be computed recursively using the following two steps: prediction and updating. We will detail these steps for PF implementation in Section IV.

2.4.2 Bayesian Inference

As discussed, we require two equations describing the state-space model; one expresses the evolution of the state and one connects the relation between states and

observations. We assume that each observation $\mathbf{y}_n$ depends solely on the current state $\mathbf{x}_n$, and the observations up to time n are conditionally independent given the states $\mathbf{x}_n$, therefore

$$p(\mathbf{Y}_n|\mathbf{X}_n) = \prod_{i=1}^{n} p(\mathbf{y}_i|\mathbf{X}_n). \tag{2.8}$$

The states of the model are assumed to change over time according to a first order Markov process, therefore the current state depends only the state at a previous time step yielding:

$$p(\mathbf{X}_n) = p(\mathbf{x}_0) \prod_{i=1}^{n} p(\mathbf{x}_i|\mathbf{x}_{i-1}). \tag{2.9}$$

The goal of the PF is to gather the posterior PDF of the unknown states when the observed data is available at time step n, $p(\mathbf{X}_n|\mathbf{Y}_n)$, and it can be given as:

$$p(\mathbf{X}_n|\mathbf{Y}_n) = \frac{p(\mathbf{Y}_n|\mathbf{X}_n)p(\mathbf{x}_0)}{p(\mathbf{Y}_n)}. \tag{2.10}$$

From Eqs. (2.8) and (2.9), we can express the posterior distribution $p(\mathbf{X}_n|\mathbf{Y}_n)$ as

$$p(\mathbf{X}_n|\mathbf{Y}_n) = \frac{p(\mathbf{x}_0) \prod_{i=1}^{n} p(\mathbf{y}_i|\mathbf{x}_i)p(\mathbf{x}_i|\mathbf{x}_{i-1})}{p(\mathbf{Y}_n)}, \tag{2.11}$$

where $p(\mathbf{x}_0)$ is the prior density and we assume it to be a uniform density in this work, i.e., the chance of the existence of the modal frequencies is assumed to be equal over the search interval. The observation $\mathbf{y}_n$ is independent of the states at all other times and we assume that the observation data up to step n are also independent. Bayesian framework recursively estimates the marginal PDF $p(\mathbf{x}_n|\mathbf{Y}_n)$ from the previous marginal PDF $p(\mathbf{x}_{n-1}|\mathbf{Y}_n)$. By assuming that the marginal PDF

$p(\mathbf{x}_{n-1}|\mathbf{Y}_{n-1})$ is available, the prediction of the PDF $p(\mathbf{x}_n|\mathbf{Y}_{n-1})$ can be computed from transitional PDF $p(\mathbf{x}_n|\mathbf{x}_{n-1})$ obtained from the state equation of Eq. (2.6). We can then rewrite Eq. (2.11) as:

$$p(\mathbf{X}_n|\mathbf{Y}_n) = \frac{p(\mathbf{y}_n|\mathbf{x}_n)p(\mathbf{x}_n|\mathbf{x}_{n-1})p(\mathbf{X}_{n-1}|\mathbf{Y}_{n-1})}{p(\mathbf{y}_n|\mathbf{Y}_{n-1})}, \tag{2.12}$$

where

$$\begin{aligned} p(\mathbf{y}_n|\mathbf{Y}_{n-1}) = \int\int & p(\mathbf{y}_n|\mathbf{x}_n)p(\mathbf{x}_n|\mathbf{x}_{n-1}) \\ & \times p(\mathbf{X}_{n-1}|\mathbf{Y}_{n-1})\mathrm{d}\mathbf{x}_{n-1}\mathrm{d}\mathbf{x}_n. \end{aligned} \tag{2.13}$$

Moreover, the PDF $p(\mathbf{x}_n|\mathbf{Y}_{n-1})$ can be expressed as the so called Chapman-Kolmogorov equation:

$$\begin{aligned} p(\mathbf{x}_n|\mathbf{Y}_{n-1}) &= \int p(\mathbf{x}_n|\mathbf{x}_{n-1},\mathbf{Y}_{n-1})p(\mathbf{x}_{n-1}|\mathbf{Y}_{n-1})\mathrm{d}\mathbf{x}_{n-1} \\ &= \int p(\mathbf{x}_n|\mathbf{x}_{n-1})p(\mathbf{x}_{n-1}|\mathbf{Y}_{n-1})\mathrm{d}\mathbf{x}_{n-1}. \end{aligned} \tag{2.14}$$

the new estimate of the states at time step n is:

$$p(\mathbf{x}_n|\mathbf{Y}_n) = \frac{p(\mathbf{y}_n|\mathbf{x}_n)p(\mathbf{x}_n|\mathbf{Y}_{n-1})}{p(\mathbf{y}_n|\mathbf{Y}_{n-1})}. \tag{2.15}$$

Assume that the observation data $\mathbf{Y}_n$ is available, the likelihood of the state vector $\mathbf{x}_n$ is obtained from the density $p(\mathbf{y}_n|\mathbf{x}_n)$. Since the posterior PDF of the states is available according to the sequential update discussed above, the interference can then be performed using this probability distribution. The estimate function of the state can be calculated from

$$\begin{aligned}\widehat{F}(\mathbf{x}_n) &= \mathbf{E}_{p(\mathbf{x}_n|\mathbf{Y}_n)}[F(\mathbf{x}_n)|\mathbf{Y}_n] \\ &= \int F(\mathbf{x}_n)p(\mathbf{x}_n|\mathbf{Y}_n)\mathrm{d}\mathbf{x}_n. \end{aligned} \tag{2.16}$$

2.4.3 Particle filtering

Working in a sequential filtering framework, we implement PFs for identifying the trajectories of the modal frequencies with time of the ocean acoustics signal. It must be clear that the KF families cannot be applied to our problem because the relationship between the observed data and the states is highly nonlinear.

For each time step, the PF approximates a probability density of $p(\mathbf{x}_n|\mathbf{x}_n)$ by constructing by a set of random samples with their associated weights as

$$p(\mathbf{x}_n|\mathbf{y}_n) \approx \sum_{i=1}^{N} w_n^i \delta(\mathbf{x}_n - \mathbf{x}_n^i) \tag{2.17}$$

and

$$w_n^i \propto \frac{p(\mathbf{X}_n^i|\mathbf{Y}_n)}{q(\mathbf{X}_n^i|\mathbf{Y}_n)}, \tag{2.18}$$

where δ is the Dirac delta function, N is the number of particles used in the approximation, and the quantity $q(\mathbf{X}_n^i|\mathbf{Y}_n)$ is the importance density. The accuracy of the filter, i.e., the performance of the approximated distribution to the true continuous density increases as the increasing of N [8,29]. In other words, $\sum_{i=1}^{N} w_n^i \delta(\mathbf{x}_n - \mathbf{x}_n^i) \rightarrow p(\mathbf{x}_n|\mathbf{y}_n)$ as $N \rightarrow \infty$. Since we assume that our process follows the first order Markov process, the results from the previous time step $n-1$ and the importance density can be chosen that the minimization of the IS errors is achieved, we therefore obtain the importance weight for each particle as (for full derivation details, please consult [29])

$$w_n^i = p(\mathbf{y}_n|\mathbf{x}_n^i)w_{n-1}^i. \tag{2.19}$$

The degradation of the sequential IS (SIS) performance stems from the problem that the variance of the importance weights always increases monotonically over time. After running a filtering process for a few iterations, only few particles tend to occupy high weights but the rest of particles holds the weights that are close to zero. In some extreme cases, just only one particle is a survival and it holds a unit weight. This means that the diversity of the particle distribution is not achieved and results in a failure of the posterior probability distribution representation using this framework. This problem is called degeneracy. There are improvement algorithms proposed to overcome degeneracy problem, the wildly use method is called resampling scheme. The trick is to eliminate small importance weight particles and, on the other hand, those of the large weights are regenerated. The amount of regeneration depends on the importance weights of the parent particles. We call the process that combines SIS and resampling as sequential importance resampling (SIR). The resampling process is typically performed when the effective number of particles N^{eff} falls below a threshold as discussed in [12, 18]. The effective number of particles is determined as

$$N^{eff} = \frac{1}{\sum_{i=1}^{N}(w_n^i)^2}. \tag{2.20}$$

Even that the resampling reduces the effects of degeneracy, two new problems occurs [29]. First, resampling step introduces the limitation of the ability to parallelize the SIS algorithm because all weights have to be summed during normalization. Second, the assumption of statistical independence is no longer valid after resampling. A problem that may arise after resampling is the loss of particle diversity due to all of the particles are identical breaking down to a noninformative distribution. Therefore, convergence issues are generated along the process if resampling takes serious loss of particle diversity. This is well-known as sample impoverishment which is commonly

exhibited in PF applications. Recently, there are some developments of PFs [13,21,29] that have been designed to resolve these problems.

2.4.4 Classical Likelihood Formulation

This section offers a consideration of likelihood formulation which is the core of the PF since the likelihood for each particle is used to form a posterior PDF of the modal frequency of the signal. We provide the likelihood formulation here in this section just for from the classical approach used in literature and some modifications according to our problem. Note that this functions are not accurate as discussed in the previous section, the correct likelihood formulation will be discussed in the next chapter.

2.4.4.1 Treating model as known amplitude

The length of $\mathbf{y_k}$ is the range of frequencies of interest. The likelihood for the unknown frequencies evaluated for a particle given the Gaussian noise assumption is:

$$p(\mathbf{y}_k|\mathbf{x}_k) \propto exp\{-\frac{1}{2\xi_w^2}\|\mathbf{y}_k - \sum_{j=1}^{M} a_{kj}[sinc(f - x_{kj})]^2\|^2\}. \tag{2.21}$$

2.4.4.2 Multiple Model Particle Filter

The estimation problem for the multiple model scenario needs careful consideration. In a noisy environment, the PF favors the model with the highest order because there is an inherent bias towards large dimensionality. Let's consider the situation where we have a time-series with one modal frequency with an amplitude of one. There are infinite ways to generate combinations of multiple modes with the exact same modal frequencies and different amplitudes in such a way that their sum is the true mode. To compensate for this, a penalizing factor is added to the original likelihood for remedying the typical preference of high-order models. This penalty factor comes from the prior density on the order. In this work we select uniform priors:

$$p(a_{kj}) = 1 \tag{2.22}$$

$$p(x_{kj}) = \frac{1}{L} \tag{2.23}$$

where L is the length of the Fourier transform that supports the frequency space. The likelihood function in this case is given by

$$p(\mathbf{y}_k|\mathbf{x}_k) \propto \frac{1}{L^{r_k}} exp\{-\frac{1}{2\xi^2}\|\mathbf{y}_k - \sum_{j=1}^{r_k} a_{kj}[sinc(f - x_{kj})]^2\|^2\}. \tag{2.24}$$

The penalizing term $\frac{1}{L^{r_k}}$ impacts the value of the likelihood. For small values of r_k, this term has a value associated with a higher probability than that for larger values of $r(k)$.

2.4.4.3 Treating noise variance as an unknown parameter

The observation equation and the structure of the measurement noise are the same as discussed in the previous subsections except that the noise variance is now added to the state vector. The likelihood function in this case is given by:

$$p(\mathbf{y}_k|\mathbf{x}_k, \mathbf{a_k}, \mathbf{r_k}) \propto (\frac{1}{\sigma_k^2})^{L/2} \frac{1}{L^{r_k}} exp\{-\frac{1}{2\sigma_k^2}\|\mathbf{y}_k - \sum_{j=1}^{r_k} a_{kj}[sinc(f - x_{kj})]^2\|^2\}. \tag{2.25}$$

The following non-informative prior for the variance of the additive white Gaussian noise is employed [1, 7]:

$$p(\sigma^2) \propto \frac{1}{\sigma^2}. \tag{2.26}$$

By including the above prior density, the joint posterior density of the unknown parameters given the observed data is:

$$p(\mathbf{x_k}, \mathbf{a_k}, \mathbf{r_k}, \sigma_k^2|\mathbf{y}_k) \propto \frac{1}{\sigma_k^2} \frac{1}{(2\pi\sigma_k^2)^{L/2}} \frac{1}{L^{r_k}} exp\{-\frac{1}{2\sigma_k^2}\|\mathbf{y}_k - \sum_{j=1}^{r_k} a_{kj}[sinc(f - x_{kj})]^2\|^2\}. \tag{2.27}$$

CHAPTER 3

THE PROPOSED METHOD

3.1 Probability distribution of a noisy time-series

Consider a noisy signal $x[n]$ of length N, which is composed of a deterministic part $s[n]$ and noise part $g[n]$, i.e., $x[n] = s[n] + g[n]$, where $g[n]$ is assumed to be zero mean white Gaussian noise with variance σ^2. From the assumption, the distribution of each sample $x[n]$ is

$$x[n] \sim \mathcal{N}(g[n], \mathbf{C}) \tag{3.1}$$

where $\mathcal{N}(a, b)$ is the normal distribution with mean a and variance b, and here $\mathbf{C}$ is the autocorrelation function.

The spectrogram $S_x(l, k)$ at time l and frequency k of signal $x[n]$ obtained from STFT is calculated from the squared modulus of the STFT as

$$S_x(l, k) = X_r(l, k)^2 + X_{im}(l, k)^2, \tag{3.2}$$

$X_r(l, k)$ and $X_{im}(l, k)$ are real and imaginary parts of the STFT and they are computed by

$$X_r(l, k) = \sum_{n=1}^{N} w(n - l)x(n) \cos(-2\pi k \frac{n}{L}), \tag{3.3}$$

and

$$X_{im}(l, k) = \sum_{n=1}^{N} w(n - l)x(n) \sin(-2\pi k \frac{n}{L}), \tag{3.4}$$

where $w(n)$ is the analysis window with length N.

From the assumption of the signal model, the signal in the time-domain $x[n]$ is distributed according to Eq. (3.1). Following the property of the normal distribution that a linear combination of the Gaussian distributions is also Gaussian distributed. Since both $X_r(l,k)$ and $X_{im}(l,k)$ are linear combinations of N Gaussian random variables with coefficients $w(n-l)\cos(-2\pi k\frac{n}{L})$ and $w(n-l)\sin(-2\pi k\frac{n}{L})$, respectively, therefore, these two quantities are Gaussian random variables as well. It can be shown that the variance of both real and imaginary parts of STFT is $\sigma^2/2$, the half of the noise variance of noise part in the time-domain [15].

According to Eq. (3.2), the spectrogram $S_x(n,k)$ is the sum of two squared Gaussian random variables. It can be shown that $S_x(n,k)$ follows the χ^2 distribution with two degrees of freedom. The degrees of freedom of a χ^2 distribution depends on number of elements in the combination; here we have real and imaginary parts, squared and added together to generate the spectrogram as previously described.

In general, let us now consider a random variable $X_i \sim \mathcal{N}(0,\sigma_i^2)$, $i = 1, \ldots, 2, \ldots, N$, X is the sum of the squares of X_i. Let $X = \sum_{i=1}^{N} X_i^2$, and it is distributed as a χ^2 variable. This distribution can be characterized by three parameters, a χ^2 PDF of a random variable X can be given as:

$$f_{X;a,b,c}(X) = \frac{1}{2b}\left(\frac{x}{c}\right)^{\frac{a-2}{4}} e^{-(x+c)/2b} I_{\frac{a-2}{2}}\left(\frac{\sqrt{xc}}{b}\right), \tag{3.5}$$

where $I_n(.)$ stands for the n-order modified Bessel function of the first kind. The parameters a, b and c are the degrees of freedom, coefficient of proportionality, and non-centrality parameter, respectively. Theses parameters will be defined according to our problem which will be discussed later

In this chapter, we describe the proposed statistical model and the adaptive resmpling technique used in this project. The likelihood estimation is based on the stochastic property of the signal which will be explained later. Next, the adaptive

resampling to enhance the quality of the estimates from the PF will be discussed subsequently.

3.2 Adaptive Resampling

Even with the resampling step reducing the effects of degeneracy, new problems still occurs [29]. First, resampling step introduces the limitation of the ability to parallelize the SIS algorithm because all weights have to be summed during normalization. Second, the assumption of statistical independence is no longer valid after resampling. Therefore, convergence issues are generated along the process if resampling takes a serious loss of particle validity. For some cases, a problem that may arise after resampling is the loss of particle diversity due to all of the particles being identical as a result from a replication of those particles with high importance weights, breaking down to a noninformative distribution. This is well-known as sample impoverishment which is commonly exhibited when the noise level in the observed data is low. Recently, there are some developments of PFs [9, 13, 21, 29] that have been designed to resolve these problems.

In this work we incorporated the *adaptive resampling* scheme for eliminating the loss of particle diversity problem. This is one of the main concerns of the conventional SIR problems. The scheme was introduced in a seismic event tracking application [14] and it was successfully applied to the PF for frequency estimation using a time-varying autoregressive model [3]. New particles for the next state are constructed based on the weights of their parent particles. Number of the offspring particles, $m_k^i = \lceil N w_k^i \rceil + M$, is calculated and then the process generates the offspring particles from their parents $\mathcal{N}(x_k^i, \lambda_k^i)$. M is an integer chosen empirically. Note that $\lceil \bullet \rceil$ creates the roundup to the nearest integer. Amount of new particles also depends on the weights of their parents and the quantity λ_k^i, called fission factor, that is used to control the offsprings construction. The fission factor of the ith particle can be computed by [14]

$$\lambda_k^i = \Big[1 + exp\Big(\frac{w_k^i - \overline{w}_k}{\max\limits_i \; w_k^i - \overline{w}_k}\Big)\Big]^{-1}, \tag{3.6}$$

where $\overline{w}_k$ represents the mean of the weights at time step k. Then we create new particles based on the parent particles and the corresponding fission factor as

$$x_k^j \sim \mathcal{N}(x_k^i, \lambda_k^i), \tag{3.7}$$

where x_k^j and x_k^i are the offspring the parent particles, respectively.

Eq. (3.6) works as follows: if a parent particle occupies low weight, the higher fission degree is obtained, dictating the process to create higher quality particles. On the other hand, if the parent particle has high weight, the lower fission degree acts as a protector to conserve the high quality parent particle. In summary, the adaptive resampling process creates a new better set of particles based on the importance weights of their parent particles, and then propagates this new set into the next time step.

3.3 Particle filtering implementation

In this work, the dimension of the state is unknown, therefore we need to estimate number of frequencies present at each time step, resulting in the requirement of additional state variable. The transition probability matrix is used to dictate the probabilities of order changes; that is, frequency trajectories may leave or enter at each step [19] . If at time step $n-1$, the signal is composed of m_{n-1} modes (number of central frequencies). Then it becomes m_n in the next time step n with probability $p(m_n = j|m_{n-1} = i) = \pi_{ij}$. It should be noted that the constraint $\sum_j \pi_{ij} = 1$ must be satisfied.

According to Eq. (2.5), we obtain the measurement equation that relates the observation data $\mathbf{y}_n$ and frequency particles x_{nj} for the STFT method as follows:

$$\mathbf{y}_n = \sum_{j=1}^{m_n} a_{nj}[sinc(f - x_{nj})]^2 + \mathbf{w}_n. \tag{3.8}$$

Note that $\mathbf{y}_n$ is the FT of the acoustic time series: our approach relies on modeling the signal in the frequency domain at consecutive time slices.

Although we desire to estimate the frequencies of the signal, constructing the likelihood of the observation data requires a construction of replica of the signal. We, therefore not only estimate the frequency, but also need to estimate its corresponding amplitude as well. Since the amplitudes a_n are unknown, we create a new state vector containing these unknown quantities and treat it similarly to the unknown frequencies x_{nj}. Moreover, we also estimate the noise variance since we normally treat it to be an unknown parameter. To summarize, the state transition equations are given by:

$$\mathbf{f}_n = \mathbf{f}_{n-1} + \mathbf{v}_{1,n-1}, \tag{3.9}$$

$$\mathbf{a}_n = \mathbf{a}_{n-1} + \mathbf{v}_{2,n-1}, \tag{3.10}$$

and

$$\sigma_n^2 = \sigma_{n-1}^2 + \mathbf{v}_{3,n-1}. \tag{3.11}$$

Therefore, frequency particle and amplitude particle can be sampled from the following densities:

$$\mathbf{f}_n^i \sim \mathcal{N}(\mathbf{f}_{n-1}^i, \sigma_{v_1,n}^2), \tag{3.12}$$

$$\mathbf{a}_n^i \sim \mathcal{N}(\mathbf{a}_{n-1}^i, \sigma_{v_2,n}^2), \tag{3.13}$$

and the measurement noise variance particle can be drawn from the density:

$$\sigma_{w,n}^{2,i} \sim \mathcal{N}(\sigma_{w,n-1}^{2,i}, \varsigma_{v_3,n}^2), \tag{3.14}$$

where $\sigma_{v_1,n}^2$ and $\sigma_{v_2,n}^2$ are the frequency and amplitude state perturbation variances, while $\varsigma_{v_3,n}^2$ is the variance of the state perturbation of measurement noise variance. After sampling is employed, the likelihood can be computed via the measurement equation.

The implementation of the method for frequency estimation using particle filtering is from what was developed and presented in previous section. The χ^2 behavior of the data implies a likelihood function that will be used for weight/probablity calculation for individual particle. The χ^2 behavior of the FT shaping the form of the likelihood is explained as follows. According to Eq. (3.5), the real and imaginary parts of the FFT are normally distributed with non-zero '*means*'. These '*means*' are the corresponding FTs of the signal. Follow the statistical independent property, the sum of the squares of the real and imaginary parts follows non-central χ^2 distribution with two degrees of freedom. The sum of the squares of the means of the real and imaginary parts is the non-central parameter.

The above analysis is just for a single point in the frequency domain. For the complete length of the Fourier transform for a slice of the spectrogram, the non-central parameter is a vector of length L, which is actually the replica of the squared spectrum of the signal. The χ^2 parameters are as follows: the noncentral parameter is the replica of the signal in our problem and the number of degrees of freedom is two as discussed earlier. The coefficient of proportionality is based on the fact that both real and imaginary parts of the STFT are Gaussian random variables with common variance $\sigma^2/2$ [16]. Therefore, the coefficient of proportionality is $\sigma^2/2$. Let $\mathbf{x}_n$ is a state vector containing $\mathbf{f}_n$, $\mathbf{a}_n$, and m_n, from the discussion in Section II, the likelihood function can be given by:

$$l(\mathbf{y}_n|\mathbf{x}_n) \propto \frac{1}{L^{m_n}} exp\Big(\frac{-(\mathbf{y}_n + \sum_{j=1}^{m_n} a_{nj}[sinc(f - x_{nj})]^2)}{\sigma_{w,n}^2}\Big) \\ I_0\left[\frac{\sqrt{< \mathbf{y}_n, \sum_{j=1}^{m_n} a_{nj}[sinc(f - x_{nj})]^2 >}}{\sigma_{w,n}^2/2}\right]. \tag{3.15}$$

where $< \bullet, \bullet >$ stands for a dot product operator. Please be noted that the term $\frac{1}{L^{m_n}}$ is a prior density acting as penalizing term that impacts the value of the likelihood. For small values of m_n, this term has a value associated with a higher probability than that for larger values of m_n.

We can merge all the steps from SIS and resamping step to construct the SIR algorithm which is the essential of particle filtering approach used in this work. The SIR algorithm is outlined as follows.

- **Initialization** Since the PDFs of parameters at $n = 0$ are not known. Therefore, to construct the joint PDF of all unknown parameters, the prior densities for the parameters to be estimated need to be initialized at the beginning of the filtering process. The initial particles are sampled from these prior PDFs. Statistical properties of the priors depend on the knowledge about the data and state variables. In this work, prior densities are drawn from the uniform distributions depending on the entire support space for each parameter. Using Bayes theorem, the likelihood must be multiplied by the priors of all unknown parameters in order to create the joint PDF of the parameters.

- **Prediction** This stage starts with a set of equal weight particles from the previous time. The frequency, amplitude, and measurement noise variance particles from the precedent step are propagated via normal densities prescribed by the transition densities of Eqs. (3.12)- (3.14), respectively.

- **Updating** As previously described that the SIS is utilized to the PF at the prediction step and it needs a transition prior as its importance sampling

density. Now, the updating process starts with a set of equal weight particles, $w_{n-1}^i = 1/N$. From the measurement equation and the noise in the data acquisition process, the weight of each particle is computed using the data (spectrogram slice) just arrived.

- **Resample** This stage is introduced to remedy the sampling degeneracy. A new set of particle $\{\mathbf{x}_n^j, w_n^j = 1/N\}_{i=1}^N$ are sampled from an approximated density $p(\mathbf{x}_n|\mathbf{Y}_n)$ computed at the updating stage. Resampling creates new particles according to the weights of their parent particles w_n^i, generating more particles where the parents have high weights. After resampling, all particles occupy the same weight.

To decide what frequency is the one that we are seeking for, we select the most frequent value as a point estimates of elements of frequency state vector, namely, for a frequency state vector $\mathbf{f}_{jn}$ of a modal frequency j at time n is computed as

$$\widehat{f}_{jn} = MAP_i(f_{ijn}), \quad j = 1,\ 2,\ \ldots,\ m_n. \tag{3.16}$$

where $MAP_i(f_{ijn})$ represents the mode most frequent value of f_{ijn} for mode j at time step n among all particle i.

CHAPTER 4

SIMULATION RESULTS

In previous discussions, we described the fundamentals of Bayesian filtering for frequency estimation and the proposed model and also an adaptive resampling scheme to enhance the quality of the estimates from the PF. This chapter delivers the simulation results from the filters comprehensively.

4.1 Tracking Results from PF with adaptive resampling

4.1.1 Modal Identification

To test the performance of the AR-PF, we employed the SIR-PF and AR-PF to the data generated for a realistic underwater medium. Fig. 4.1 displays a noise-free spectrogram of an ocean acoustics signal calculated from a length of the time-segment 180 via a short-time Fourier transform with hamming window. A slice of the spectrogram at time 200 ms is shown in Fig. 4.2. We can see that there are a few modes that appear at this time slice. It should be noted that we can have up to six modes but the possibility for this scenario is very low. To justify the number of modes, the filter allows itself to track model order and the decision is based on the weights of particles. We assume that the signal contains at least one modal component and may not exceed six modes. Particle filter initialization is constructed with a uniform prior for the searching frequency interval of 200-600 Hz, therefore we initiated the frequency particles with $\mathbf{x} \sim \mathcal{U}[200, 600]$, where $\mathbf{x} \sim \mathcal{U}[a, b]$ is the uniform distribution PDF with parameters a and b. Also, the noise variance particles are initiated according to work reported in [6].

Next we show the modal estimates from the SIR-PF and AR-PF where the signal is clean, as seen in Fig. 4.3. The number or particles used in this experiment

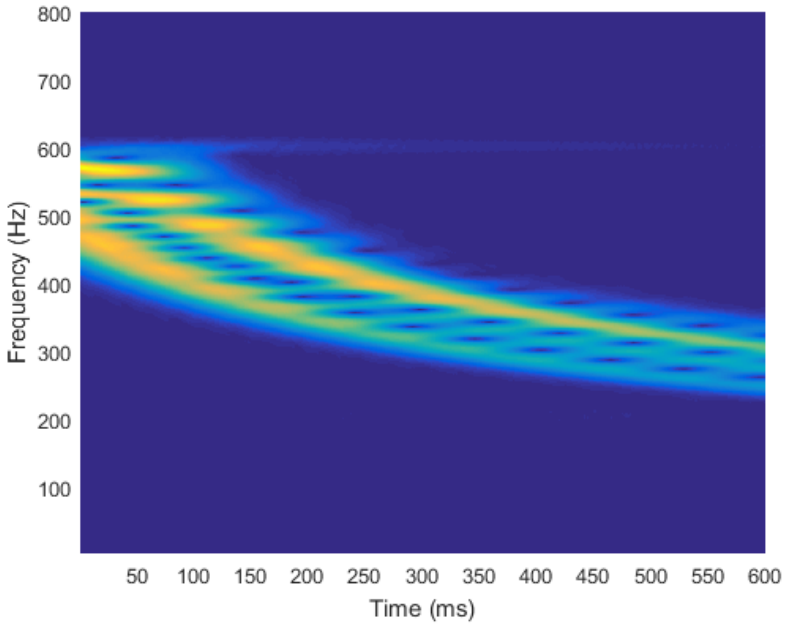

Figure 4.1 Spectrogram of an ocean acoustics signal.

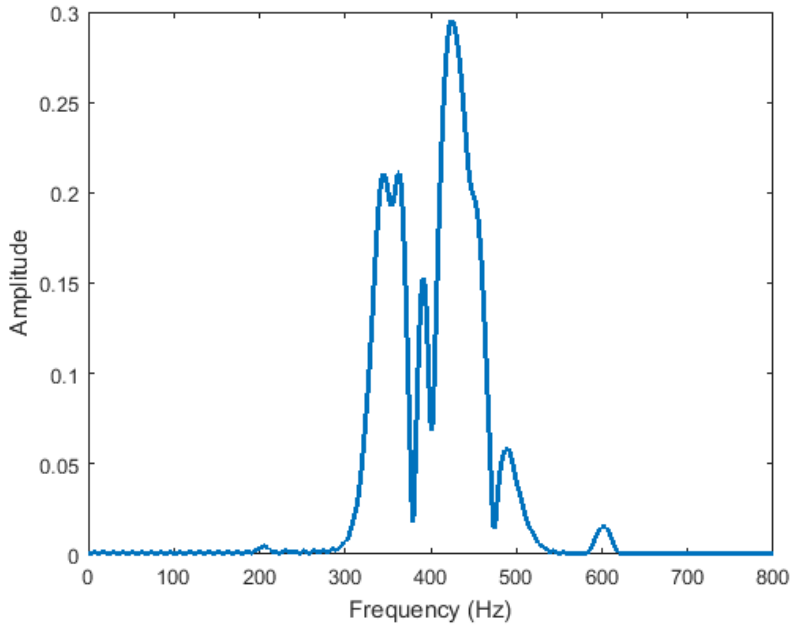

Figure 4.2 A slice of the spectrogram at time 200 ms.

was 500 for both filters. The results shown in Fig. 4.3 are the estimated spectrums as obtained by SIR-PF that is shown with red colour, and by AR-PR as displayed with

green colour. The modal frequencies (spectral peaks) are calculated from the highest posterior probability, i.e., the modal frequencies are identified via the *maximum a posterior* (MAP) estimator, i.e., the most frequent value of the tracking parameter is chosen. From the results, the estimated spectrums from both filters coincide nicely with the squared FT magnitude of the acoustic data. This is not surprising that the SIR-PF can capture almost all of the useful information embedded in the data since the noise level is extremely small. For this case AR-PF may not be necessary.

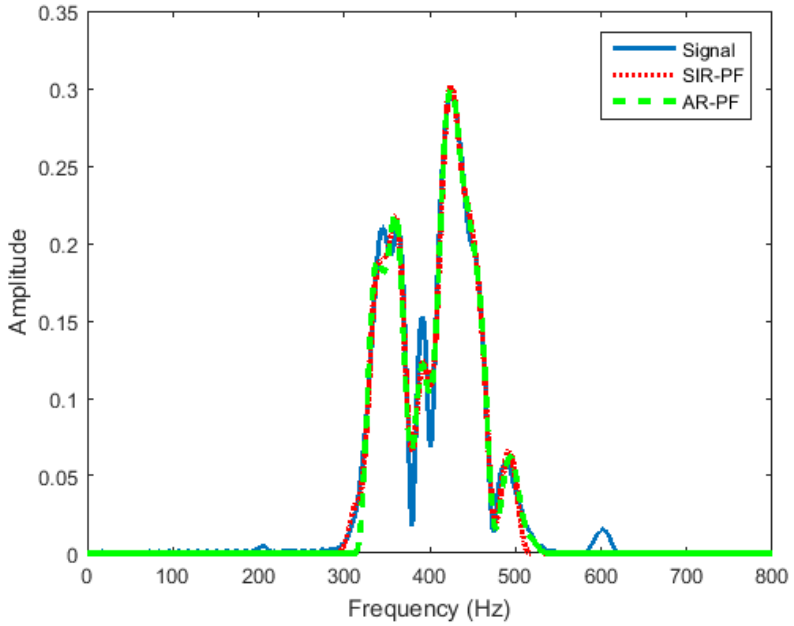

Figure 4.3 A slice of the spectrogram at time 200 ms (solid line) with the modal spectrum constructed using the MAP estimates for the SIR-PF and AR-PF superimposed.

We further illustrate the tracking results when the noise level becomes higher. Noise is assumed to contaminate the signal in the frequency domain and we added the same amount for all time slices. Since the spectrogram becomes weaker as time progresses, a single signal-to-noise ratio (SNR) cannot be defined but is decreasing as time evolves.

We demonstrated, with number of particles of 1000 for both filters, in Fig. 4.4 that the performance of the AR-PF becomes superior than the SIR-PF when the noise level is increased. The SIR-PF can estimate the modal frequencies in the spectrogram only with those modes that occupy high amplitudes. For the frequencies with low amplitudes, SIR-PF fails to do so but the AR-PF. A zoomed in version of Fig. 4.4 is provided to demonstrates the AR-PF. This evidence is presented in Fig. 4.5 which obviously presents that a modal frequency of 458 Hz can be captured by the AR-PF while the SIR-PF cannot track it. The AR-PF, therefore, exhibits an excellent match between the estimated spectrum and the observed noisy data.

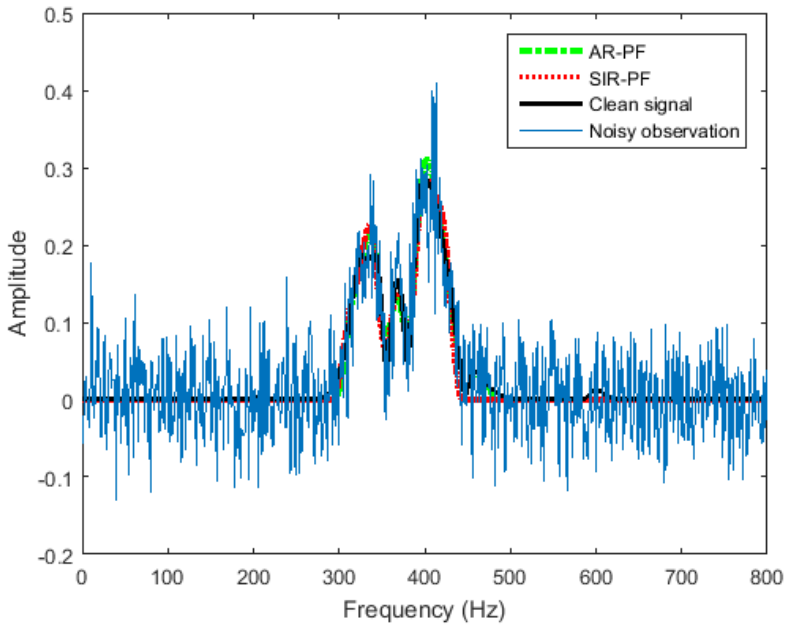

Figure 4.4 A slice of the spectrogram at time 250 ms (solid line) with the modal spectrum constructed using the MAP estimates for the SIR-PF and AR-PF superimposed.

Finally, we demonstrated the robustness of the AR-PF where the acoustic signal was contaminated by a high level of noise, i.e., the SNR is low. Again, the number of particles used for this test was 5000. The illustrating example of the modal identification at time slide 250 ms is shown in Fig. 4.6. In Fig. 4.6(a), we show the

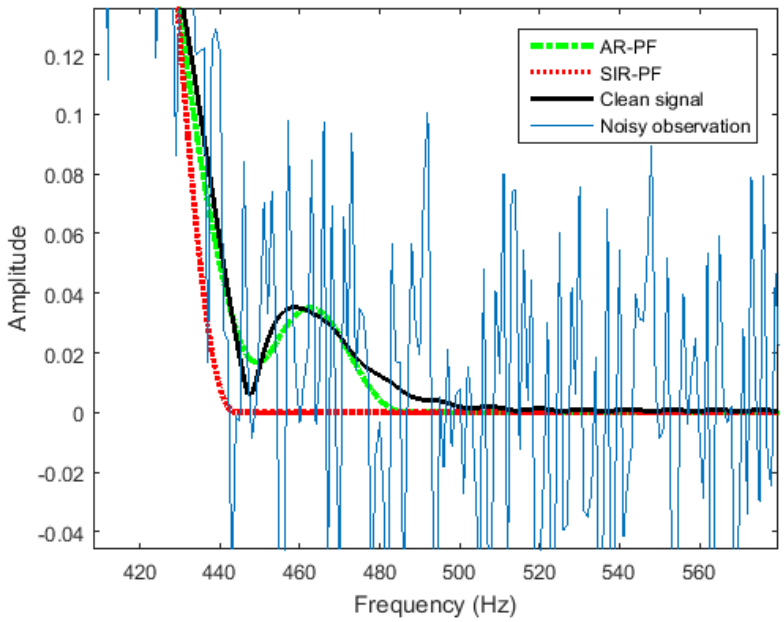

Figure 4.5 Illustration of the ability of AR-PF to capture a mode with modal frequency of 458 Hz.

original signal and its noisy realization, while the estimates from SIR-PF and AR-PF, and plot of original signal are presented in 4.6(b). The estimates from SIR-PF are displayed using red colour, the estimates from AR-PF are indicated by the green colour, and the black line is the original signal. The estimated spectrum as obtained from the AR-PF clearly outperforms that from the SIR-PF. For this case, we obviously observed that the SIR-PF loses its capability to track the modal frequencies effectively since most peaks of the estimates from the SIR-PF do not match with those of the original ones. On the other hand, peaks and modal amplitudes are almost similar to the original signal, therefore, AR-PF offers an estimated spectrum that is closed to the original signal. Another observation is that the SIR-PF also misses a modal frequency at 455 Hz, but not with the AR-PF. This demonstration is to emphasize the robustness capability of the AR-PF.

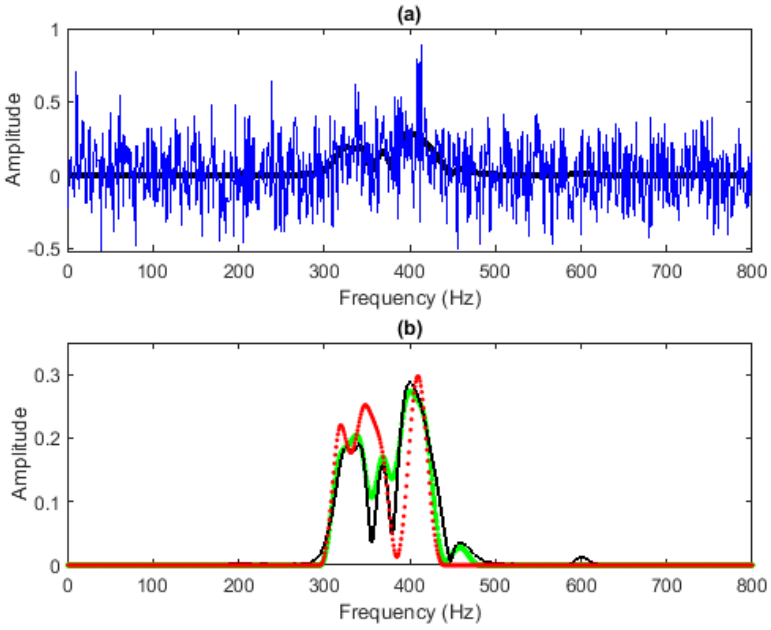

Figure 4.6 Original and estimated spectrums at time 250 ms from AR-PF and SIR-PF for low SNR: (a) original signal (black) and its noisy realization (blue); (b) original signal (black), estimated spectrum as obtained by the SIR-PF (red), and estimated spectrum as obtained by the AR-PF (green).

4.1.2 Dispersion Tracking

We now perform the full sequential Bayesian filtering framework to obtain dispersion curves of the ocean acoustics signal. According to the acoustic model of the propagated signal under the dispersive media discussed in Section 3, we utilized the particle filtering along with the adaptive resampling scheme to extract the modal frequencies of the acoustic signal. These frequencies form the dispersion characteristic of the ocean acoustics property via the dispersion curves that were obtained from the PF.

We showed in Fig. 4.7 the spectrogram of the noisy ocean acoustics signal. It should be noted that the signal is weaker as time increases, therefore the SNR cannot be defined as a single SNR for the whole signal but it is decreasing as time evolves. We set the number of particles for this experiment to 2000 for both filters. The tracking results from the SIR-PF and AR-PF are shown in Figs. 4.8-4.9. For the first 350 ms, the tracks from the SIR-PF and AR-PF are not significantly different. However, the

tracks from AR-PF are better than those from the SIR-PF as clearly seen from the present of more uncertainty in the tracks from SIR-PF, meaning that the ability to handle the noise of the SIR-PF is inferior to that of the AR-PF. Moreover, at time 450-475 ms, we observed that the estimates from AR-PF do not deliver ambiguity but SIR-PF, as seen at the top most tracks.

To get a better justification of the performance of the filters, we compute the RMS error (RMSE) defined by the L_2 norm averaged over K spectrogram slides:

$$RMSE = \sqrt{\frac{1}{K}\sum_{k=1}^{K} ||\mathbf{f}_k^{'} - \hat{\mathbf{f}}^{'}_k||^2} \tag{4.1}$$

where $\mathbf{f}_k^{'}$ is the vector of true values of the normalized frequencies and $\hat{\mathbf{f}}^{'}_k$ is the vector containing the normalized frequency estimates at time step k. The RMSE values from both filters are shown in Table 4.1. Please be noted that the SNR for each case is the average SNR over all slices since the SNR for each slice varies with time as mentioned earlier. From the Table, for any SNR levels, the AR-PF provides lower RMSEs than the SIR-PF. Moreover, the quality of the estimation by the AR-PF is much better when the SNR levels become lower as seen from much higher RMSEs for the SIR-PF compared to RMSEs for AR-PF.

Table 4.1 Prediction performance of PF via RMSE with different SNR levels.

Average SNR (dB)	**RMSE**$_{(SIR-PF)}$	**RMSE**$_{(AR-PF)}$
3	0.2122	0.1565
-3	0.2982	0.1855
-7	0.3653	0.2321
-10	0.4592	0.2959

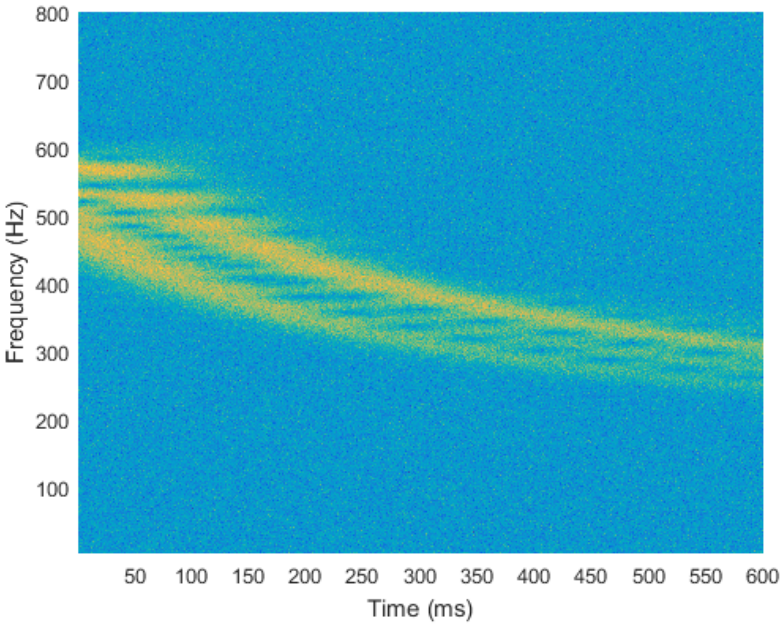

Figure 4.7 Spectrogram of a noisy ocean acoustics signal.

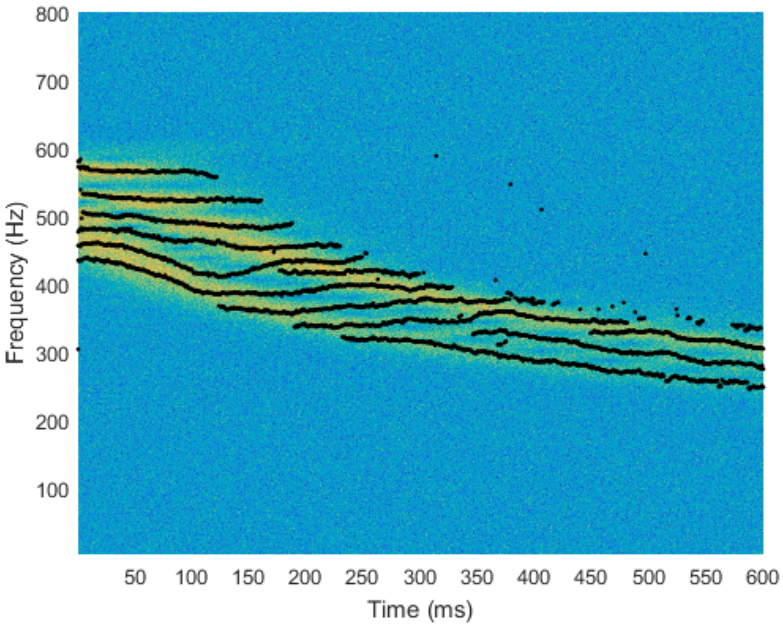

Figure 4.8 Frequency tracks of a noisy ocean acoustics signal as estimated by the SIR-PF.

Next, we present the robustness of the proposed filter by considering two different SNRs, the SNRs vs time for the two noise levels are displayed in Fig. 4.10.

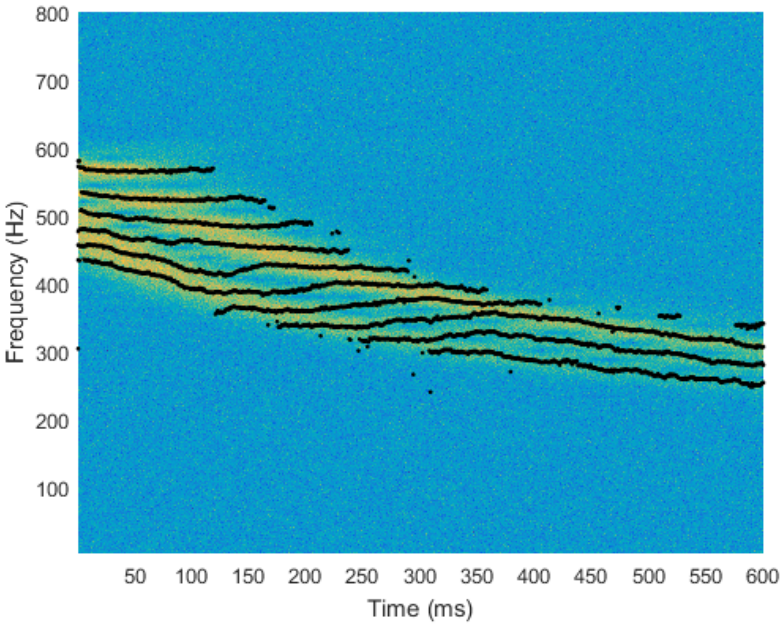

Figure 4.9 Frequency tracks of a noisy ocean acoustics signal as estimated by the AR-PF.

For the SNR level of Fig. 4.10(a), in Fig. 4.11 we demonstrated how the proposed filter is robust to the noise. It can be obviously seen that the quality of the frequency estimates from the AR-PF is much better than those from the SIR-PF, resulting in an excellent tracking as the dispersion curves can be followed nicer by using AR-PF. We observed from the tracks from the SIR-PF that the appearance of noisy tracks is more obvious as the decreasing of the SNR. More evidence to show the robustness of the proposed filter is also revealed in the tracks from AR-PF shown in Fig. 4.12, where the noise level for this test is given in Fig. 4.10(b). The frequency estimates that were obtained from the AR-PF is superior to those obtained from the SIR-PF, the tracks after 250 ms from the AR-PF is much better since more modes can be tracked very well while the SIR-PF losses its capability to do so.

We showed in Fig. 4.13(a) the frequency estimates from the SIR-PF, while in Fig. 4.13(b) the frequency estimates from the AR-PF, the average SNR level in this case was -7 dB. The quality of the frequency trajectories from AR-PF is

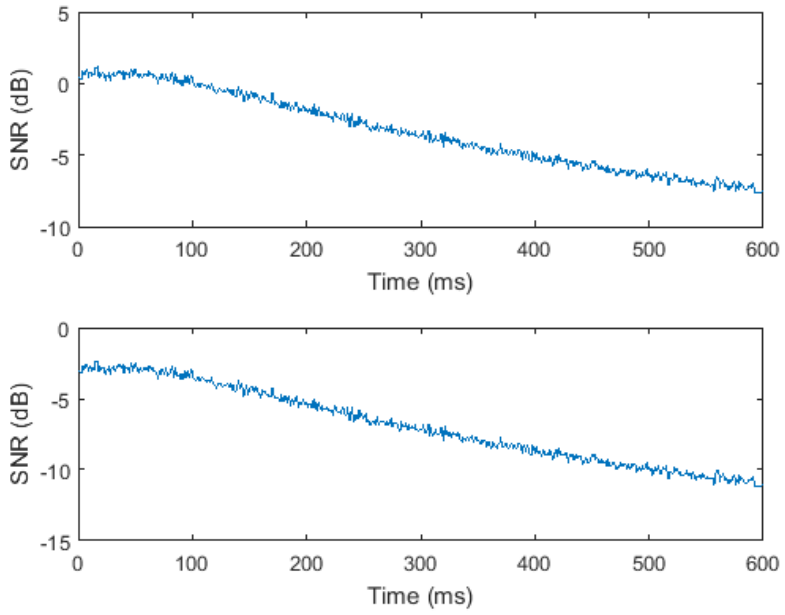

Figure 4.10 The SNR of a noisy ocean acoustics signal for two different noise levels as a function of time.

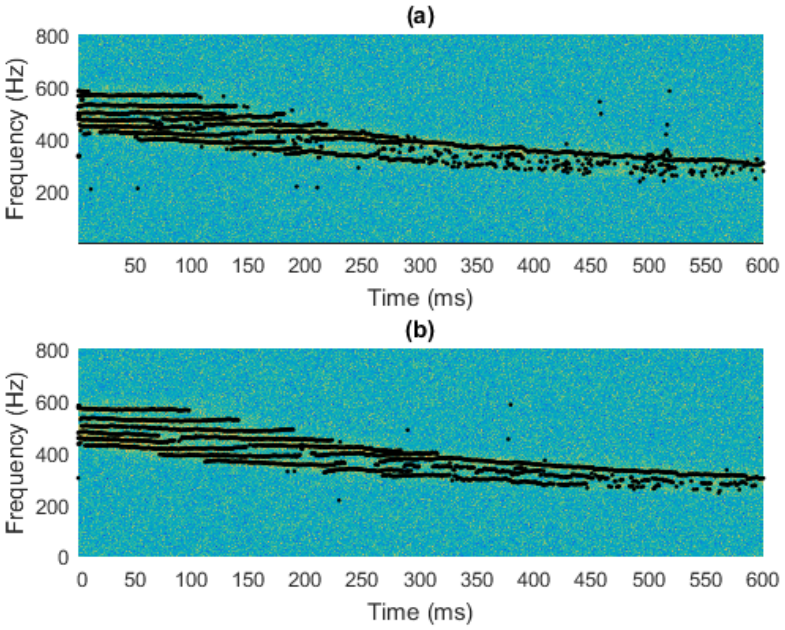

Figure 4.11 Frequency tracks of a noisy ocean acoustics signal with SNR of Fig. 4.10(a) as estimated by: (a) SIR-PF and (b) AR-PF.

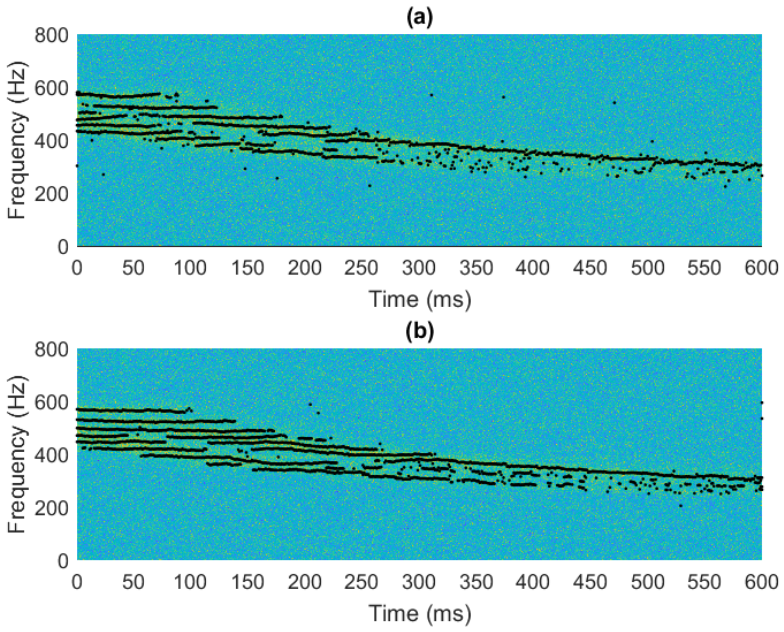

Figure 4.12 Frequency tracks of a noisy ocean acoustics signal with SNR of Fig. 4.10(b) as estimated by: (a) SIR-PF and (b) AR-PF.

maintained better than the ones obtained from the SIR-PF, especially when the signal becomes weaker, i.e. for noisier situations. Therefore the AR-PF offers a better estimated dispersion curves than the SIR-PF. To investigate the capability in capturing the modal frequencies PDFs of the ocean acoustics signal of both filters, Fig. 4.14 demonstrates the frequency PDFs at time 200 ms obtained from the filters. At time 200 ms, the signal contains 3 modes: the true values of modal frequencies are 358, 389, and 396 Hz. It is obviously seen that the AR-PF delivers high likelihood regions to the true values and it can detect all modes, but the SIR-PF can detect only two modes. Moreover, the AR-PF provides lower uncertainty in frequency estimation, resulting in a better tracking performance.

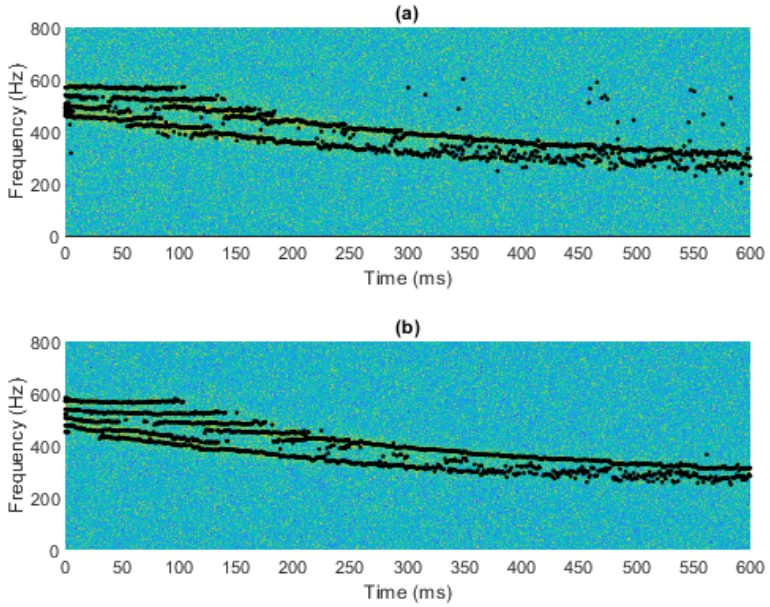

Figure 4.13 Tracking for two filters: (a) SIR-PF and (b) AR-PF. The numbers of particles was 10,000.

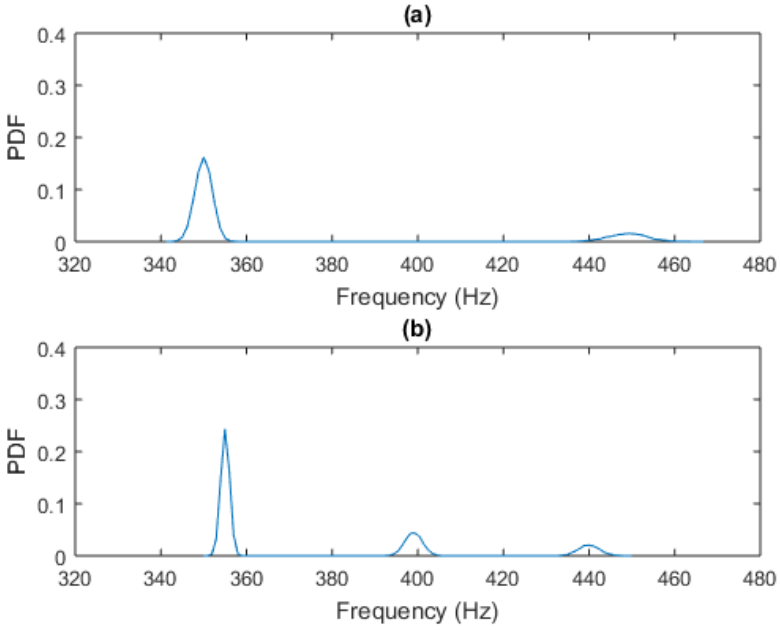

Figure 4.14 The frequency probability density functions for the signal at time 200 ms. (a) The frequency PDFs as obtained by SIR-PF and (b) the frequency PDFs as obtained by AR-PF.

4.2 Tracking results using a realistic probability density function of the spectrogram

In this work, a frequency content between 200-600 Hz generated from a source is propagating in the ocean and is observed at a hydrophone. The signal was generated according to the environment that is similar to that of the Gulf of Mexico experiment [23], the sampling rate was 2000 Hz. The ocean acoustics time-series is shown in Fig. 4.15. The spectrogram of the signal as obtained from the STFT is displayed in Fig. 4.16.

As seen in Fig. 4.16 that the pattern of the dispersion curves of the signal is obviously seen after 0.3 s, therefore, we process the signal after this time. In addition, our tracking process assumption is that we are tracking the separated modal frequencies of the signal, the mentioned starting time is reasonable in this case since the pattern shows that the modes are quite well separated after this time segment. For this simulation result, the signal in Fig. 4.16 is used for the tracking process but the white Gaussian noise was added to the acoustic time-series before the STFT and spectrogram calculation. The MAP frequency trajectory estimates obtained for the PDFs as provided by the PF are illustrated in Fig. 4.17 with black dots and they are superimposed on a segment of the spectrogram.

To illustrate the validity of the model and the performance of the filter, we show in Fig. 4.18 the spectrogram slice of the signal at a particular time using a solid line; and displayed using red stars, a MAP replica of the signal obtained from the filter. We can see that the squared STFT magnitude are coinciding with MAP replica spectrum; this shows how the mathematical and statistical models made in this work are successfully combined to estimate the frequency of the ocean acoustics signal.

We further investigate the robustness of the proposed model to noise by adding higher level of noise into the original signal. It should be noted that, in our work,

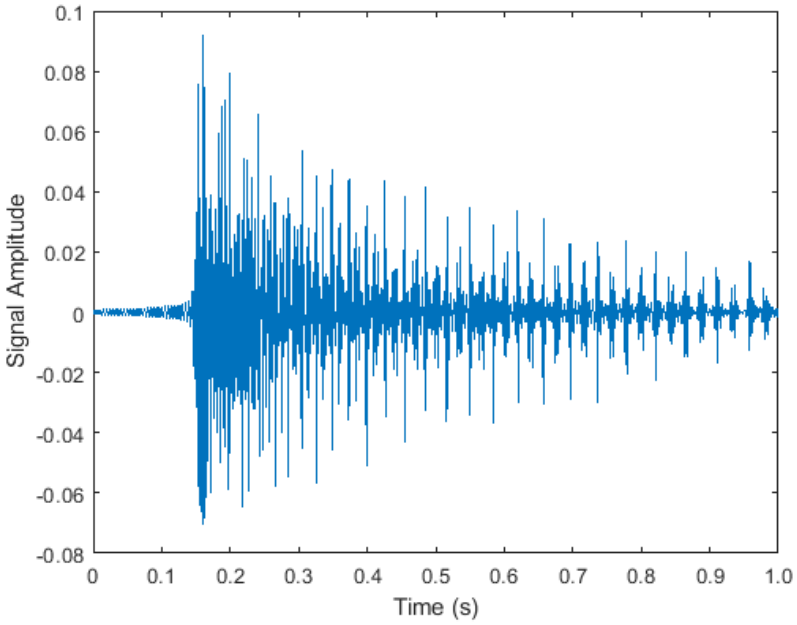

Figure 4.15 The synthetic ocean acoustics time-series.

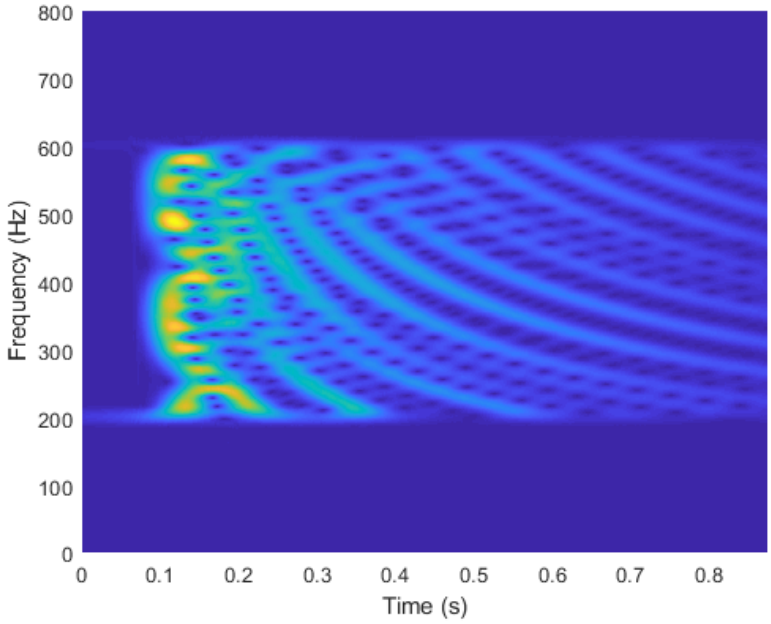

Figure 4.16 The spectrogram of synthetic ocean acoustics time-series.

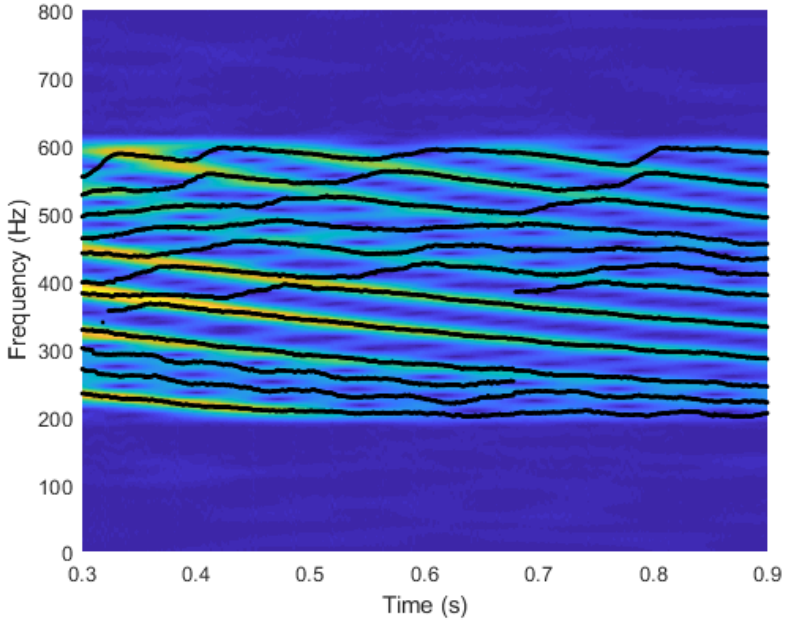

Figure 4.17 A segment of the spectrogram of synthetic ocean acoustics time-series to be processed.

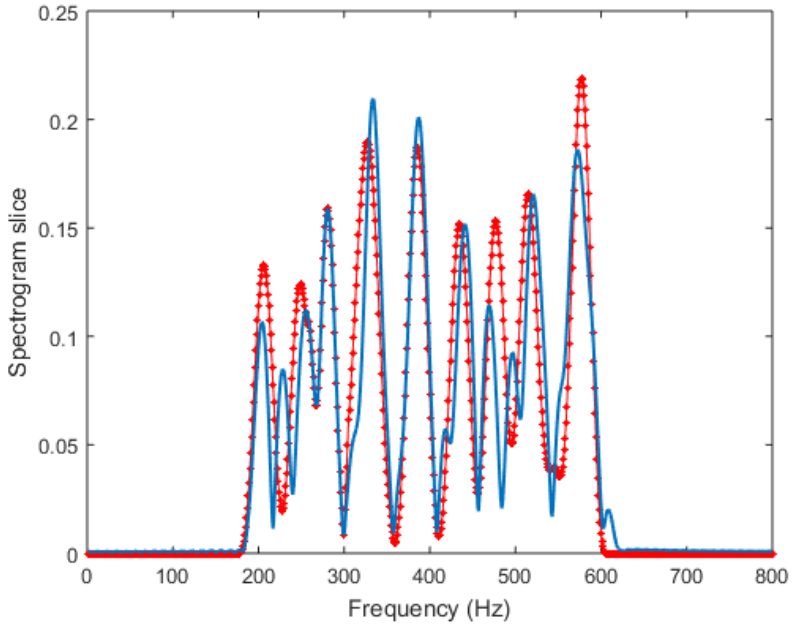

Figure 4.18 A spectrogram slice of the synthetic ocean acoustics time-series at a particular time (solid line) and the replica spectrum constructed using the results from the PF superimposed (red stars).

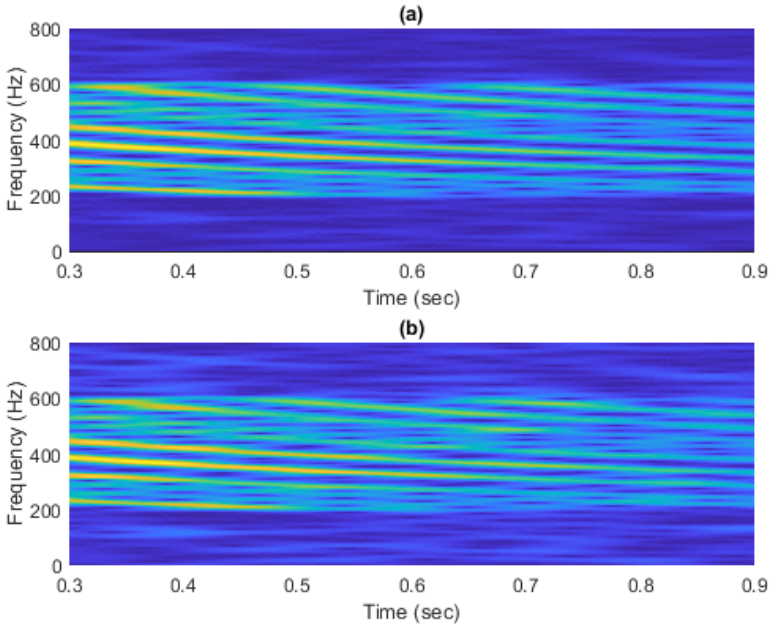

Figure 4.19 Two noisy realization spectrograms of the synthetic ocean acoustics time-series for two different noise levels.

we cannot define a single signal to noise ratio (SNR) value since the signal becomes weaker as time progresses due to the attenuation of signal with time. Two noisy realizations for different SNR levels are shown in Fig. 4.19, where the signal in later case was contaminated by a higher noise level as we can see from Fig. 4.19(b) that the spectrogram is noisier, resulting in more uncertainty in the dispersive pattern. The frequency estimates as obtained by the PF are shown in Figs 4.20-4.21. The quality of the tracking results from the filter for both cases are quite similar even the noise level in the measured signal is higher. This could be an evidence of the noise robustness of the filter which is a result of the proposed accurate statistical characteristic of the TF representation of the signal.

We provide a tracking result from a severe case where the signal is corrupted by extreme amount of noise, the spectrogram is shown in Fig. 4.22. The MAP frequency trajectory estimates obtained from the PF are revealed in Fig. 4.23. Although some modes are missing in the tracking results, the frequency estimates are fairly satisfied,

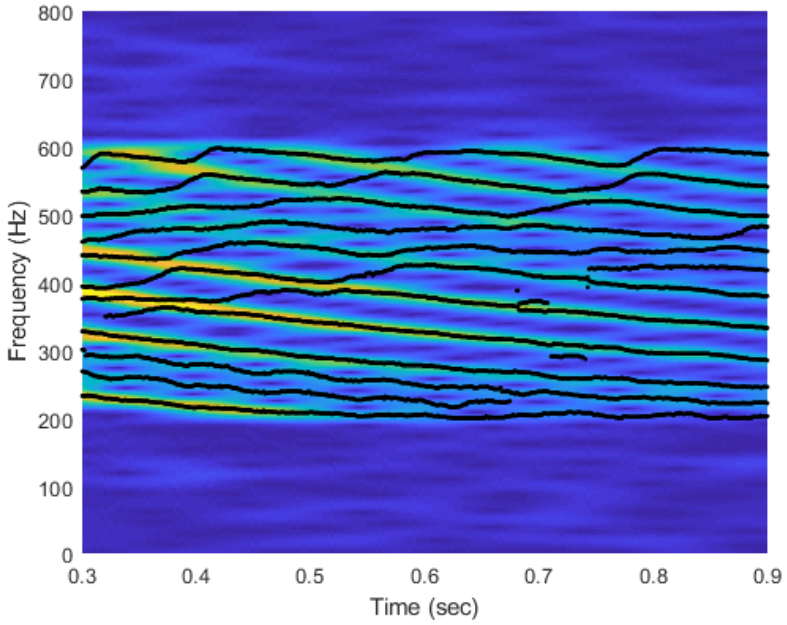

Figure 4.20 Tracking results as provided by the PF; the average SNR is 19.3 dB.

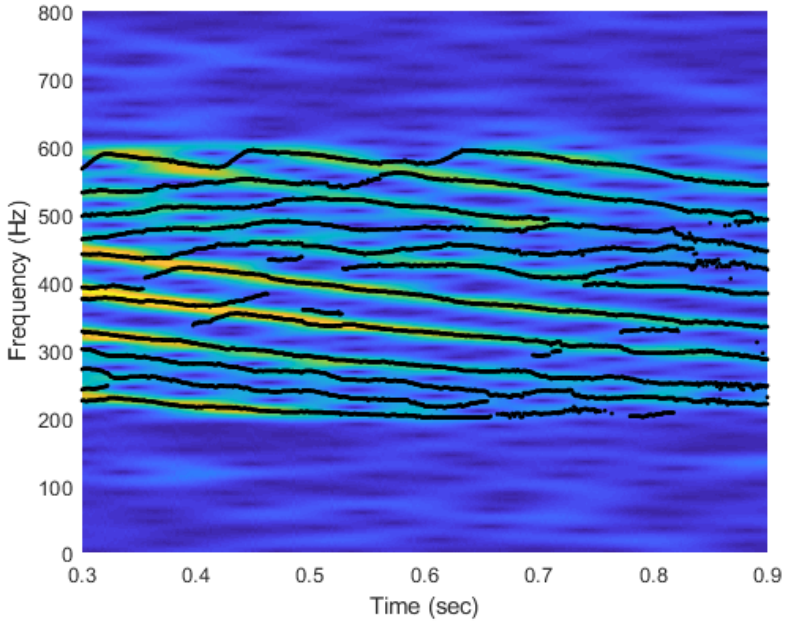

Figure 4.21 Tracking results as provided by the PF; the average SNR is 14.6 dB.

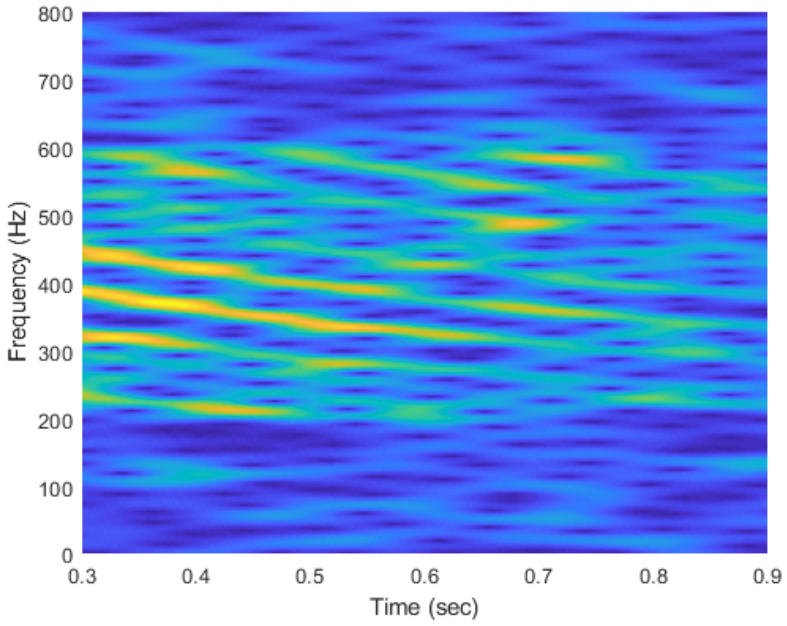

Figure 4.22 Spectrogram of extreme noisy ocean acoustics time-series; the average SNR is 5 dB.

and the estimated dispersion is adequate for further processing since a few modes are nicely traced by the filter and these are sufficient for the inversion for sediment sound speed profile and other geoacoustics properties [24, 25].

Root Mean Squared Error (RMSE) results from the PF implementation are shown in Fig. 4.24, with stars, diamonds and circles indicating the RMS errors for the average SNRs 15, 10, and 5 dB, respectively. To compare the performance of the filter, we perform conventional Maximum a Posteriori (MAP) estimation which is equivalent to the Maximum Likelihood (ML) estimation since uniform priors are chosen in our work. It is not surprising that for a small number of particles, the proposed method delivers high RMSE than that of the MAP estimation. This is because of a limited number of particles in the processor cannot capture a stochastic behavior of the signal. However, the errors for all cases significantly decrease as the increase of the number of particles. More importantly, the PF errors become

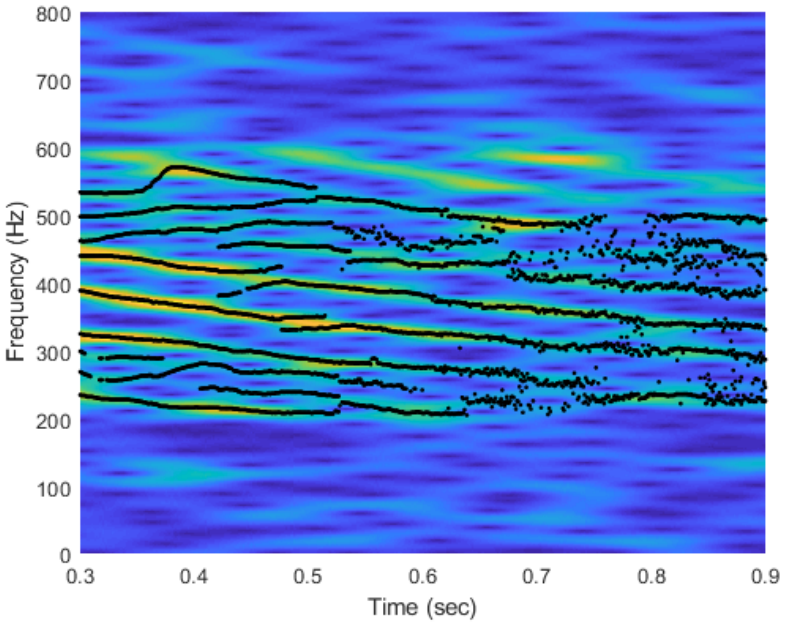

Figure 4.23 Frequency tracks as estimated by the PF for the extreme noisy ocean acoustics time-series; the average SNR is 5 dB.

dramatically lower than the corresponding conventional MAP errors, illustrating the superiority of the proposed method to the MAP estimation.

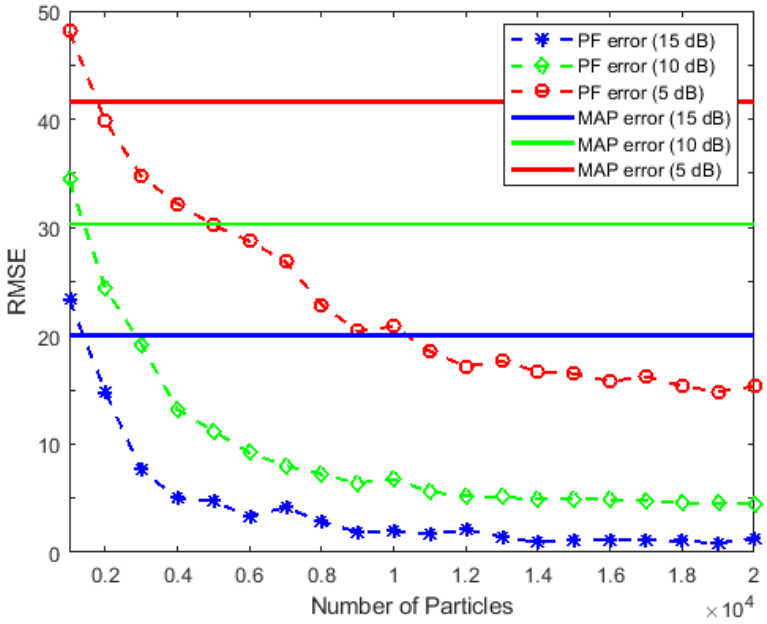

Figure 4.24 Comparison of PF estimation for different noise levels. Maximum likelihood estimates are superimposed.

CHAPTER 5

CONCLUSIONS

5.1 Conclusions

In this work, we developed an approach for sequentially estimating modal frequencies, amplitudes, number of modes, and noise variance. The main goal was the identification of a dispersion pattern of a signal propagating in the ocean. Our technique is a Monte Carlo method for drawing inferences from state-space models, where the state of a system evolves with time or space and information about the state is obtained via noisy observations made at each time step.

A standard approach for frequency estimation was based on the assumption that the additive white Gaussian noise was assumed to corrupt the original signal in the frequency domain, which was not accurate. The signal for our FT domain does not fall in Gaussian error. Therefore, we have to fix this inaccurate setting. Consequently, the main contribution of this work was the stochastic characterization derivation of the ocean acoustics time-series. We have derived that the probability density function of the spectrogram can be written as a form of the noncentral χ^2 distribution with two degrees of freedom. We then implemented a PF based on the accurate model to track the modal frequencies and dispersion curves of the ocean acoustics signal, the tracking results outperforms the conventional method.

An extra implementation that we have done in this project is devoted to the improvement on the resampling step, a step that plays a crucial role in PF, by using the so called adaptive resampling method. The adaptive resampling utilized in this project creates a new effective set of particles for constructing a posterior PDF of the tracking parameters including modal frequency, its corresponding amplitude, number

of modes, and noise variance. The method delivers better tracking results evaluated via RMSE, as reported in the previous chapter.

In summary, this project have created two new analysis and implementations of the particle filter to accurately estimate the modal frequencies and dispersion curves of the ocean acoustics time-series. By using the RMSE metric to evaluate the performance of the proposed methods, our work has shown its superiority to the conventional MAP estimator significantly.

5.2 Future Work

There are several aspects of this work that will be addressed and improved by developing more sophisticated algorithms.

We expect that modal frequency estimation will become more accurate after the implementation of a smoothing scheme. Specifically, once our filter, which is a "forward" process moving from one time instant to the next, estimates tracks, a smoother will be employed to refine the estimates of the frequency PDFs and, thus, the MAP inference on the modal frequencies.

We will also look for the new transform techniques that can reduce the effect of the low resolution problem of the STFT approach, TVAR model may be a good choice to start with.

APPENDIX A

ACCEPTED PAPERS

Followings are the accepted papers from this project [4, 31].

1. P. Taveeapiradeecharoen, K. Chamnongthai, and N. Aunsri, Bayesian Compressed Vector Autoregression for Financial Time-series Analysis and Forecasting, *IEEE ACCESS* 7:16777-16786, 2019.

1. N. Aunsri, Effect of Window Functions on the Sequential Bayesian Filtering Based Frequency Estimation, *The 21st International Symposium on Wireless Personal Multimedia Communications (WPMC- 2018)* pp. 411-415, 2018.

IEEE Access
Multidisciplinary | Rapid Review | Open Access Journal

Received October 9, 2018, accepted January 7, 2019, date of publication January 25, 2019, date of current version February 14, 2019.

Digital Object Identifier 10.1109/ACCESS.2019.2895022

Bayesian Compressed Vector Autoregression for Financial Time-Series Analysis and Forecasting

PAPONPAT TAVEEAPIRADEECHAROEN[1], KOSIN CHAMNONGTHAI[2], (Senior Member, IEEE), AND NATTAPOL AUNSRI[3,4]

[1]School of Management, Mae Fah Luang University, Chiang Rai 57100, Thailand
[2]Faculty of Engineering, King Mongkut's University of Technology Thonburi, Bangkok 10140, Thailand
[3]School of Information Technology, Mae Fah Luang University, Chiang Rai 57100, Thailand
[4]Brain Science and Engineering Innovation Research Group, Mae Fah Luang University, Chiang Rai 57100, Thailand

Corresponding author: Nattapol Aunsri (nattapol.aun@mfu.ac.th)

This work was supported in part by the Thailand Research Fund (TRF) and the Office of the Higher Education Commission (OHEC) under Grant MRG6080152, and in part by the Mae Fah Luang University.

ABSTRACT Advanced time series models have been intensively developed and used to predict in financial data such as foreign exchange data (forex). In this paper, we implement the random compression method to reduce a large dimensional forex data into much smaller matrix form. Then, Bayesian inferences on vector autoregression are used to obtain all interesting parameters. Subsequently, the models are able to perform out-of-sample prediction up to 14 days ahead of forecast. For empirical works, 30 forex pairs are used in this paper. The results show that Bayesian compressed vector autoregression (BCVAR) and time-varying BCVAR (TVP-BCVAR) deliver excellent forecasting on AUD-JPY, CAD-CHF, CAD-JPY, EUR-DKK, EUR-MXN, and EUR-TRY forex datasets according to mean square forecasting error, outperforming the traditional benchmark Bayesian Autoregression.

INDEX TERMS Bayesian methods, compression algorithms, finance, autoregressive processes, forecasting, Bayesian model averaging, dymamic model averaging, Kalman filter.

I. INTRODUCTION

Recently, econometricians have been working intensively on developing tools for forecasting big economic data with the concerns of dealing with the financial big data which is available recently. Vector autoregressions (VARs) method has been a crucial tool in finance and economics since the seminal work of Sims [1]. Given a large dimension of data in forecasting process especially in VARs, computational burden is always one of the main problems. Specifically, Bayesian VARs which include the method of Markov Chain Monte Carlo (MCMC) is almost impossible where the number of predictors is as a scale of hundreds or thousands. In literatures, number of works concerning about this issue reported previously that some works successfully tackled this kind of problem such as [2]–[4], for examples. The curse of dimensionality usually arises when the number of available observations is often less than the number of predictors in VARs equations. This is one of the reasons why we call the method that is dealing with this kind of problem as ''high dimensional method''. Econometricians typically work through prior shrinkage on the parameters in order to avoid such over-parametrization; the Minnesota prior, for example, is one among the other famous shrinkage methods. In addition, another approach such as least absolute shrinkage and selection operator were proposed, see [5]. There are many sources of literatures where researchers work with compressing the data instead of parameters; see [6]. Recently, Guhaniyogi and Dunson [7] developed the compressing strategy with a Bayesian regression, where the number of predictors in model equations is randomly compressed by introducing a special matrix to perform that task.

The advances of computer and computational Bayesian approach play an important role in solving sophisticated financial problems via numerical methods by means of Monte Carlo simulation, allowing the approximated posterior distribution of the underlying parameters is obtained without difficulty [8], [9]. Compression method has been utilized in many applications including signal processing, compressed sensing, machine learning, and image processing, etc [10], [11].

The associate editor coordinating the review of this manuscript and approving it for publication was Luis Javier Garcia Villalba.

The compression is performed with the similar idea to that of the principal component analysis (PCA). The PCA method treats the random variable as factor to be the representative of the variation from large dimensional matrix. It has been known that the PCA requires computational burden; compression, however, is computationally simpler. From a large dimensional matrix, we compress it with random algorithm. In literature, Guhaniyogi and Dunson [7] illustrated an application in using compression involving up to 84,363 explanatory variables. Among the others see [3] and [12] where these works adapted dynamic model averaging developed by Raftery *et al.* [13], and implemented it to be applicable in VAR model for forecasting the macroeconomic and daily forex, respectively. Moreover, Ji *et al.* [14] presented the compression method for signal processing in a Bayesian compressing fashion.

In this work, we propose a random compression method to reduce a large dimensional forex data into much smaller matrix. Then the Bayesian model averaging (BMA) approach is employed to the weight of each random compressed VAR for achieving the best prediction model.

The rest of the paper is structured as follows. Section II, a foundation of Bayesian compressed vector autoregression is presented. Then Section III describes how the BCVAR is formulated for forecasting. In Section IV, we provide the details of the extension of the method to the time-varying parameters. Empirical works including data preparation and forecasting results are found in Section V. Conclusions are made in Section VI, and data appendix is provided in Section VII.

II. BAYESIAN COMPRESSED VECTOR AUTOREGRESSION

For better comprehension, the notations that are used in this work are provied in details in Table 1.

Consider a general form of VAR model,

$$Y_t = BY_{t-p} + \epsilon_t \tag{1}$$

where Y_t is $n \times T$ series of dependent variable matrix of T observations. B is $n \times n$ matrix of VAR parameters that we wish to estimate, Y_{t-p} are predictors which typically are the lags of dependent variables with p lags selected according to the problem at hands. Residual, ϵ_t, is normally distributed and it follows the assumption $\epsilon_t \sim N(0, \Omega)$.

For the large size VAR model, suppose we want to estimate 100 n variables with $p = 1$, the dimension of the predictors Y_{t-1} would be $k \times T$, where $k = n \times p + 1$ in case of constant term included and $k = n \times p$ in case of no intercept, and B is extremely large and if we need to estimate up to 10, 000 parameters. In this case, the curse of dimensionality is unavoidable, see literature for instances [15]–[17]. In addition, the computation can be cumbersome especially when working with a Markov Chain Monte Carlo method such as Gibbs-sampling in Bayesian VAR.

The idea of compressed VAR is that we randomly generate "the projection matrix" Φ to compress the predictors in matrix Y_{t-p}. Instead of fully estimate VAR model in equation (1), we can rewrite the VAR equation as follow:

$$Y_t = B^c(\Phi Y_{t-1} + \epsilon_t) \tag{2}$$

where Φ is $m \times k$ matrix with $m \ll k$, subject to normalization $\Phi\Phi' = I$. We may define $\widetilde{Y}_{t-1} = \Phi Y_{t-1}$ with the dimension of $m \times T$. We see that the matrix of predictors in VAR is relatively small for the uncompressed VAR.

As mentioned above that compression method is done by treating Φ_{ij} as random matrix. It is thus necessary to define the elements in projection matrix. We adopt [18], the method of drawing Φ_{ij} to this work, where it is sampled from the following distribution:

$$\begin{aligned} \mathbf{Pr}(\Phi_{ij} = \frac{1}{\varphi}) &= \varphi^2, \\ \mathbf{Pr}(\Phi_{ij} = 0) &= 2(1-\varphi)\varphi, \\ \mathbf{Pr}(\Phi_{ij} = -\frac{1}{\varphi}) &= (1-\varphi)^2, \end{aligned} \tag{3}$$

where φ and m are also treated as unknown parameters. Since we have no prior information about those parameters, we then initialize Φ_{ij} in a fully random fashion $\Phi_{ij}^{(r)}$ where $r = 1, \ldots, R$ denotes number of generations. Specifically, we follow [7] where φ is drawn from $U[a, b]$, a uniform distribution, where a and b are set to the constant numbers of slightly above zero and below than one, respectively. In addition, Guhaniyogi and Dunson [7] suggest to simulate number of compression matrix m from $U[2log(k), min(T, k)]$ distribution. Since we need to find $\Phi_{ij}^{(r)}$ that performs the best on forecasting based on the available data, we therefore apply Bayesian Model Averaging (BMA) to augment weight for each random $\Phi_{ij}^{(r)}$ by calculating the marginal likelihood

TABLE 1. Mathematic symbol notations.

Notations	Descriptions
t	Time observation of data
p	Number of lag in predictor matrix in VAR
k	Number of predictors before random compression
m	Number of predictors after random compression
Y_t	Dependent Variables in VAR
Y_{t-p}	Predictors in VAR
B	Parameters in compact form of VAR
ϵ_t	Residuals in VAR
Ω	Variance of residual matrix in VAR
Φ	Random projection matrix
B^c	compact VAR parameters after compression
m	Number of predictors after random compression
φ	Unknown parameters for generate random compression matrix
A	Lower triangular matrix
Z_t	Predictor matrix after rearranging reduced-form VAR
Θ	Parameters after rearranging reduced-form VAR
Σ	Diagonal matrix contains variance of residuals
Θ_i^c	Compressed VAR parameters of equation i
Z_t^i	Compressed VAR predictors of equation i
σ_i	Compressed VAR residuals variance of equation i
$V_{i,t}$	Disturbance term in state equation of equation i
$\Lambda_{i,t}$	Variance of disturbance term in state equation of equation i
$\underline{\Theta}_i^c$	Prior mean of Θ_i^c
$\underline{V}_i$	Prior variance of Θ_i^c
$\underline{s}_i^{-2}$	Prior mean of variance of residuals
$\underline{v}_i$	Prior variance of variance of residuals
$a_{i,t}^{(r)}$	Posterior mean of $\Theta_{i,t}^c$ of equation i in model r
$R_{i,t}^{(r)}$	Posterior variance of $\Theta_{i,t}^c$ of equation i in model r
$\lambda_{i,t}^{-1}$	Forgetting factor to determine the degree of variation in parameters

for each model and average across the various models in forecasting exercise.

After defining random projection matrix, we are able to estimate compressed parameters in VAR (B^c) using typical natural conjugate prior in Bayesian fashion conditional on $\Phi_{ij}^{(r)}$. The posterior distribution of interested parameters, marginal likelihood, and predictive density of the compressed VAR in equation (2) can be obtained, see [19] for details. Please note that the compressed VAR approach involves multiplying both sides of the equation (1) by Φ, thus we also compress the dependent variables. To finish compressing VAR model, we need to define the estimation of error covariance matrix as well. Koop *et al.* [20] suggest to work with a re-parameterized version of the Bayesian compressed VAR (BCVAR) which allows compression enters into the error covariance matrix by the following a triangular decomposition of Ω as in [21] and [22].

$$A\Omega A' = \Sigma\Sigma \tag{4}$$

where A is a lower triangular matrix with ones on the main diagonal, and Σ is diagonal matrix with $\sigma_i (i = 1, \ldots, n)$ on its diagonal. We rewrite $A = I_n + \widetilde{A}$, where $\widetilde{A}$ is a lower triangular matrix with zeros on its main diagonal [20]. Rearranging the reduced-form VAR in equation (1), then we obtain:

$$\begin{aligned} Y_t &= \Gamma Y_{t-p} + \widetilde{A}(-Y_t) + \Sigma E_t \\ &= \Theta Z_t + \Sigma E_t \end{aligned} \tag{5}$$

where $Z_t = [Y_{t-p}, -Y_t]'$, $\Gamma = AB$, $\Theta = [\Gamma, \widetilde{A}]$, and $E_t \sim N(0, I_n)$. Due to the lower triangular structure of $\widetilde{A}$, each specific VAR equation includes as follow: if $i = 1$, i.e., the first equation in BCVAR, predictor Z_t would contain $(Y_{t-p}, Y_{t-p+1}, \ldots, Y_{t-1})$, if $i = 2$, i.e., the second equation in BCVAR, the predictor matrix contains $(Y'_{t-p}, Y'_{t-p+1}, \ldots, Y'_{t-1}, -Y_{1,t})'$, the third equation includes $(Y'_{t-p}, Y'_{t-p+1}, \ldots, Y'_{t-1}, -Y_{1,t}, -Y_{2,t})'$.[1] In this sense, Koop *et al.* [20] exploited the estimation and proved that VAR estimations can be done equation-by-equation at a time.

Given such above manipulation, we can now rewrite the compressed version VAR as follow:

$$Y_{i,t} = \Theta_i^c(\Phi_i Z_t^i) + \sigma_i E_{i,t}, \tag{6}$$

where $i = 1, \ldots, n$.

Now estimating the compressed parameters can be employed using the MCMC from Bayesian inference.

III. FORECASTING USING BAYESIAN COMPRESSED VECTOR AUTOREGRESSION

For each estimation of posterior draws of Θ_i^c and σ_i, we follow a standard Bayesian method as discussed in [23] for the prior distribution so called "seemingly unrelated regression model" (SUR-Model):

$$\Theta_i^c|\sigma_i^2 \sim N(\underline{\Theta}_i^c, \sigma_i^2 \underline{V}_i) \tag{7}$$

[1] $Y_{i,t}$ denotes the i-th element of the vector Y_t

$$\sigma_i^{-2} \sim G(\underline{s}_i^{-2}, \underline{\nu}_i) \tag{8}$$

The quantities $\underline{\Theta}_i^c$ and $\underline{V}_i$ are unknown parameters. However we set $\underline{\Theta}_i^c = 0$ and $\underline{V}_i = 0.5 \times I$ as suggested by Koop *et al.* [20]. The prior σ_i^{-2} follows Gamma distribution with mean $\underline{s}_i^{-2}$ and degrees of freedom $\underline{\nu}_i$. Once the priors and Bayesian compressed VAR model specifications have been defined, the one-step ahead forecasting density is available in a simple computational effort. Despite that, $h-$step ahead predictive densities for $h > 1$ are not available according to BCVAR specification in equation (6). To compute predictive densities for $h > 1$ according to [20], we convert BCVAR from equation (6) into triangular VAR in equation (5) and now the interested parameters become:

$$\begin{aligned} \Theta = [&(\Theta_1^c \Phi_1^{(r)}, \mathbf{0}_n)', (\Theta_2^c \Phi_2^{(r)}, \mathbf{0}_{n-1})', \\ &\ldots, (\Theta_{n-1}^c \Phi_{n-1}^{(r)}, \mathbf{0}_2)', (\Theta_n^c \Phi_n^{(r)}, 0)']' \end{aligned} \tag{9}$$

where $\Phi_i^{(r)}$ denotes r number of random projection matrices of equation i-th in BCVAR. After this transformation has been performed, typical Bayesian VAR inference can be used to derive $h-$step ahead predictive densities.

Since we apply up to R random projection matrix, i.e., $\Phi_i^{(r)}$, where $r = 1, \ldots, R$. Given R models, predictive density distribution can be obtained using the following specification:

$$\mathbf{p}(Y_{t+h}|D^t) = \sum_{r=1}^{R} \frac{\mathbf{exp}(-0.5\Psi_r)}{\sum_{r=1}^{R} \mathbf{exp}(-0.5\Psi_r)} \mathbf{p}(Y_{t+h}|\Phi^{(r)}, D^t), \tag{10}$$

where D^t is the available information at time t, Ψ_r is $BIC_r - BIC_{min}$. The quantity BIC_r is the Bayesian information criteria of model using $\Phi^{(r)}$ and BIC_{min} is the minimum value of BIC across all $\Phi^{(R)}$ models, calculated from $k_i \times ln(T) + T \times ln(\frac{SSE}{T})$, and k_i denotes number of predictors in i-th equation in equation (6), T is number of data observations and SSE is a sum of square error from equation (6).

Finally we only need to specify the parameter of φ (elements in random projection matrix) and m (the number of predictors after the compression) as from the distribution in equation (3). In this work, we draw φ from the uniform $U[0.1, 0.8]$ and m is simulated from discrete distribution of $U[1, 5ln(k_i)]$.

IV. COMPRESSED VAR WITH TIME-VARYING PARAMETERS

Work in [3] adapted the algorithm that is based on Kalman filter approach to update the parameter to be time-variant. This algorithm is efficient in computational perspective. Found in [21], where all VAR equations are estimated jointly by using MCMC method. Even after compressing VAR model as in equation (6), the dimensions of VAR is still large and the computational burden arises. Therefore it is necessary to perform the compressed TVP-VAR via computational Bayesian perspective [3]. The model involves only updating process via Kalman filter in state-space model which we can rewrite the

Time-varying compressed VAR (TVP-BCVAR) as follows:

$$Y_{i,t} = \Theta^{c}_{i,t}(\Phi_i Z_{i,t}) + \sigma_{i,t}E_{i,t}, \tag{11}$$

and

$$\Theta^{c}_{i,t} = \Theta^{c}_{i,t-1} + V_{i,t} \tag{12}$$

where $V_{i,t} \sim N(0, \Lambda_{i,t})$. Instead of estimating full covariance matrix $\Lambda_{i,t}$ which can be daunting from the computational point of view, we avoid this concern by using forgetting factor. In this sense, the compressed parameters of above equations follow the random walk.

Below, we briefly describe the Kalman recursions of equation i-th at a specific time instant. We also refer the reader to [3] and [24] for further details. Given the information up to time $t-1$, compressed time-varying parameters $\Theta^{c}_{i,t}$ at time t follow $\Theta^{c}_{i,t} \sim N(a^{(r)}_{i,t}, R^{(r)}_{i,t})$, where $a^{(r)}_{i,t}$ and $R^{(r)}_{i,t}$ are mean and variance of compressed coefficients of equation i-th estimated with different random projection matrices $\Phi^{(r)}_{ij}$ at time t. The brief version of Kalman recursion can be written as follow:

$$\begin{aligned} a^{(r)}_{i,t} &= m^{(r)}_{i,t-1} \\ R^{(r)}_{i,t} &= C^{(r)}_{i,t-1} + \Lambda^{(r)}_{t} \end{aligned} \tag{13}$$

We replace $\Lambda^{(r)}_{i,t}$ as $\Lambda^{(r)}_{i,t} = \frac{(1-\lambda_{i,t})}{\lambda_{i,t}} C^{(r)}_{i,t-1}$ using forgetting factors $\lambda_{i,t}$. Re-arranging equation we have:

$$R^{(r)}_{i,t} = \lambda^{-1}_{i,t} C^{(r)}_{i,t-1} \tag{14}$$

The one-step-ahead predictive mean and variance of $Y_{i,t}$ follow a normal distribution with mean $f^{(r)}_{i,t}$ and variance $Q^{(r)}_{i,t}$, where:

$$\begin{aligned} f^{(r)}_{i,t} &= (\Phi^{(r)}_{i} Z^{(r)}_{i,t}) a^{(r)}_{i,t} \\ Q^{(r)}_{i,t} &= Z^{(r)}_{i,t} R^{(r)}_{i,t} Z^{(r)}_{i,t} + \sigma^{(r)}_{i,t}, \end{aligned} \tag{15}$$

here $\sigma^2_{i,t} = \kappa_{i,t}\sigma^2_{i,t-1} + (1-\kappa_{i,t})\widehat{E}^2_{i,t}$. The updated posterior distribution for $\Theta^{c}_{i,t}$ given the information at time t is written as:

$$\begin{aligned} m^{(r)}_{i,t} &= a^{(r)}_{i,t} + A^{(r)}_{i,t} e^{(r)}_{i,t} \\ C^{(r)}_{i,t} &= R^{(r)}_{i,t} - A^{(r)}_{i,t} A^{(r)'}_{i,t} Q^{(r)}_{i,t}, \end{aligned} \tag{16}$$

where $A^{(r)}_{i,t}$ is the adaptive coefficient matrix, i,e., $A^{(r)}_{i,t} = \frac{R^{(r)}_{i,t}(\Phi^{(r)}_{i} Z^{(r)}_{i,t})}{Q^{(r)}_{i,t}}$. Re-arranging from equations (13) through (16), we finally have:

$$\Theta^{c}_{i,t} = \Theta^{c}_{i,t-1} + \sqrt{\frac{(1-\lambda_{i,t}) var(\Theta^{c}_{i,t-1|t-1})}{\lambda_{i,t}}} u_{i,t} \tag{17}$$

In this sense, the compressed parameters matrix $\Theta^{c}_{i,t}$ follows a random walk using forgetting factor approximation to its error scalar, where subscription i and t imply the time-varying coefficients of equation i at time t. In addition, $var(\Theta_{i,t-1|t-1})^{c}$ is a variance from prediction equation of $\Theta^{c}_{i,t-1}$ given information up to time $t-1$, and $u_{i,t} \sim N(0, 1)$.

TABLE 2. BCVAR-Mean square forecasting error (MSFE) $h = 1, \ldots, 7$.

Forex Pairs	$h=1$	$h=2$	$h=3$	$h=4$	$h=5$	$h=6$	$h=7$
AUD-CAD	0.920	0.809	0.815	0.833	0.738	0.721	0.838
AUD-CHF	1.014	0.987	0.971	0.934	0.923	0.923	0.923
AUD-JPY	0.122	0.264	0.387	0.498	0.591	0.649	0.729
AUD-NZD	1.148	1.243	1.221	1.179	1.080	1.060	1.070
BGN-RON	0.529	0.541	0.492	0.511	0.765	0.956	0.970
CAD-CHF	0.521	0.577	0.592	0.546	0.520	0.524	0.554
CAD-JPY	**0.045**	**0.125**	**0.203**	**0.284**	**0.365**	**0.436**	0.514
CHF-BGN	0.738	0.721	0.695	0.645	0.623	0.582	0.534
CHF-JPY	0.952	0.964	0.873	0.862	0.807	0.740	0.748
CHF-RON	0.690	0.693	0.668	0.617	0.624	0.647	0.618
CHF-TRY	0.818	1.122	1.118	0.996	1.059	1.051	1.013
EUR-AUD	1.067	1.012	1.007	0.937	0.919	0.935	0.887
EUR-CAD	0.619	0.552	0.587	0.524	0.497	0.529	0.520
EUR-CHF	0.719	0.678	0.646	0.598	0.577	0.540	**0.505**
EUR-CZK	1.079	1.198	1.117	1.093	1.263	1.508	1.494
EUR-DKK	**0.070**	**0.191**	**0.320**	0.458	0.614	0.766	0.895
EUR-GBP	0.723	0.804	0.786	0.772	0.753	0.669	0.662
EUR-HKD	1.095	1.115	1.148	1.145	1.116	0.893	0.893
EUR-HUF	2.275	2.570	2.521	2.453	2.247	2.208	2.274
EUR-ILS	0.759	0.681	0.641	0.653	0.673	0.631	0.595
EUR-JPY	1.014	0.906	0.881	0.865	0.824	0.735	0.716
EUR-MXN	0.893	1.067	1.002	1.015	1.130	1.144	1.139
EUR-NOK	0.690	0.879	0.897	0.827	0.801	0.807	0.776
EUR-NZD	1.064	1.128	1.103	1.060	1.019	1.047	1.039
EUR-PLN	1.151	1.444	1.386	1.349	1.334	1.459	1.486
EUR-RON	0.703	0.716	0.663	0.641	0.960	1.203	1.231
EUR-RUB	0.410	0.502	0.485	**0.454**	**0.407**	**0.395**	**0.350**
EUR-SEK	1.086	1.466	1.390	1.334	1.400	1.429	1.389
EUR-SGD	1.532	1.448	1.442	1.340	1.303	1.260	1.130
EUR-TRY	**0.012**	**0.046**	**0.088**	**0.123**	**0.156**	**0.189**	**0.209**

Here $\sigma^2_{i,t}$ is considered to have similar properties as Exponentially Weighted Moving Average. $\widehat{E}^2_{i,t}$ is the squared prediction error at time t calculated from the i-th equation of VAR, see [3] for more details. The important parameters that need to be set are $\lambda_{i,t}$ and $\kappa_{i,t}$, where these parameters control the degree of time variation in TVP-BCVAR parameters and also $\sigma^2_{i,t}$. Given the use of the forgetting factor, if we set $\lambda_{i,t}$ and $\kappa_{i,t}$ to 1, the VAR becomes constant parameter with no stochastic volatility. Koop *et al.* [20] developed algorithm that allows these parameter to be varying over time via the following formulae:

$$\lambda_{i,t} = \underline{\lambda} + (1-\underline{\lambda}) \times \mathbf{exp}(-0.5 \times \frac{\widehat{E}^2_{i,t-1}}{\widehat{\sigma}^2_{i,t-1}}), \tag{18}$$

and

$$\kappa_{i,t} = \underline{\kappa} + (1-\underline{\kappa}) \times \mathbf{exp}(-0.5 \times kurt(\widehat{E}_{i,t-30:t-1})), \tag{19}$$

where $\widehat{\sigma}^2_{i,t-1}$ is the variance estimate of time $t-1$ and $kurt(\widehat{E}_{i,t-30:t-1})$ is the excess kurtosis of the VAR prediction error estimated over a month ago (based on our daily data used, we estimated over 30 observations). $\underline{\lambda}$ and $\underline{\kappa}$ are set as the minimum values of optimal forgetting and decay factors. In this work, we follow [20] where $\underline{\lambda}$ and $\underline{\kappa}$ were set as 0.98 and 0.94, respectively.

V. EMPIRICAL WORKS

A. DATA AND CONFIGURATIONS

We use the BCVAR to forecast daily forex up to 30 pairs.[2] All pairs are transformed to be stationary similar to the suggestion from [20]. There forex spans from 7 FEBRUARY

[2]For forex pair details such as transformation code before running this algorithm and source can be seen at VI.

TABLE 3. BCVAR-Mean square forecasting error (MSFE) $h = 8, \ldots, 14$.

Forex Pairs	$h=8$	$h=9$	$h=10$	$h=11$	$h=12$	$h=13$	$h=14$
AUD-CAD	0.850	0.840	0.831	0.792	0.817	0.771	0.843
AUD-CHF	0.925	0.917	0.700	0.709	0.690	0.692	0.698
AUD-JPY	0.819	0.860	0.856	0.844	0.800	0.775	0.796
AUD-NZD	1.074	1.049	1.001	0.989	0.992	0.998	1.001
BGN-RON	0.967	1.011	0.998	0.997	0.997	0.948	0.924
CAD-CHF	0.556	0.561	0.464	0.479	0.475	0.504	0.511
CAD-JPY	0.586	0.635	0.651	0.651	0.641	0.637	0.643
CHF-BGN	0.538	0.502	0.451	0.451	0.463	0.450	0.468
CHF-JPY	0.758	0.759	0.721	0.755	0.922	0.888	0.958
CHF-RON	0.623	0.612	0.548	0.552	0.561	0.541	0.538
CHF-TRY	1.013	1.010	0.996	1.034	1.070	1.095	1.244
EUR-AUD	0.891	0.881	0.710	0.763	0.753	0.742	0.736
EUR-CAD	0.522	0.514	0.475	0.466	0.471	0.451	0.500
EUR-CHF	**0.510**	**0.489**	**0.443**	**0.446**	**0.459**	**0.448**	**0.462**
EUR-CZK	1.484	1.499	1.421	1.417	1.429	1.397	1.403
EUR-DKK	1.019	1.127	1.181	1.215	1.232	1.219	1.171
EUR-GBP	0.639	0.605	0.558	0.554	0.545	0.575	0.556
EUR-HKD	0.910	0.897	0.874	0.883	0.910	0.824	0.851
EUR-HUF	2.440	2.440	2.443	2.454	2.265	2.257	2.257
EUR-ILS	0.595	0.584	0.553	0.603	0.663	0.633	0.642
EUR-JPY	0.735	0.736	0.656	0.669	0.773	0.739	0.835
EUR-MXN	1.148	1.106	1.049	0.978	0.955	0.955	0.936
EUR-NOK	0.752	0.719	0.658	0.672	0.657	0.651	0.648
EUR-NZD	1.042	0.046	1.003	0.976	0.903	0.901	0.899
EUR-PLN	1.453	1.481	1.423	1.446	1.416	1.431	1.437
EUR-RON	1.229	1.268	1.243	1.250	1.256	1.195	1.164
EUR-RUB	**0.334**	**0.304**	**0.269**	**0.251**	**0.263**	**0.278**	**0.271**
EUR-SEK	1.388	1.344	1.202	1.245	1.234	1.205	1.213
EUR-SGD	1.197	1.199	1.139	1.202	1.199	1.087	1.054
EUR-TRY	**0.223**	**0.242**	**0.258**	**0.279**	**0.304**	**0.336**	**0.384**

TABLE 4. TVP-BCVAR-Mean square forecasting error (MSFE) $h = 1, \ldots, 7$.

Forex Pairs	$h=1$	$h=2$	$h=3$	$h=4$	$h=5$	$h=6$	$h=7$
AUD-CAD	0.902	0.810	0.827	0.843	0.746	0.728	0.850
AUD-CHF	0.988	0.969	0.961	0.946	0.935	0.940	0.937
AUD-JPY	0.121	0.276	0.425	0.563	0.685	0.769	0.872
AUD-NZD	1.099	1.232	1.189	1.170	1.075	1.060	1.077
BGN-RON	0.545	0.548	0.490	0.515	0.775	0.968	0.982
CAD-CHF	0.532	0.566	0.585	0.545	0.517	0.527	0.559
CAD-JPY	**0.045**	**0.130**	**0.214**	**0.303**	**0.390**	**0.467**	0.561
CHF-BGN	0.721	0.713	0.698	0.660	0.624	0.583	0.535
CHF-JPY	0.962	0.973	0.866	0.857	0.806	0.741	0.757
CHF-RON	0.672	0.684	0.663	0.619	0.614	0.639	0.613
CHF-TRY	0.824	1.115	1.091	0.960	1.017	1.010	0.993
EUR-AUD	1.056	0.998	0.987	0.928	0.924	0.940	0.891
EUR-CAD	0.626	0.530	0.561	0.499	0.479	0.512	0.516
EUR-CHF	0.697	0.670	0.642	0.608	0.573	0.538	**0.501**
EUR-CZK	1.071	1.218	1.121	1.074	1.228	1.480	1.485
EUR-DKK	**0.067**	**0.181**	**0.304**	**0.436**	0.589	0.739	0.870
EUR-GBP	0.747	0.829	0.797	0.781	0.759	0.690	0.677
EUR-HKD	1.126	1.149	1.169	1.153	1.111	0.850	0.861
EUR-HUF	2.310	2.563	2.482	2.398	2.214	2.178	2.264
EUR-ILS	0.812	0.739	0.691	0.723	0.696	0.622	0.599
EUR-JPY	0.989	0.885	0.873	0.862	0.821	0.740	0.722
EUR-MXN	0.918	1.042	0.977	0.994	1.126	1.136	1.138
EUR-NOK	0.701	0.881	0.897	0.815	0.791	0.812	0.788
EUR-NZD	1.000	1.083	1.070	1.038	1.035	1.063	1.039
EUR-PLN	1.126	1.442	1.386	1.348	1.351	1.473	1.488
EUR-RON	0.725	0.739	0.671	0.649	0.974	1.221	1.254
EUR-RUB	0.421	0.510	0.492	0.457	**0.425**	**0.420**	**0.370**
EUR-SEK	1.050	1.447	1.367	1.274	1.360	1.414	1.390
EUR-SGD	1.532	1.428	1.426	1.318	1.289	1.240	1.121
EUR-TRY	**0.009**	**0.034**	**0.065**	**0.092**	**0.115**	**0.133**	**0.141**

2018 through 2 AUGUST 2018. 70 % of all data observations are trained and the rest 30 % of the data are used for predictive performance evaluation of each model. We also include the alternative models which are treated to be one of the best model to handle large size VAR such as Dynamic Factor Model (DFM), Minnesota Prior Bayesian VAR (BVAR-Minn), and Bayesian AR (B-AR).

Four lagged dependent variable is selected, i.e., $p = 4$. Forecasting horizon is 14 day-ahead. We measure predicting performance using Mean square forecasting error (MSFE)

TABLE 5. TVP-BCVAR-Mean square forecasting error (MSFE) $h = 8, \ldots, 14$.

Forex Pairs	$h=8$	$h=9$	$h=10$	$h=11$	$h=12$	$h=13$	$h=14$
AUD-CAD	0.858	0.850	0.835	0.804	0.826	0.787	0.868
AUD-CHF	0.937	0.925	0.701	0.708	0.687	0.692	0.698
AUD-JPY	0.986	1.050	1.062	1.067	1.031	1.002	1.032
AUD-NZD	1.073	1.060	1.014	0.997	1.002	1.020	1.024
BGN-RON	0.979	1.028	1.015	1.019	1.016	0.964	0.940
CAD-CHF	0.560	0.564	0.470	0.482	0.477	0.516	0.528
CAD-JPY	0.648	0.717	0.753	0.768	0.765	0.760	0.764
CHF-BGN	0.543	0.494	0.442	0.444	0.459	0.446	0.467
CHF-JPY	0.765	0.769	0.736	0.767	0.928	0.887	0.957
CHF-RON	0.620	0.601	0.539	0.548	0.564	0.545	0.545
CHF-TRY	0.998	0.999	0.987	1.027	1.054	1.068	1.232
EUR-AUD	0.891	0.889	0.707	0.761	0.755	0.748	0.740
EUR-CAD	0.520	0.513	0.479	0.469	0.471	0.457	0.507
EUR-CHF	**0.512**	**0.477**	**0.430**	**0.436**	**0.455**	**0.443**	**0.457**
EUR-CZK	1.481	1.492	1.421	1.421	1.442	1.417	1.431
EUR-DKK	0.998	1.111	1.185	1.245	1.274	1.258	1.215
EUR-GBP	0.652	0.614	0.562	0.559	0.553	0.585	0.565
EUR-HKD	0.910	0.915	0.904	0.882	0.889	0.809	0.868
EUR-HUF	2.440	2.438	2.434	2.430	2.227	2.234	2.251
EUR-ILS	0.601	0.595	0.579	0.581	0.607	0.573	0.593
EUR-JPY	0.743	0.740	0.662	0.670	0.770	0.735	0.834
EUR-MXN	1.134	1.105	1.049	0.970	0.940	0.932	0.906
EUR-NOK	0.761	0.746	0.685	0.703	0.688	0.674	0.663
EUR-NZD	1.038	1.046	1.001	0.977	0.912	0.926	0.932
EUR-PLN	1.455	1.480	1.427	1.441	1.407	1.427	1.463
EUR-RON	1.256	1.295	1.264	1.281	1.287	1.220	1.186
EUR-RUB	**0.355**	**0.322**	**0.276**	**0.256**	**0.270**	**0.285**	**0.272**
EUR-SEK	1.404	1a.363	1.214	1.264	1.258	1.214	1.217
EUR-SGD	1.201	1.208	1.162	1.205	1.188	1.089	1.067
EUR-TRY	**0.145**	**0.153**	**0.163**	**0.177**	**0.190**	**0.204**	**0.220**

TABLE 6. Out-of-sample predictive performance of AUD-xxx forex pairs relative to Bayesian-AR.

Forex Pairs	Model	$h=1$	$h=2$	$h=3$	$h=4$	$h=5$	$h=6$	$h=7$	$h=8$	$h=9$	$h=10$	$h=11$	$h=12$	$h=13$	$h=14$
AUD-CAD	BCVAR	0.895	0.921	0.935	0.986	0.984	0.966	0.967	0.965	0.969	0.984	0.998	1.002	1.003	1.019
	TVP-BCVAR	0.879	0.922	0.949	0.998	0.996	0.975	0.981	0.974	0.982	0.990	1.013	1.013	1.024	1.050
	BVAR-MINN	1.065	0.993	0.958	1.051	1.027	1.001	0.975	0.928	0.938	0.954	0.986	0.979	0.971	0.994
	BDFM	1.050	1.073	1.051	1.053	1.027	0.954	0.986	0.996	0.976	0.995	1.008	0.996	1.015	1.044
AUD-CHF	BCVAR	0.987	0.973	0.967	0.927	0.957	0.961	0.961	0.959	0.988	0.991	0.982	0.994	1.002	0.991
	TVP-BCVAR	0.961	0.954	0.958	0.938	0.969	0.979	0.976	0.971	0.997	0.993	0.981	0.990	1.002	0.991
	BVAR-MINN	0.987	0.912	0.914	0.810	0.915	0.954	0.955	0.957	1.006	1.018	0.987	1.010	1.034	0.983
	BDFM	1.000	0.943	1.001	0.981	0.991	1.016	0.997	0.975	1.009	1.023	0.992	1.009	1.010	0.998
AUD-JPY	BCVAR	0.993	1.020	1.055	1.091	1.072	1.056	1.050	1.046	1.055	1.074	1.080	1.074	1.085	1.111
	TVP-BCVAR	0.985	1.065	1.158	1.234	1.244	1.252	1.256	1.258	1.289	1.333	1.367	1.384	1.404	1.442
	BVAR-MINN	1.223	1.305	1.267	1.154	1.072	1.028	0.986	0.919	0.904	0.876	0.859	0.840	0.864	0.910
	BDFM	3.707	1.950	1.371	1.152	1.021	0.945	0.912	0.860	0.838	0.844	0.852	0.818	0.839	0.877
AUD-NZD	BCVAR	1.035	1.008	1.003	1.007	1.029	1.024	1.036	1.027	1.014	1.005	1.009	1.007	1.010	1.017
	TVP-BCVAR	0.991	0.999	0.977	0.999	1.025	1.025	1.043	1.026	1.025	1.018	1.017	1.017	1.032	1.040
	BVAR-MINN	1.230	1.124	1.052	1.046	1.101	1.088	1.103	1.067	1.062	1.040	1.040	1.036	1.059	1.084
	BDFM	0.992	1.012	1.002	0.991	0.981	0.978	0.992	0.980	0.975	0.959	0.984	0.993	0.999	1.012

and Mean absolute forecasting error (MAFE) relative to AR using Bayesian inference. MSFE and MAFE which are below one suggesting that the proposed model is able to beat B-AR benchmark.

The mean square forecasting error of 30 pairs of forex using Bayesian compressed VAR (BCVAR) and Time-varying Bayesian compressed VAR (TVP-BCVAR) are shown in Tables 2-3 and Tables 4-5, respectively. For each table, three lowest Mean Square Forecasting Error are presented by boldface. From the results, BCVAR gives the best forecast for EUR-TRY pair in every forecasting exercise i.e. ($h = 1, 2, \ldots, 14$) (one-day-ahead through fourteen-day-ahead prediction). Other forex pairs that are worth to mention include CAD-JPY, EUR-DKK and EUR-RUB.

It can be observed that the forecasting errors between different foreign exchange pairs are very different when referring to the result, some forex pair such as EUR-HUF has extremely high MSFE relative to others. The possible reason behind this is that the information that we use as the predictors in each equations are four lagged dependent variables and random compressed of other forex pairs. Therefore higher MSFE means that those predictive information is not relevant to changes in EUR-HUF forex pair. It is obvious that BCVAR

TABLE 7. Out-of-sample predictive performance of CHF-xxx forex pairs relative to Bayesian-AR.

Forex Pairs	Model	$h=1$	$h=2$	$h=3$	$h=4$	$h=5$	$h=6$	$h=7$	$h=8$	$h=9$	$h=10$	$h=11$	$h=12$	$h=13$	$h=14$
BGN-RON	BCVAR	1.265	1.244	0.982	1.001	0.997	1.011	1.009	1.008	1.006	1.000	1.006	1.004	0.997	0.996
	TVP-BCVAR	1.303	1.260	0.979	1.009	1.009	1.023	1.022	1.020	1.022	1.018	1.028	1.024	1.013	1.013
	BVAR-MINN	1.453	1.360	1.069	1.161	1.104	1.071	1.064	1.068	1.092	1.094	1.082	1.061	1.045	1.058
	BDFM	1.404	1.321	0.892	0.911	0.962	0.972	0.955	0.961	0.960	0.954	0.959	0.965	0.959	0.957
CAD-CHF	BCVAR	1.138	0.987	1.021	0.942	0.927	0.925	0.920	0.915	0.944	0.960	0.980	1.000	1.017	1.015
	TVP-BCVAR	1.164	0.968	1.008	0.940	0.923	0.930	0.928	0.923	0.948	0.971	0.986	1.005	1.041	1.049
	BVAR-MINN	1.418	1.154	1.188	0.989	0.899	0.962	0.956	0.929	0.970	1.027	1.036	1.043	1.083	1.063
	BDFM	1.074	0.990	1.123	1.003	0.986	1.008	0.940	0.903	0.963	0.998	0.969	0.997	1.032	1.042
CAD-JPY	BCVAR	1.237	1.156	1.130	1.142	1.140	1.143	1.142	1.132	1.124	1.102	1.071	1.025	0.983	0.949
	TVP-BCVAR	1.253	1.199	1.192	1.215	1.221	1.227	1.246	1.252	1.268	1.274	1.264	1.223	1.173	1.127
	BVAR-MINN	1.531	1.432	1.281	1.189	1.123	1.079	1.049	0.993	0.939	0.839	0.750	0.662	0.610	0.564
	BDFM	6.086	2.770	2.056	1.870	1.737	1.624	1.520	1.389	1.272	1.184	1.116	1.036	0.970	0.901
CHF-BGN	BCVAR	1.054	1.095	1.074	1.015	0.993	1.022	0.987	0.948	0.958	0.983	0.991	1.038	1.021	0.952
	TVP-BCVAR	1.031	1.083	1.078	1.039	0.0993	1.025	0.988	0.956	0.944	0.963	0.975	1.030	1.011	0.950
	BVAR-MINN	1.817	1.881	1.655	1.423	1.330	1.393	1.322	1.263	1.250	1.284	1.292	1.354	1.343	1.267
	BDFM	1.124	1.183	1.197	1.080	1.071	1.119	1.115	1.106	1.136	1.234	1.236	1.258	1.178	1.169
CHF-JPY	BCVAR	1.039	1.048	1.006	0.954	0.954	0.967	0.967	0.973	0.973	0.976	0.976	0.962	0.963	0.972
	TVP-BCVAR	1.050	1.057	0.997	0.948	0.953	0.969	0.979	0.981	0.987	0.996	0.992	0.968	0.962	0.970
	BVAR-MINN	1.198	1.107	1.026	0.963	0.950	0.984	0.971	0.969	1.002	0.984	0.997	0.960	0.953	0.966
	BDFM	1.242	1.257	1.162	1.048	0.982	0.934	0.945	0.947	0.969	0.956	0.950	0.933	0.907	0.946
CHF-RON	BCVAR	1.064	1.105	1.084	1.052	1.046	1.102	1.068	1.037	1.063	1.095	1.099	1.137	1.129	1.044
	TVP-BCVAR	1.037	1.092	1.076	1.057	1.029	1.088	1.060	1.033	1.043	1.078	1.090	1.144	1.139	1.058
	BVAR-MINN	1.892	1.882	1.687	1.576	1.486	1.539	1.460	1.402	1.421	1.475	1.466	1.521	1.542	1.425
	BDFM	1.129	1.152	1.138	1.077	1.101	1.185	1.156	1.142	1.168	1.223	1.216	1.256	1.208	1.185
CHF-TRY	BCVAR	1.098	1.061	1.056	1.031	1.029	1.029	1.005	1.002	0.995	0.991	0.996	1.001	1.019	1.016
	TVP-BCVAR	1.106	1.055	1.031	0.994	0.987	0.988	0.985	0.988	0.984	0.982	0.988	0.985	0.993	1.007
	BVAR-MINN	1.398	1.232	1.211	1.144	1.117	1.096	1.064	1.075	1.018	0.980	0.963	0.946	0.949	0.983
	BDFM	1.378	1.131	1.134	1.164	1.155	1.178	1.125	1.07	1.068	1.065	1.038	1.003	0.987	0.996

TABLE 8. Out-of-sample predictive performance of EUR-xxx forex pairs relative to Bayesian-AR.

Forex Pairs	Model	$h=1$	$h=2$	$h=3$	$h=4$	$h=5$	$h=6$	$h=7$	$h=8$	$h=9$	$h=10$	$h=11$	$h=12$	$h=13$	$h=14$
EUR-AUD	BCVAR	1.057	1.092	1.118	1.061	1.039	1.030	1.027	1.025	1.021	0.991	1.033	1.031	1.014	1.015
	TVP-BCVAR	1.046	1.078	1.095	1.050	1.045	1.036	1.031	1.025	1.030	0.988	1.030	1.033	1.021	1.020
	BVAR-MINN	1.250	1.189	1.162	1.050	1.077	1.083	1.078	1.110	1.129	1.069	1.077	1.078	1.053	1.058
	BDFM	1.155	1.181	1.220	1.249	1.218	1.167	1.155	1.142	1.111	1.075	1.091	1.107	1.072	1.047
EUR-CAD	BCVAR	1.122	1.121	1.199	1.091	1.102	1.089	1.036	0.984	0.976	0.962	0.964	0.979	0.934	0.932
	TVP-BCVAR	1.134	1.076	1.144	1.040	1.063	1.054	1.028	0.981	0.974	0.970	0.969	0.980	0.947	0.945
	BVAR-MINN	1.710	1.825	1.699	1.381	1.328	1.323	1.228	1.117	1.072	1.046	1.030	1.036	0.984	0.991
	BDFM	1.229	1.292	1.365	1.283	1.272	1.235	1.067	0.994	0.990	1.011	0.992	0.999	0.970	0.980
EUR-CHF	BCVAR	1.032	1.079	1.065	1.000	0.992	1.019	0.984	0.944	0.953	0.974	0.987	1.036	1.020	0.949
	TVP-BCVAR	1.001	1.066	1.059	1.017	0.986	1.015	0.976	0.948	0.930	0.946	0.964	1.026	1.010	0.939
	BVAR-MINN	1.756	1.823	1.641	1.398	1.355	1.413	1.329	1.268	1.239	1.266	1.278	1.342	1.331	1.255
	BDFM	1.107	1.167	1.188	1.069	1.066	1.109	1.111	1.104	1.127	1.217	1.220	1.243	1.164	1.159
EUR-CZK	BCVAR	1.033	1.043	1.025	1.033	1.009	1.035	1.032	1.032	1.045	1.053	1.044	1.041	1.040	1.030
	TVP-BCVAR	1.025	1.062	1.028	1.015	0.980	1.015	1.025	1.030	1.040	1.053	1.048	1.051	1.054	1.051
	BVAR-MINN	1.193	1.114	1.043	1.045	1.041	1.104	1.091	1.108	1.100	1.0966	1.089	1.099	1.120	1.108
	BDFM	1.005	1.037	1.030	0.999	1.036	1.065	1.043	1.040	1.045	1.043	1.021	1.011	1.032	1.027
EUR-DKK	BCVAR	1.012	0.813	0.760	0.720	0.699	0.673	0.662	0.668	0.678	0.688	0.699	0.705	0.705	0.702
	TVP-BCVAR	0.961	0.771	0.722	0.685	0.670	0.650	0.643	0.654	0.669	0.690	0.716	0.729	0.728	0.728
	BVAR-MINN	1.315	1.282	1.329	1.291	1.221	1.179	1.150	1.120	1.091	1.064	1.043	1.023	1.004	0.979
	BDFM	5.540	2.151	1.423	1.113	0.970	0.881	0.816	0.778	0.773	0.769	0.768	0.766	0.757	0.730
EUR-GBP	BCVAR	0.993	1.087	1.070	1.061	1.115	1.092	1.079	1.037	1.012	0.998	0.991	0.990	1.005	1.007
	TVP-BCVAR	1.027	1.120	1.086	1.073	1.124	1.125	1.104	1.059	1.028	1.006	0.999	1.004	1.022	1.022
	BVAR-MINN	1.343	1.440	1.184	1.191	1.256	1.259	1.166	1.041	1.005	0.998	0.997	0.978	0.998	0.998
	BDFM	1.149	1.079	1.072	1.108	1.043	1.039	1.025	1.012	1.004	1.003	1.011	0.999	1.051	1.037
EUR-HKD	BCVAR	1.047	1.030	1.034	1.019	1.030	1.109	1.123	1.097	1.081	1.056	1.043	1.056	1.049	1.017
	TVP-BCVAR	1.077	1.061	1.053	1.026	1.026	1.056	1.083	1.097	1.103	1.093	1.041	1.031	1.031	1.038
	BVAR-MINN	1.435	1.387	1.223	1.155	1.166	1.252	1.224	1.209	1.147	1.044	1.020	1.046	1.070	1.096
	BDFM	1.209	1.195	1.126	1.068	1.058	1.036	1.039	1.082	1.074	1.065	1.045	1.048	1.032	1.028
EUR-HUF	BCVAR	1.121	1.088	1.087	1.052	1.050	1.024	1.005	1.006	1.008	1.010	1.007	1.024	1.026	1.027
	TVP-BCVAR	1.138	1.085	1.070	1.028	1.035	1.010	1.000	1.006	1.007	1.006	0.997	1.007	1.015	1.024
	BVAR-MINN	1.254	1.158	1.096	1.039	1.043	1.026	1.018	1.046	1.057	1.067	1.067	1.106	1.114	1.120
	BDFM	1.104	1.079	1.058	1.051	1.091	1.066	1.027	1.032	1.037	1.031	1.019	1.046	1.052	1.055
EUR-ILS	BCVAR	1.048	0.965	0.934	0.970	1.015	1.077	1.051	1.048	1.039	0.999	1.031	1.069	1.070	1.059
	TVP-BCVAR	1.121	1.047	1.008	1.073	1.049	1.062	1.058	1.060	1.059	1.046	0.993	0.980	0.968	0.978
	BVAR-MINN	1.178	1.092	1.023	1.054	1.085	1.141	1.078	1.032	1.022	0.946	0.902	0.936	0.951	0.988
	BDFM	1.075	1.059	1.074	1.109	1.148	1.164	1.107	1.165	1.142	1.112	1.093	1.085	1.072	1.041
EUR-JPY	BCVAR	1.025	0.970	0.961	0.921	0.958	0.982	0.959	0.958	0.966	0.973	0.981	1.000	0.994	0.978
	TVP-BCVAR	1.001	0.947	0.952	0.917	0.941	0.989	0.966	0.968	0.972	0.981	0.983	0.996	0.988	0.976
	BVAR-MINN	1.433	1.230	1.033	0.899	0.943	1.000	0.951	0.948	0.962	0.920	0.944	0.961	0.945	0.956
	BDFM	1.186	1.060	0.991	0.923	0.917	0.877	0.875	0.939	0.953	0.938	0.953	0.986	0.962	0.981
EUR-MXN	BCVAR	0.834	0.822	0.817	0.848	0.903	0.951	0.955	0.927	0.887	0.959	0.851	0.843	0.857	0.871
	TVP-BCVAR	0.857	0.803	0.797	0.829	0.899	0.944	0.954	0.916	0.886	0.859	0.844	0.829	0.836	0.844
	BVAR-MINN	0.872	0.820	0.956	1.026	0.958	0.985	0.997	0.988	0.992	0.955	0.942	0.916	0.921	0.937
	BDFM	0.955	0.950	0.969	0.982	0.960	0.955	0.899	0.884	0.904	0.900	0.905	0.886	0.879	0.900
EUR-NOK	BCVAR	1.038	1.018	1.165	1.102	1.065	1.038	1.034	0.996	0.967	0.954	0.971	1.003	0.995	0.988
	TVP-BCVAR	1.055	1.020	1.165	1.086	1.052	1.044	1.049	1.022	1.003	0.993	1.015	1.050	1.029	1.011
	BVAR-MINN	1.055	0.995	1.220	1.054	1.021	0.979	0.979	0.960	0.933	0.949	1.013	1.051	1.054	1.031
	BDFM	1.114	1.021	1.024	1.041	1.029	0.983	1.004	1.005	0.995	0.997	1.012	0.995	0.976	0.974
EUR-NZD	BCVAR	1.215	1.129	1.107	1.067	1.003	1.063	1.067	1.081	1.082	1.069	1.068	1.064	1.054	1.048
	TVP-BCVAR	1.143	1.084	1.075	1.045	1.018	1.079	1.066	1.076	1.082	1.066	1.070	1.075	1.083	1.087
	BVAR-MINN	1.602	1.437	1.404	1.295	1.252	1.317	1.319	1.302	1.250	1.204	1.189	1.188	1.170	1.144
	BDFM	1.221	1.201	1.159	1.132	1.088	1.138	1.151	1.132	1.130	1.125	1.097	1.082	1.068	1.059
EUR-PLN	BCVAR	1.016	1.025	0.995	0.985	0.987	1.028	1.020	0.998	1.022	1.049	1.057	1.053	1.054	1.057
	TVP-BCVAR	0.994	1.024	0.995	0.984	0.999	1.037	1.021	0.999	1.021	1.052	1.054	1.047	1.051	1.076
	BVAR-MINN	1.111	1.058	1.099	1.054	1.042	1.098	1.092	1.095	1.085	1.093	1.095	1.092	1.098	1.086
	BDFM	1.019	0.994	0.958	0.942	1.020	1.067	1.039	1.015	1.031	1.054	1.041	1.028	1.048	1.065
EUR-RON	BCVAR	1.136	1.141	0.978	0.998	0.989	1.010	1.011	1.011	1.004	0.995	1.004	1.006	0.999	0.997
	TVP-BCVAR	1.172	1.177	0.991	1.010	1.003	1.026	1.030	1.033	1.026	1.013	1.029	1.031	1.020	1.016
	BVAR-MINN	1.134	1.236	1.046	1.173	1.088	1.074	1.082	1.082	1.103	1.102	1.097	1.081	1.065	1.075
	BDFM	1.237	1.163	0.891	0.910	0.960	0.987	0.971	0.975	0.974	0.967	0.974	0.982	0.978	0.976
EUR-RUB	BCVAR	1.268	1.316	1.234	1.219	1.267	1.289	1.214	1.096	1.008	0.950	0.916	0.958	0.999	0.969
	TVP-BCVAR	1.303	1.337	1.252	1.226	1.321	1.368	1.283	1.165	1.066	0.976	0.934	0.982	1.024	0.972
	BVAR-MINN	1.848	1.665	1.247	1.103	1.137	1.185	1.122	1.015	0.983	0.919	0.940	1.016	1.011	1.021
	BDFM	1.699	1.376	1.191	1.236	1.237	1.181	1.124	1.066	0.960	0.876	0.908	0.933	0.929	0.963
EUR-SEK	BCVAR	1.065	1.008	1.067	1.046	1.067	1.066	1.037	1.032	1.019	1.014	1.018	1.014	0.991	0.994
	TVP-BCVAR	1.030	0.995	1.050	0.999	1.036	1.055	1.038	1.044	1.033	1.025	1.034	1.033	0.998	0.997
	BVAR-MINN	1.058	1.086	1.206	1.122	1.151	1.132	1.089	1.070	1.044	1.038	1.054	1.049	1.020	1.009
	BDFM	1.295	1.082	1.096	1.098	1.068	1.033	1.033	1.050	1.035	1.029	1.024	0.974	0.936	0.953
EUR-SGD	BCVAR	1.163	1.129	1.112	1.058	1.038	1.047	1.066	1.049	1.049	1.032	1.036	1.040	1.024	1.008
	TVP-BCVAR	1.163	1.114	1.099	1.041	1.027	1.031	1.058	1.052	1.056	1.053	1.039	1.030	1.025	1.020
	BVAR-MINN	1.508	1.415	1.233	1.125	1.107	1.100	1.069	1.081	1.035	0.988	1.000	1.013	1.022	1.052
	BDFM	1.181	1.153	1.061	1.083	1.061	1.026	1.046	1.046	1.043	1.045	1.042	1.025	1.016	1.029
EUR-TRY	BCVAR	1.376	1.368	1.338	1.334	1.367	1.405	1.411	1.405	1.407	1.400	1.396	1.401	1.438	1.520
	TVP-BCVAR	1.017	1.006	0.997	1.002	1.006	0.992	0.954	0.914	0.893	0.881	0.882	0.875	0.872	0.872
	BVAR-MINN	1.414	1.353	1.299	1.279	1.293	1.295	1.253	1.202	1.170	1.1128	1.066	0.985	0.933	0.901
	BDFM	16.312	6.612	4.448	3.768	3.591	3.590	3.664	3.752	3.833	3.920	3.919	3.882	3.873	3.967

and TVP-BCVAR models predict poorly on EUR-HUF in all forecasting exercises.

The results from TVP-BCVAR model are similar to the results from the BCVAR model, where the TVP-BCVAR model predicts the best mostly on EUR-TRY pairs as seen in Table 5. Moreover, EUR-CHF, EUR-RUB and CAD-JPY are honorable mentions in these forex pair lists. It is thus reasonable to conclude that the advanced time series model such as BCVAR and TVP-BCVAR are capable of tracking the movement of those mentioned forex pairs with the lowest MSFE especially when allowing time-variation in TVP-BCVAR model, the MSFE is substantially reduced for every prediction exercises, i.e., $h = 1, 2, \ldots, 14$ as shown in Tables 4-5.

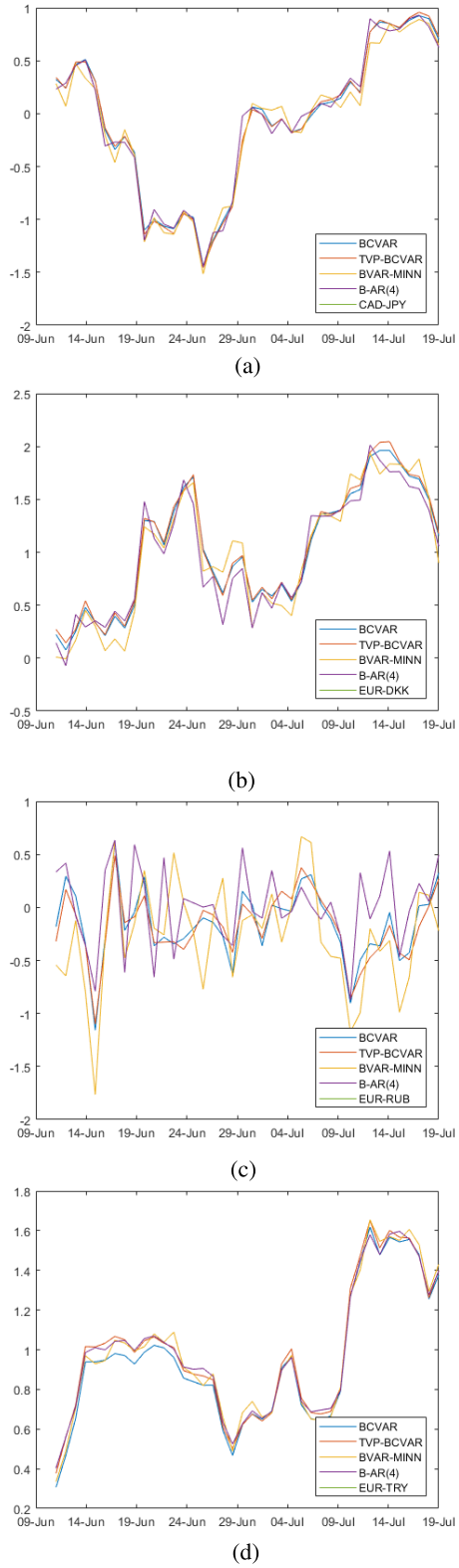

FIGURE 1. Forecasted value and actual value at $h = 1$. (a) CAD-JPY. (b) EUR-DKK. (c) EUR-RUB. (d) EUR-TRY.

In addition, we summarize the MSFE relative to Bayesian AR with four lags B-AR(4) model. The details are presented in Tables 6-8. These tables report the ratio between the MSFE of model i and the MSFE of the benchmark B-AR(1),

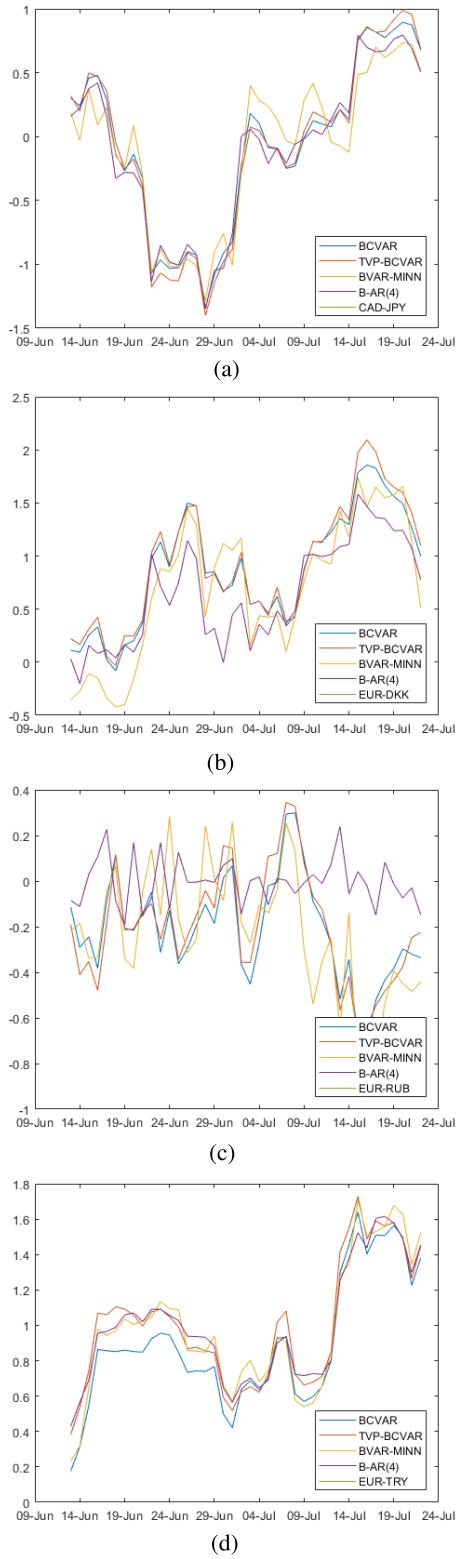

FIGURE 2. Forecasted Value and actual value at $h = 3$. (a) CAD-JPY. (b) EUR-DKK. (c) EUR-RUB. (d) EUR-TRY.

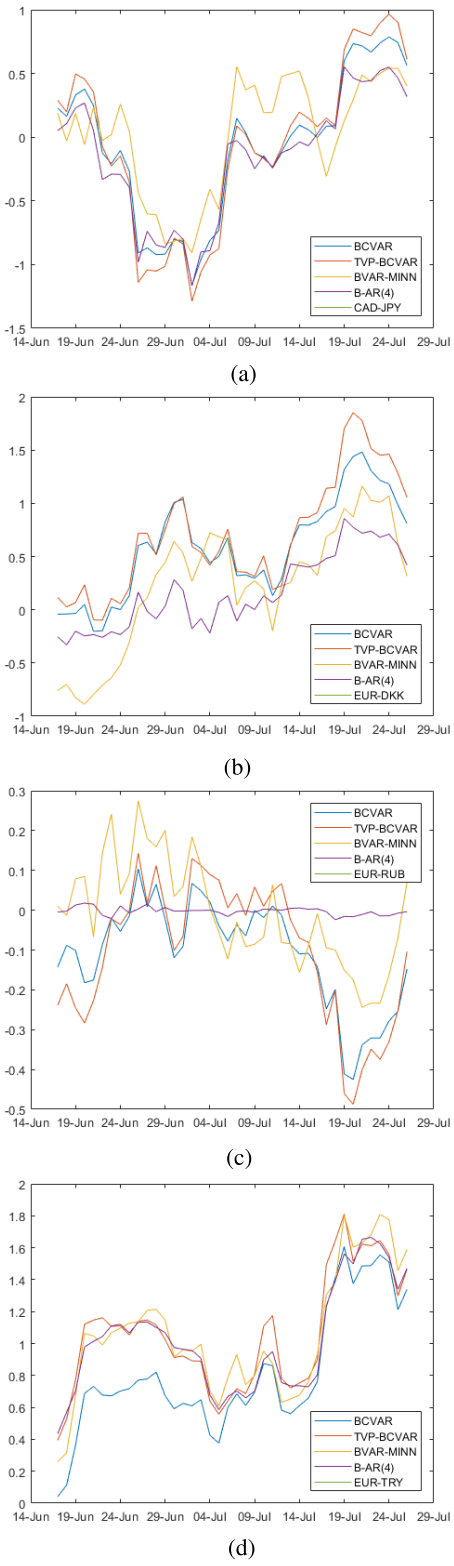

FIGURE 3. Forecasted value and actual Value at $h = 7$. (a) CAD-JPY. (b) EUR-DKK. (c) EUR-RUB. (d) EUR-TRY.

computed as

$$MSFE_{i,j,h} = \sum_{\tau=\underline{t}}^{\bar{t}-h} e^2_{i,j,\tau+h} / \sum_{\tau=\underline{t}}^{\bar{t}-h} e^2_{bcmk,j,\tau+h}, \tag{20}$$

where $e^2_{i,j,\tau+h}$ and $e^2_{bcmk,j\tau+h}$ are the squared forecasting errors of variable j at time τ and forecast horizon h modeled by model i and the Benchmark model Bayesian-AR(1) model,

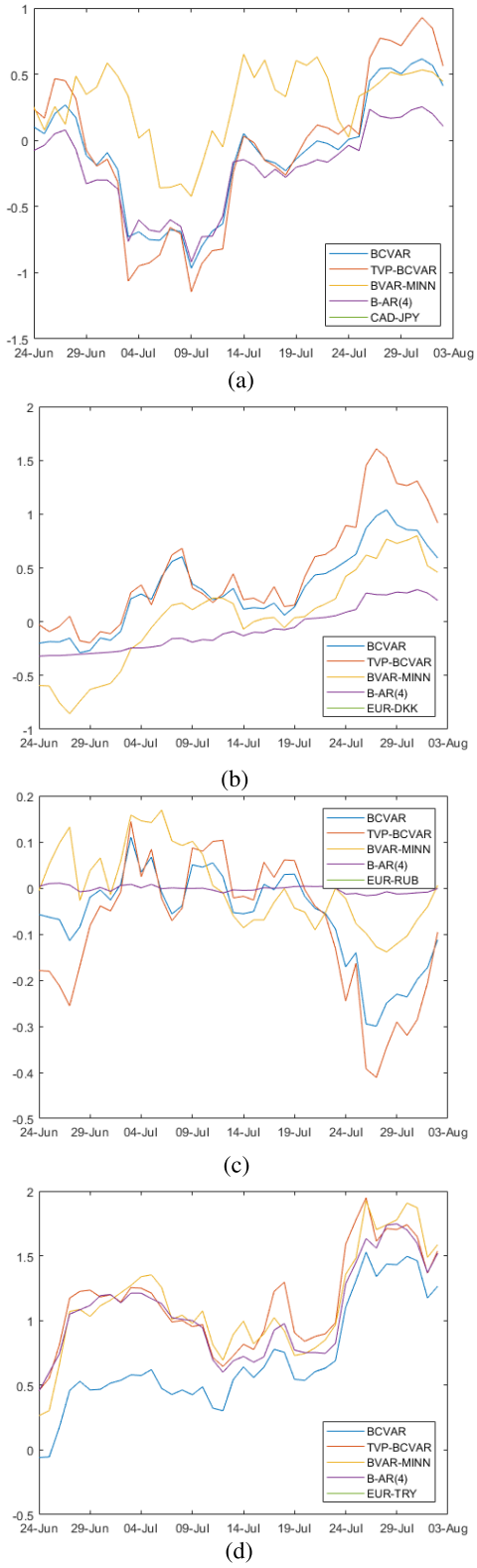

FIGURE 4. Forecasted value and actual value at $h = 14$. (a) CAD-JPY. (b) EUR-DKK. (c) EUR-RUB. (d) EUR-TRY.

respectively.[3] Variables $\underline{t}$ and $\bar{t}$ denote the start and end of the out of sample forecasting periods.

[3]$(i \in BCVAR, TVP-BCVAR, BVAR-MINN, BDFM)$

According to Tables 7 and 8, we found that the BCVAR and TVP-BCVAR are not fully suitable to forecast all the forex pairs. In other words, these methods are based closely on the information of the predictors. Therefore, it is possibly because of the predictors included in our model are not completely informative in prediction the movement of forex pairs. Nevetheless, we found the huge advantage in predictive performance on EUR-MXN, EUR-DKK and EUR-TRY of model BCVAR and TVP-BCVAR relative to traditional model B-AR. Another empirical result that is worth to mention is that predictive performance is gained substantially when using TVP-BCVAR relative to BCVAR to forecast EUR-TRY. This implies that by allowing the time variation in the model, it can help to achieve better forecasting this forex pair, see Table 8. Moreover, for forecasting EUR-DKK exercise, after three-period-ahead prediction ($h = 3$), the MSE of BCVFAR and TVP-BCVAR relative to B-AR is tremendously reduced. This means that the EUR-DKK pair is extremely correlated to the selected predictors. In other words, other forex pairs rather than EUR-DKK are informative enough to forecast EUR-DKK pair. This was proved by the BDFM model result in Table 8 showing that after the 4-days-ahead forecast, the MSFE is decreased dramatically.

We present more results on how BCVAR, TVP-BCVAR and other models can forecast the selected forex pairs, we illustrate the accuracy more obviously by showing the actual value vs. the forecasted values from multiple models in Figs. 1-4. The predicting exercises are $h = 1, 3, 7$ and 14. Forex pairs which are presented in those figures are CAD-JPY, EUR-DKK, EUR-RUB and EUR-TRY. We selected these pairs based on the lowest MSFE. According to the results, it can be concluded that BCVAR, TVP-BCVAR and other models provide the best forecasting when the horizon of 1. The longer out-of-sample forecast, the higher of mean square forecasting error. The benchmark model, i.e., Bayesian AR(4) cannot track the actual movement of EUR-RUB by using the lag predictors. In other words, by implementing the forex pair predictors, BCVAR and TVP-BCVAR, the accuracy is gained considerably.

VI. CONCLUSIONS

We propose multiple the advanced time series models[4] to forecasting forex up to 30 pairs. All forex data range between 7 FEBRUARY 2018 and 2 AUGUST 2018. Each forex was transformed to be stationary based on Augmented-Dickey Fuller test (ADF-test), see Table 9 for more details on transformation code. We found that Bayesian compressed VAR (BCVAR) and time-varying Bayesian compressed VAR (TVP-BCVAR) were able to deliver the best forecasting on the forex CAD-JPY, EUR-DKK, EUR-RUB and EUR-TRY by means of Mean Square Forecasting Error (MSFE). We found the huge advantage on using BCVAR and

[4]Bayesian compressed VAR (BCVAR), time-varying Bayesian compressed VAR (TVP-BCVAR), Minnesota prior Bayesian VAR (BVAR-Minn), Bayesian dynamic factor model (BDFM), Bayesian Autoregression (B-AR)

TABLE 9. Stationary forex tranformation.

Forex Pairs	Transformation Code	Sources
AUD-CAD	2	Yahoo Finance
AUD-CHF	2	
AUD-JPY	1	
AUD-NZD	2	
BGN-RON	2	
CAD-CHF	2	
CAD-JPY	1	
CHF-BGN	2	
CHF-JPY	2	
CHF-RON	2	
CHF-TRY	2	
EUR-AUD	2	
EUR-CAD	2	
EUR-CHF	2	
EUR-CZK	2	
EUR-DKK	1	
EUR-GBP	2	
EUR-HKD	2	
EUR-HUF	2	
EUR-ILS	2	
EUR-JPY	2	
EUR-MXN	2	
EUR-NOK	2	
EUR-NZD	2	
EUR-PLN	2	
EUR-RON	2	
EUR-RUB	2	
EUR-SEK	2	
EUR-SGD	2	
EUR-TRY	1	

Transformation code = 1 is level data, 2 is first differentiate.

TVP-BCVAR relative to typical Bayesian AR(4) to predict EUR-DKK for all forecasting exercises $h = 1, 2, \ldots, 14$ (one-day through fourteen-day-ahead forecast).

According to the lowest MSFE in all tables represented above, for those who are interested in applying Bayesian compressed VAR model to predict forex pairs, EUR-TRY, EUR-DKK and CAD-JPY are best forex pairs when forecasting one-day-ahead until five-day-ahead and EUR-TRY, EUR-RUB and EUR-CHF when forecasting eight-day-ahead until fourteen-day-ahead. Those predictive performance evaluations can be seen in Table 4 and Table 5. We also suggest that in order to gain the highest profit from using these methodologies, forecasting EUR-TRY might be the best choice according to the empirical results.

DATA APPENDIX

See Table 9.

REFERENCES

[1] C. A. Sims, "Macroeconomics and reality," *Econometric, J. Econ. Soc.*, pp. 1–48, 1980.

[2] M. Bańbura, D. Giannone, and L. Reichlin, "Large Bayesian vector auto regressions," *J. Appl. Econometrics*, vol. 25, no. 1, pp. 71–92, 2010.

[3] G. Koop and D. Korobilis, "Large time-varying parameter VARs," *J. Econometrics*, vol. 177, no. 2, pp. 185–198, 2013.

[4] G. M. Koop, "Forecasting with medium and large Bayesian VARs," *J. Appl. Econometrics*, vol. 28, no. 2, pp. 177–203, 2013.

[5] T. Park and G. Casella, "The Bayesian Lasso," *J. Amer. Stat. Assoc.*, vol. 103, no. 482, pp. 681–686, 2008.

[6] D. L. Donoho, "Compressed sensing," *IEEE Trans. Inf. Theory*, vol. 52, no. 4, pp. 1289–1306, Apr. 2006.

[7] R. Guhaniyogi and D. B. Dunson, "Bayesian compressed regression," *J. Amer. Stat. Assoc.*, vol. 110, no. 512, pp. 1500–1514, 2015.

[8] F. Zhu, W. Quan, Z. Zheng, and S. Wan, "A Bayesian learning method for financial time-series analysis," *IEEE Access*, vol. 6, pp. 38959–38966, 2018.

[9] H. Jang and J. Lee, "An empirical study on modeling and prediction of bitcoin prices with Bayesian neural networks based on blockchain information," *IEEE Access*, vol. 6, pp. 5427–5437, 2018.

[10] J. Wei, Y. Huang, K. Lu, and L. Wang, "Nonlocal low-rank-based compressed sensing for remote sensing image reconstruction," *IEEE Geosci. Remote Sens. Lett.*, vol. 13, no. 10, pp. 1557–1561, Oct. 2016.

[11] X. Huang, J. Wu, Y. Wen, F. Hu, Y. Wang, and T. Jiang, "Rate-adaptive feedback with Bayesian compressive sensing in multiuser MIMO beamforming systems," *IEEE Trans. Wireless Commun.*, vol. 15, no. 7, pp. 4839–4851, Jul. 2016.

[12] P. Taveeapiradeecharoen and N. Aunsri, "Dynamic model averaging for daily forex prediction: A comparative study," in *Proc. Int. Conf. Digit. Arts, Media Technol. (ICDAMT)*, Feb. 2018, pp. 321–325.

[13] A. E. Raftery, M. Kárnỳ, and P. Ettler, "Online prediction under model uncertainty via dynamic model averaging: Application to a cold rolling mill," *Technometrics*, vol. 52, no. 1, pp. 52–66, 2010.

[14] S. Ji, Y. Xue, and L. Carin, "Bayesian compressive sensing," *IEEE Trans. Signal Process.*, vol. 56, no. 6, pp 2346–2356, Jun. 2008.

[15] A. Carriero, G. Kapetanios, and M. Marcellino, "Forecasting exchange rates with a large Bayesian VAR," *Int. J. Forecasting*, vol. 25, no. 2, pp. 400–417, 2009.

[16] V. Kuzin, M. Marcellino, and C. Schumacher, "Midas vs. mixed-frequency VAR: Nowcasting GDP in the euro area," *Int. J. Forecasting*, vol. 27, no. 2, pp. 529–542, 2011.

[17] F. Schorfheide and D. Song, "Real-time forecasting with a mixed-frequency var," *J. Bus., Econ. Statist.*, vol. 33, no. 3, pp. 366–380, 2015.

[18] D. Achlioptas, "Database-friendly random projections: Johnson-Lindenstrauss with binary coins," *J. Comput. Syst. Sci.*, vol. 66, no. 4, pp. 671–687, 2003.

[19] G. Koop and D. Korobilis, "Manual to accompany MATLAB package for Bayesian VAR models," *Retrieved*, vol. 10, p. 2012, Sep. 2009.

[20] G. Koop, D. Korobilis, and D. Pettenuzzo, "Bayesian compressed vector autoregressions," *J. Econometrics*, Nov. 2018. [Online]. Available: http://www.sciencedirect.com/science/article/pii/S0304407618302100, doi: 10.1016/j.jeconom.2018.11.009.

[21] M. D. Negro and G. E. Primiceri, "Time varying structural vector autoregressions and monetary policy: A corrigendum," *Rev. Econ. Stud.*, vol. 72, no. 3, pp. 821–852, 2005.

[22] A. Carriero, T. E. Clark, and M. Marcellino, "Bayesian VARs: Specification choices and forecast accuracy," *J. Appl. Econometrics*, vol. 30, no. 1, pp. 46–73, 2015.

[23] A. Zellner, *An Introduction to Bayesian Inference in Econometrics*. Hoboken, NJ, USA: Wiley, 1971.

[24] R. Prado and M. West, *Time Series: Modeling, Computation, and Inference*. Boca Raton, FL, USA: CRC Press, 2010.

PAPONPAT TAVEEAPIRADEECHAROEN received the Bachelor of Economics and Master of Economics degrees with specializing in econometrics from Chiang Mai University, Thailand, in 2012 and 2014, respectively. He was with Bangkok Bang Limited Company for one year. He joined Mae Fah Luang University as a Lecturer. Since 2014, he has been a Researcher with the Office of Border Economy and Logistics Study, Chiang Rai, Thailand. His research interests include advance modeling in time series model especially in economic and financial data, Bayesian econometrics, vector autoregression, stochastic volatility, and model averaging and selection.

KOSIN CHAMNONGTHAI (S'88–M'90–SM'06) received the B.Eng. degree in applied electronics from the University of Electro-Communications, Tokyo, Japan, in 1985, the M.Eng. degree in electrical engineering from the Nippon Institute of Technology, Saitama, Japan, in 1987, and the Ph.D. degree in electrical engineering from Keio University, Tokyo, in 1991. He is currently a Professor with the Electronic and Telecommunication Engineering Department, Faculty of Engineering, King Mongkut's University of Technology Thonburi. His research interests include computer vision, image processing, robot vision, signal processing, and pattern recognition. He is a member of IEICE, TESA, ECTI, AIAT, APSIPA, TRS, and EEAAT. He served as an Editor for *ECTI E-magazine*, from 2011 to 2015, and an Associate Editor for ELEX (IEICE Transactions), from 2008 to 2010, ECTI-EEC Transactions, from 2003 to 2010, and ECTI-CIT Transactions, from 2011 to 2016. He served as the Chairman for the IEEE COMSOC Thailand, from 2004 to 2007. He serves as the President for the ECTI Association, from 2018 to 2019.

NATTAPOL AUNSRI received the B.Eng. degree in electrical engineering from Khon Kaen University, Thailand, in 1999, the M.Eng. degree in electrical engineering from Chulalongkorn University, Thailand, in 2003, and the M.Sc. degree in applied mathematics and the Ph.D. degree in mathematical sciences from the New Jersey Institute of Technology, Newark, NJ, USA, in 2008 and 2014, respectively.

Since 2017, he has been an Assistant Professor of computer engineering with the School of Information Technology, Mae Fah Luang University, Chiang Rai, Thailand, where he is currently with the Brain Science and Engineering Innovation Research Group. His research interests include ocean acoustics, Bayesian estimation and filtering, signal processing, biomedical signal processing, drug–drug interactions, and mathematical and statistical modeling.

Effect of Window Functions on the Sequential Bayesian Filtering Based Frequency Estimation

Nattapol Aunsri
School of Information Technology
Brain Science and Engineering Innovation Research Group
Mae Fah Luang University
Chiang Rai, Thailand 57100
Email: nattapol.aun@mfu.ac.th

***Abstract*—Window functions are typically used in time-frequency (TF) signal analysis, especially in spectrogram calculation. In frequency estimation problems, most methods for solving such tasks rely on the spectrogram-based approach where the time-series of the signal is considered in the frequency domain via the short-time Fourier transform (STFT). Sequential Bayesian filtering has been one of the most powerful methods for sequential estimation of time-varying parameters where the signal model and observation data are complicated in terms of nonliear/non-Gaussian assumptions. The method integrates mathematical and statistical properties of the signal in order to construct a posterior probability density functions of the interesting parameters. Therefore, when window function is applied in STFT, the statistical property of the transformed domain may be destroy, resulting in the movement of the frequency estimates according to the window type used in spectrogram calculation. Therefore, we investigate in this work the effect of windows on the accuracy of the sequential Bayesian filtering based frequency estimation. Simulation results show that window has some effect only when the noise level is high.**

***Index Terms*—Window functions, spectrogram; frequency estimation; particle filter; sequential Bayesian filtering; signal processing**

I. Introduction

Frequency estimation has been one of the most important tasks in signal processing, ranging from various kinds of applications [1], [2], [3], [4], [5], [6]. Number of techniques have been proposed to such problems extensively. We focus in this work for spectrogram based time-frequency representation of the signal since it is a conventional approach for most applications. [5], [7], [8] for instances.

This study is based on the sequential Bayesian filtering framework, a particle filtering, in particular. The main reason that this method was considered is from the nature of the signals what we are tracking. Since frequency content of the signal is varied with time, i.e., the number of frequency components and their strength vary and they are considered as a function of time. The particle filter (PF), is therefore a suitable approach too deal with this kind of signal. One may consider a Kalman filter (KF) as a choice, but the limitations of KF prevent its usability for nonlinear and non-Gaussian problems, our problem here is also a case that KF cannot work properly [9], [10], [11].

The rest of the paper is organized as follows. Section II describes the concept of time-frequency analysis of the time-series, and the use of window functions in the analysis. We briefly introduces a sequential filtering method for frequency estimation in Section III. Section IV presents simulation results and discussion. The conclusions can be found in Section V.

II. Window Functions

In signal processing, one the signal is to be analyzed in the frequency domain via the STFT, window function is typically used in the spectrogram calculation in order to enhance the quality of the transform. In this work, we focus on the frequency estimation problem where the Fourier transform of the time-series is considered for the TF analysis. Four window functions including Rectangular, Hamming, Hanning, and Blackman windows are investigated and the functions of these windows are given in Eqs. (1)-(4), respectively.

$$w_{Rect}[n] = 1, \tag{1}$$

$$w_{Ham}[n] = 0.54 + 0.46\cos(\pi n/M), \tag{2}$$

$$w_{Han}[n] = 0.5 + 0.5\cos(\pi n/M), \tag{3}$$

and

$$w_{Black}[n] = 0.42 + 0.5\cos(\pi n/M) + 0.08\cos(2\pi n/M), \tag{4}$$

for $0 \leq n \leq M-1$.

These windows are chosen based on their usage popularity for many applications. In frequency estimation using STFT approach, these windows are typically considered as mentioned earlier.

Standard Short-Time Fourier Transform is performed in the work for a TF representation of the signals, the corresponding squared magnitude of the STFT is expressed by:

$$SG_x = \frac{1}{2\pi}\left| \int x(\tau)w(\tau - t)e^{-j\omega\tau}d\lambda \right|^2, \tag{5}$$

where $w(t)$ is the window function.

III. Sequential filtering for Spectrogram-based Frequency estimation

In Bayesian filtering, the main goal of this approach is to obtain the posterior probability density function (pdf) of the underlying parameters (frequencies for this study). This is done via a state space model where two equations are needed for describing the states and observation data. The first equation is called state transition equation which gives the relation of the states from the current time to the next time step by the perturbation noise. This equation is given as:

$$\mathbf{x}_n = \mathbf{f}_{n-1}(\mathbf{x}_{n-1}, \mathbf{v}_{n-1}) \tag{6}$$

$$\mathbf{y}_n = \mathbf{g}_n(\mathbf{x}_n, \mathbf{w}_n). \tag{7}$$

where n is time, $\mathbf{x}_n$ is a state vector containing the frequency components and the associated amplitudes of the signal. Vector $\mathbf{y}_n$ is the observed data, in this problem $\mathbf{y}_n$ is the spectrogram. Both functions $\mathbf{f}_{n-1}$ and $\mathbf{g}_n$ are known nonlinear functions, and $\mathbf{v}_{n-1}$ and $\mathbf{w}_n$ are perturbation and observation noises, respectively.

In this work, we implemented a multiple model particle filter (MMPF) to track the frequency trajectories of the signal since the number of existing frequencies is a function of time. Based on this kind of filter, it is able to adapt the order (this reflects the length of the state vector) in such a way that the particle can adequately capture the stochastic behavior of the tracking signal. To see the details of the MMPF, especially in frequency estimation and some other applications, the reader is invited to consult the works from [12], [13], [14], [15], [16], [17].

A random sample of parameter values, generated from a set of initial prior specifications (uniform prior for each parameter was chosen), is propagated via the standard Bayesian updating scheme. A combination of the prior with a likelihood is performed to yield the posterior density for each time slice. The linkage of one time slice to the next is through the state Eq. (6) of the sequential model, so that the posterior distribution for one time slice becomes the prior distribution for the next time slice. A likelihood for each particle is computed based on the observation Eq. (7). We follow the technique presented in [16], the reader is referred to that paper for details. In this work we investigate the effect of the window functions to the filtering using PF, where [16] does not consider this issue.

IV. Simulation Results

The spectrogram of the signal considered in this work is shown in Fig. 1; this spectrogram was computed using Hamming window. The signal contains multiple components and each component may appear or exit at any time. Throughout the paper, the number of particles used for performance evaluation was 500. We first illustrate the tracking results from the PF for SNR of 30 dB, the frequency estimates as provided by the PF where Hamming and Hanning windows were used in spectrogram computation are shown in Fig. 2

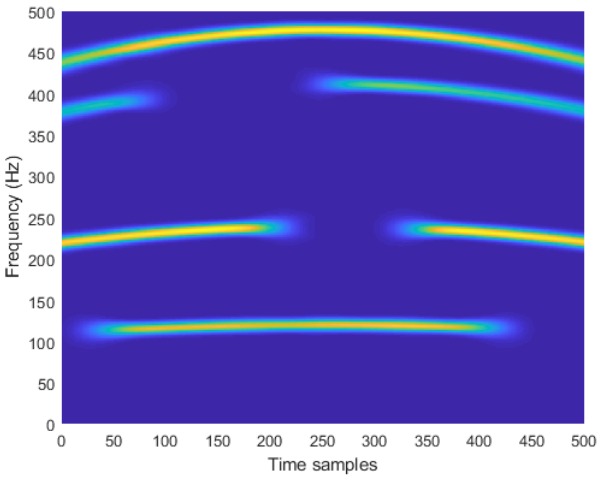

Fig. 1: Spectrogram of the signal to be investigated.

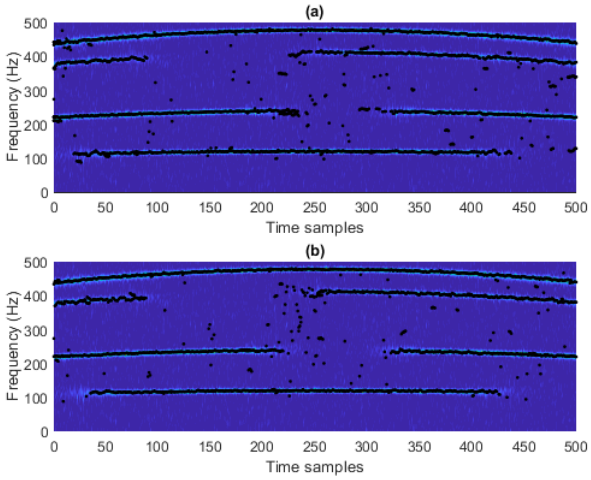

Fig. 2: Frequency estimates as obtained by the PF where the spectrogram was computed using (a) Hamming window and (b) Hanning Window. The SNR is 30 dB.

(a) and (b), respectively. Figure 3(a) and (b) display the frequency estimates from the PF where Blackman and rectangular windows were used in spectrogram computation, respectively. From the figures, it can be seen that the tracking results from all tests are almost identical except that the result from rectangular window. Frequency estimates from the PF where the rectangular window was used are not clear as compared to the other windows, and we found that some frequency components that do really exist are generated by the PF for the rectangular window case.

Next, we further demonstrate the results from the experiment where the SNR is low, in Fig. 4 we show the spectrogram of the signal with SNR of 10 dB. The frequency estimates as provided by the PF from Hamming, Hanning, Blackman, and rectangular windows are shown in Fig. 5(a) and (b) and Fig. 6(a) and (b), respectively. It can be noticed from the results

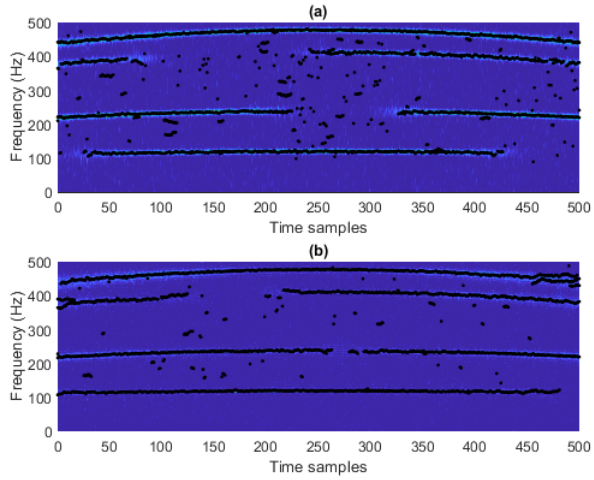

Fig. 3: Frequency estimates as obtained by the PF where the spectrogram was computed using (a) Blackman window and (b) Rectangular Window. The SNR is 30 dB.

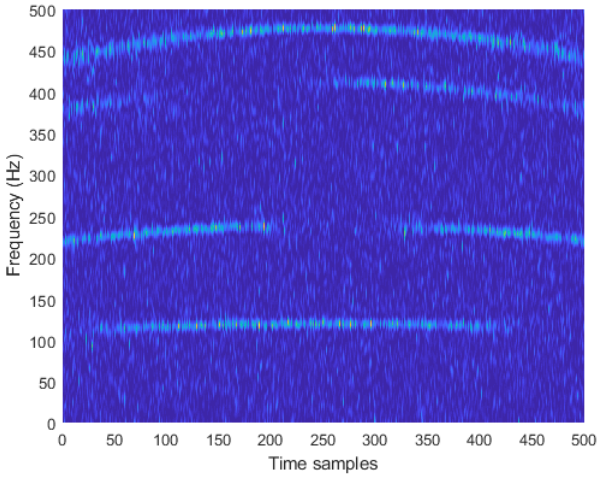

Fig. 4: Spectrogram of the signal to be investigated, the SNR is 10 dB.

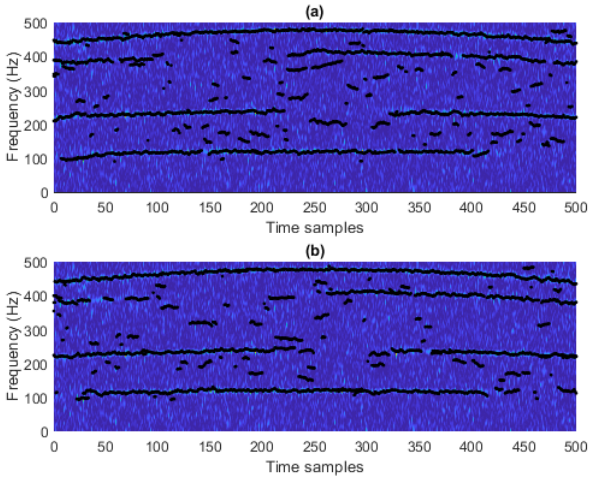

Fig. 5: Frequency estimates as obtained by the PF where the spectrogram was computed using (a) Hamming window and (b) Hanning Window. The SNR is 10 dB.

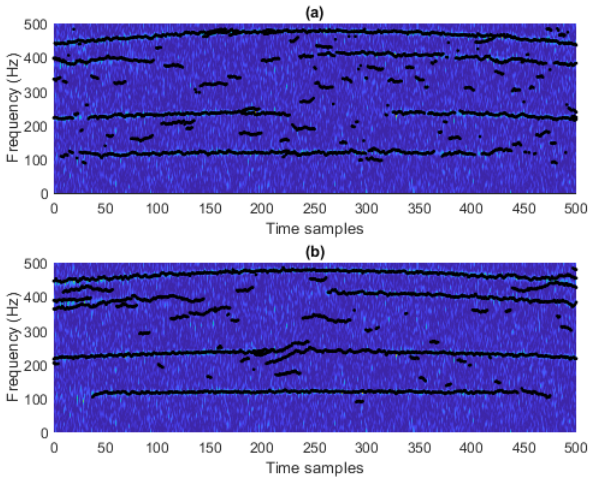

Fig. 6: Frequency estimates as obtained by the PF where the spectrogram was computed using (a) Blackman window and (b) Rectangular Window. The SNR is 10 dB.

that the tracks from Hamming and Hanning windows are better than from Blackman and rectangular windows. In addition, result from rectangular window is the worse one compared to the others, this could be a result from its function which does not provide any contribution to the windowed segment of the signal.

Finally, we illustrate the effect of the window functions when we now consider a signal with more frequency components and more complex than the precious example. The spectrogram of this signal is shown in Fig. 7. Tracking results are provided in Figs. 8-9. Spectrogram with rectangular window is the worse one again since it delivers frequency estimates with the highest errors compared to the other windows used in spectrogram calculation.

V. Conclusions

In this paper, we investigate how window functions affect the performance of frequency estimation from a sequential Bayesian filtering approach. Several frequent use window functions were considered including Hamming, Hanning, Blackman, and rectangular windows. The investigation was taken by considering two signal examples with varied SNR. Simulation results suggested that the tracking results as delivered by the PF where the spectrogram was computed with rectangular window were poor; this could be a result from no contribution of this window type in spectrogram calculation. The other windows for spectrogram calculation, allow the PF to better tracks frequency components of the signal. It should be noted that even the frequency tracks from any

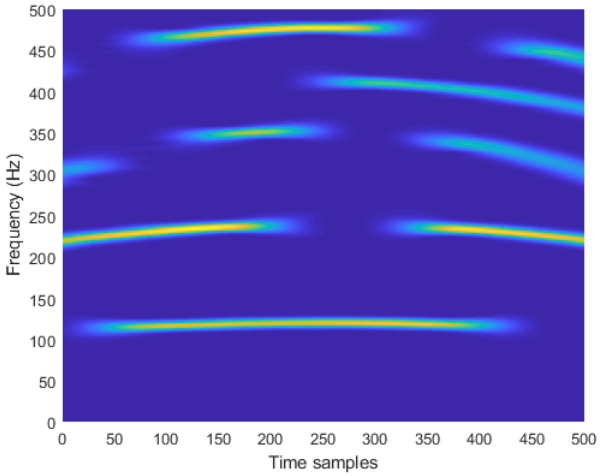

Fig. 7: Spectrogram of the signal with more frequency components.

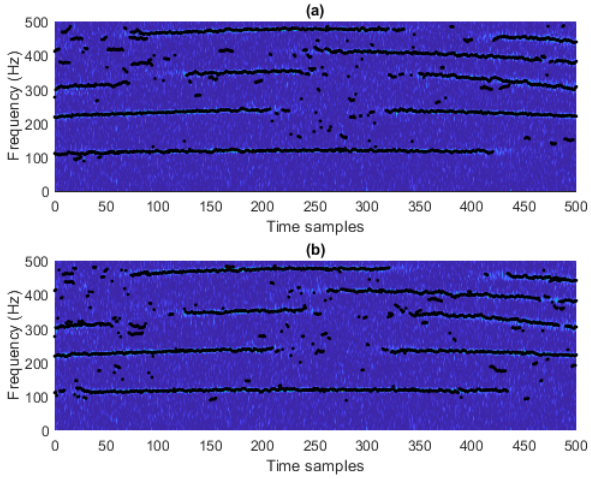

Fig. 8: Frequency estimates as obtained by the PF where the spectrogram Fig. 7 was computed using (a) Hamming window and (b) Hanning Window. The SNR is 10 dB.

window except from the rectangular window are better, one the spectrogram calculation with window function has done, the stochastic property of the TF representation would change. In this work, based on the acceptable model and its widely used in literature, we constructed the likelihood function using Gaussian error model, which was not accurate. If the other models are used, tracking results would also change, and rigorous analysis and PF implementation must be performed.

ACKNOWLEDGMENT

This work was partially supported by the Thailand Research Fund (TRF) and the Office of the Higher Education Commission under the grant MRG6080152. The author would also like to thank the School of Information Technology, Mae Fah Luang University for facilities support.

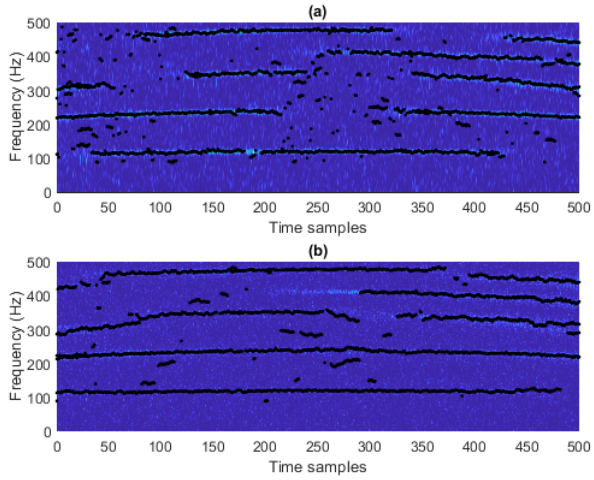

Fig. 9: Frequency estimates as obtained by the PF where the spectrogram in Fig. 7 was computed using (a) Blackman window and (b) Rectangular Window. The SNR is 10 dB.

REFERENCES

[1] C.-S. Chen, J. Miller, F. Boudreaux-Bartels, G. Potty, and C. Lazauski, "Time-frequency representations for wideband acoustic signals in shallow water," in *Proceedings of OCEANS 2003*, 2003, pp. 2903–2907.

[2] C. Dubois, M. Davy, and J. Idier, "Tracking of time-frequency components using particle filtering," in *Acoustics, Speech, and Signal Processing, 2005. Proceedings. (ICASSP '05). IEEE International Conference on*, vol. 4, March 2005, pp. iv/9 – iv12 Vol. 4.

[3] T. G. Oesterlein, C. He, J. E. Quijano, R. L. Campbell Jr., L. M. Zurk, and M. Siderius, "Extraction of time-frequency target features," in *IEEE Conference on Signals, Systems, and Computers*, November 2009.

[4] G. Zhang and S. Godsill, "Fundamental frequency estimation in speech signals with variable rate particle filters," *IEEE Transactions on Audio, Speech, and Language Processing*, vol. 24, pp. 890–900, May 2016.

[5] N. Aunsri and S. Hemrungrote, "A Bayesian approach for frequency estimation using TV AR model for ocean acoustics time-series," in *Signal and Information Processing Association Annual Summit and Conference (APSIPA), 2014 Asia-Pacific*, Dec 2014, pp. 1–4.

[6] N. Aunsri, "A Bayesian filtering approach with time-frequency representation for corrupted dual tone multi frequency identification," *Engineering Letters*, vol. 24, no. 4, pp. 370–377, 2016.

[7] Z.-H. Michalopoulou and N. Aunsri, "Environmental inversion using dispersion tracking in a shallow water environment," *The Journal of the Acoustical Society of America*, vol. 143, no. 3, pp. EL188–EL193, 2018.

[8] N. Aunsri, "A TVAR particle filter with adaptive resampling for frequency estimation," in *2016 International Symposium on Intelligent Signal Processing and Communication Systems (ISPACS)*, Oct 2016, pp. 1–5.

[9] M. Arulampalam, S. Maskell, N. Gordon, and T. Clapp, "A tutorial on particle filters for online nonlinear/non-Gaussian Bayesian tracking," *IEEE Trans. Signal Process.*, vol. 50, pp. 174–188, 2002.

[10] B. Ristic, S. Arulampalam, and N. Gordon, *Beyond the Kalman Filter: Particle Filters for Tracking Applications*. Boston, MA: Artech House, 2004.

[11] J. V. Candy, *Bayesian Signal Processing: Classical, Modern and Particle Filtering Methods*. New Jersey: John Wiley & Sons, 2009.

[12] C. Andrieu and A. Doucet, "Joint Bayesian model selection and estimation of noisy sinusoids via reversible jump MCMC," *IEEE Trans. Signal Processing*, vol. 47, no. 10, pp. 2667 –2676, Oct 1999.

[13] A. Doucet, N. J. Gordon, and V. Krishnamurthy, "Particle filters for state estimation of jump Markov linear systems," *IEEE Trans. Signal Processing*, vol. 49, no. 3, pp. 613–624, 2001.

[14] C. Andrieu, M. Davy, and A. Doucet, "Efficient particle filtering for jump Markov systems. Application to time-varying autoregressions,"

IEEE Trans. Signal Processing, vol. 51, no. 7, pp. 1762–1770, July 2003.

[15] Z.-H. Michalopoulou and R. Jain, "Particle filtering for arrival time tracking in space and source localization," *J Acoust. Soc. Am.*, vol. 132, no. 5, pp. 3041–3052, 2012.

[16] N. Aunsri and Z.-H. Michalopoulou, "Sequential filtering for dispersion tracking and sediment sound speed inversion," *J. Acoust. Soc. Am.*, vol. 136, no. 5, pp. 2665–2674, 2014.

[17] N. Aunsri, "Seismic events estimation under noisy environments using multiple model particle filter," in *2018 15th International Conference on Electrical Engineering/Electronics, Computer, Telecommunications and Information Technology (ECTI-CON)*, July 2018, pp. 793–797.

APPENDIX B

SUBMITTED MANUSCRIPTS

Following is the list of submitted manuscripts from this project and they are now under minor revision.

1. Sequential Bayesian Filtering with Stochastic Characterization of Ocean Acoustics Time-series for Frequency and Dispersion Estimation, submitted to Measurement, now *Under Review*

2. Particle Filtering with Adaptive Resampling Scheme for Modal Frequency Identification and Dispersion Curves Estimation in Ocean Acoustics, submitted to Applied Acoustics, *Under Review (minor revision)*

Sequential Bayesian Filtering with Stochastic Characterization of Ocean Acoustics Time-series for Frequency and Dispersion Estimation

Nattapol Aunsri[a,b,*], Kosin Chamnongthai[c]

[a] *School of Information Technology, Mae Fah Luang University, Chiang Rai, Thailand*
[b] *Brain Science and Engineering Innovation Research Group, Mae Fah Luang University, Chiang Rai, Thailand*
[c] *Faculty of Engineering, King Mongkuts University of Technology Thonburi, Bangkok, Thailand*

Abstract

Useful information embedded in the ocean acoustic time-series can be retrieved from frequency content of the measured time-series. Therefore, frequency estimation in ocean acoustics has long been one of the most important problems in geoacoustic inversion. A challenging task is to obtain more accurate frequency content in which the mathematical and stochastic properties are together suitably combined to obtain the required information. This paper, thus, considers the analysis and simulation of the ocean acoustics time-series in the frequency-domain where the signal in the time-domain was corrupted by white Gaussian noise for frequency and dispersion estimation. Via a sequential Bayesian filtering framework, we incorporate a mathematical description of a broadband ocean acoustics signal propagating through the ocean with statistical property of such type of noisy signal, the accurate posterior probability density function (PDF) of frequencies along with their associated amplitudes is eventually obtained. Sequential filtering is implemented for frequency and dispersion estimation to test the performance of the derived model. Although the data are noisy, simulation results demonstrate a significant advantage of the proposed method.

*Corresponding author
Email address: nattapol.aun@mfu.ac.th (Nattapol Aunsri)

Keywords: modal frequency, frequency estimation, dispersion curve, likelihood, particle filter, ocean acoustics.

1. Introduction

A frequency estimation has always been one of the most important and challenging problems in science and engineering applications including physics, signal processing, communication, and ocean acoustics; see [1, 2, 3, 4, 5, 6] for examples. Given a white Gaussian noise contaminated ocean acoustics time-series, we consider a time-frequency analysis of such time-series via a short-time Fourier transform (STFT). The goal of this work is to incorporate the statistical description of the signal in the frequency domain to a sequential frequency estimation framework, the particle filtering, in particular, to obtain the posterior PDF of the frequency and its corresponding quantities. The posterior PDF of these quantities play an important role in environmental inversion in which the geoacoustics properties of the ocean can be revealed [2, 7, 8].

Back to 1960 where the pioneer work in new filtering method named Kalman Filter (KF) was proposed as reported in [9]. The filter delivers an optimal estimator according to the minimum mean squared error metric. However, the limitation of the KF is that the evolution of the unknown parameters is assumed to be in the case of Gaussian and additive perturbations, the additive Gaussian noise model is considered in the observed data, and a linear function describing the measurements and state vector parameters.

It is not a case for most practical systems that the assumptions made for the KFs are always valid, most systems are nonlinear/non-Gaussian as well as non-additive noise structure. Variants of the KFs were developed to remedy these problems; the extended KF (EKF), unscented Kalman filters (UKFs), and ensemble Kalman filter (EnKF) are examples of KF variants that were proposed in literature. Nevertheless, a system with highly nonlinear models and complex noise processes are not easily to deal with, it requires computational or numerical approaches to formulate the desired posterior PDFs, and the inferences on the

state parameters have to be done numerically since the closed form PDFs may not be feasible to obtain, these approaches are particle filtering.

A Particle filter (PF), a class of sequential Monte Carlo method, is used for the estimation of the underlying posterior PDFs of random variables, allowing the extraction of the desired information from complex noisy observation data becomes possible. PF, derived from the importance sampling (IS) concept, is a numerical approach that was proposed to effectively handle nonlinear relations between unknown parameters and observations, complex noise processes, and unknown as well as the time-varying dynamical systems [10, 11, 12, 13, 14, 15].

Frequency estimation in ocean acoustics has long been as of interest for decades as seen in literature [16, 17, 18, 2, 19]. The importance of this problem stems from the fact that most important pattern of the frequency content with time exhibits in the dispersion characteristics of the waveguide resulting from the dispersive environments. Therefore, retrieving this information could lead us to effectively estimate parameters that are of utmost importance in environmental studies [20, 21, 22, 23, 8]. The approach described in [2] assumed that noise contaminated the signal in the frequency domain, resulting in a Gaussian form of the likelihood function. Therefore, the likelihood formulation based on this assumption is not accurate. In reality, the noise is additive Gaussian in the time domain, generating complex noise components after Fourier transform (FT) calculation. The contribution of this work is therefore to construct an accurate statistical model of the noise after FT calculation and then use the resulting model for likelihood and particle weight calculation. This work implements a PF based on the incorporation of mathematical and accurate statistical models of the ocean acoustics signal in the frequency domain to construct the accurate likelihood function and the particle weight calculation for formulating the frequency PDF and, hence, the dispersion PDF of the signal.

The remainder of this paper is structured as follows. Section II provides a time-frequency analysis of a noisy time-series and frequency approximation of ocean acoustics for our work. Section III presents a foundation of sequential Bayesian filtering framework and particle filtering used in this work. A PF

implementation based on the constructed ocean acoustics model and stochastic property of the signal is presented in Section IV. Section V discusses the tracking results of the frequency estimates from particle filter, and Section VI delivers the conclusions.

2. Time-frequency analysis of Ocean Acoustics time-series

2.1. Probability distribution of a noisy time-series

Consider a noisy signal $x[n]$ of length N, which is composed of a deterministic part $s[n]$ and noise part $g[n]$, i.e., $x[n] = s[n] + g[n]$, where $g[n]$ is assumed to be zero mean white Gaussian noise with variance σ^2. From the assumption, the distribution of each sample $x[n]$ is

$$x[n] \sim \mathcal{N}(g[n], \mathbf{C}) \tag{1}$$

where $\mathcal{N}(a, b)$ is the normal distribution with mean a and variance b, and here $\mathbf{C}$ is the autocorrelation function.

The spectrogram $S_x(l, k)$ at time l and frequency k of signal $x[n]$ obtained from STFT is calculated from the squared modulus of the STFT as

$$S_x(l, k) = X_r(l, k)^2 + X_{im}(l, k)^2, \tag{2}$$

$X_r(l, k)$ and $X_{im}(l, k)$ are real and imaginary parts of the STFT and they are computed by

$$X_r(l, k) = \sum_{n=1}^{N} w(n - l)x(n) \cos(-2\pi k \frac{n}{L}), \tag{3}$$

and

$$X_{im}(l, k) = \sum_{n=1}^{N} w(n - l)x(n) \sin(-2\pi k \frac{n}{L}), \tag{4}$$

where $w(n)$ is the analysis window with length N.

From the assumption of the signal model, the signal in the time-domain $x[n]$ is distributed according to Eq. (1). Following the property of the normal distribution that a linear combination of the Gaussian distributions is also

Gaussian distributed. Since both $X_r(l,k)$ and $X_{im}(l,k)$ are linear combinations of N Gaussian random variables with coefficients $w(n-l)\cos(-2\pi k\frac{n}{L})$ and $w(n-l)\sin(-2\pi k\frac{n}{L})$, respectively, therefore, these two quantities are Gaussian random variables as well. It can be shown that the variance of both real and imaginary parts of STFT is $\sigma^2/2$, the half of the noise variance of noise part in the time-domain [24].

According to Eq. (2), the spectrogram $S_x(n,k)$ is the sum of two squared Gaussian random variables. Therefore, $S_x(n,k)$ follows the χ^2 distribution with two degrees of freedom. The degrees of freedom of a χ^2 distribution depends on number of elements in the combination; here we have real and imaginary parts, squared and added together to generate the spectrogram as previously described.

In general, let us now consider a random variable $X_i \sim \mathcal{N}(0,\sigma_i^2)$, $i = 1, \ldots, 2, \ldots, N$, X is the sum of the squares of X_i. Let $X = \sum_{i=1}^{N} X_i^2$, and it is distributed as a χ^2 variable. This distribution can be characterized by three parameters, a χ^2 PDF of a random variable X can be given as:

$$f_{X;a,b,c}(X) = \frac{1}{2b}\Big(\frac{x}{c}\Big)^{\frac{a-2}{4}} e^{-(x+c)/2b} I_{\frac{a-2}{2}}\big(\frac{\sqrt{xc}}{b}\big), \tag{5}$$

where $I_n(.)$ stands for the n-order modified Bessel function of the first kind. The parameters a, b and c are the degrees of freedom, coefficient of proportionality, and non-centrality parameter, respectively. Theses parameters will be defined according to our problem which will be discussed later in the Section IV.

2.2. Frequency approximation of ocean acoustics signal

According to work in [2], the power spectrum can be given by

$$|P_n(\omega,t)|^2 = \frac{\pi}{|k_n''|^2}|\mu(\omega_n)G_n(r,z,z_r,\omega_n)|^2|\frac{\sin(\omega'-\omega)\Delta t}{\omega'-\omega}|^2, \tag{6}$$

for $|\omega-\omega_n| < \frac{\pi}{\Delta t}$.

Quantity r is the distance between source and receiver, z and z_r are the source and receiver depths, respectively, μ is the source spectrum, $G_n(r,z,z_r)$ is a func-

tion relating to normal mode quantity, k_n represents the modal wave number, $\omega = 2\pi f$, where f is frequency in Hz.

It is obvious that the power spectrum is approximated by a squared *sinc* pulse, weighted by the squared amplitude of the modal arrival. A linear combination of these pulses can be used to approximate the power spectrum of a multiple-mode signal, allowing a construction of a replica of the signal in particle filtering implementation which will be explained later. This approximation technique is called a modal representation of the a signal which was successfully used for broadband acoustic signals propagating in underwater media [16].

3. Bayesian Filtering Framework and its conceptual solution

In this section, the fundamentals of sequential Bayesian filtering are recalled and a construction of particle filtering method is then provided.

3.1. State space model

Consider the following nonlinear system:

$$\mathbf{x}_n = \mathbf{f}_{n-1}(\mathbf{x}_{n-1}, \mathbf{v}_{n-1}) \tag{7}$$

$$\mathbf{y}_n = \mathbf{g}_n(\mathbf{x}_n, \mathbf{w}_n). \tag{8}$$

where n is time, $\mathbf{x} \subseteq \mathbb{R}^{n_x}$ is the n_x-dimensional state vector, $\mathbf{y} \subseteq \mathbb{R}^{n_y}$ is the n_y-dimensional observation vector, $\mathbf{v}_{n-1}$ denotes n_x-dimensional process noise vector, and $\mathbf{w}_n$ denotes n_y-dimensional measuring process noise vector.

The first state equation describes how the states evolve with time; and the transition of the states from the consecutive time is followed the function of the first order process $\mathbf{f}_n$ as given in Eq. (7). The second equation is called the observation equation relating the observation data to the state vector through a nonlinear function $\mathbf{g}_n$, and this equation is given in Eq. (8). Both $\mathbf{f}_{n-1}$ and $\mathbf{g}_n$ are known in this work. The state and observation noise quantities are declared as $\mathbf{v}_{n-1}$ and $\mathbf{w}_n$, respectively. Functions $\mathbf{f}_{n-1}$ and $\mathbf{g}_n$ are typically nonlinear

and assumed to be the multivariate known functions. The evolution of the state vector with time is done via a function $\mathbf{f}_{n-1}$ relating the changes of the state parameters from the previous time to the current time according to the process noise $\mathbf{v}_{n-1}$. The relationship between the state vector and the observation vector is described by the measurement or observation function $\mathbf{g}_n$ and the measuring process noise $\mathbf{w}_n$. Both noises can by additive, multiplicative, or other forms depending on the problem at hands.

In general, let $\mathbf{X}_n = [\mathbf{x}_1, \mathbf{x}_2, \ldots, \mathbf{x}_n]$ be a sequence of the unknown state vectors up to time n, the aim of filtering is to recursively estimate the state vector $\mathbf{x}_n$ based on a set of available information from the measurements $\mathbf{Y}_n = [\mathbf{y}_1, \mathbf{y}_2, \ldots, \mathbf{y}_n]$. This problem can be addressed by computing the posterior PDF $p(\mathbf{x}_n|\mathbf{Y}_n)$. Assuming that the initial PDF of the state vector $p(\mathbf{x}_0|\mathbf{y}_0) = p(\mathbf{x}_0)$, the posterior PDF $p(\mathbf{x}_n|\mathbf{Y}_n)$ can be computed recursively using the following two steps: prediction and updating. We will detail these steps for PF implementation in Section IV.

3.2. Bayesian Inference

As discussed, we require two equations to describe the state-space model; one expresses the evolution of the state and one connects the relation between states and observations. We assume that each observation $\mathbf{y}_n$ depends solely on the current state $\mathbf{x}_n$; and the observations up to time n are conditionally independent given the states $\mathbf{x}_n$, therefore

$$p(\mathbf{Y}_n|\mathbf{X}_n) = \prod_{i=1}^{n} p(\mathbf{y}_i|\mathbf{X}_n). \tag{9}$$

The states of the model are allowed to change over time according to a first order Markov process, therefore the current state depends only the state at a previous time step, yielding:

$$p(\mathbf{X}_n) = p(\mathbf{x}_0) \prod_{i=1}^{n} p(\mathbf{x}_i|\mathbf{x}_{i-1}). \tag{10}$$

The goal of the PF is to gather the posterior PDF of the unknown states when the observed data is available at time step n, $p(\mathbf{X}_n|\mathbf{Y}_n)$, and it can be given as:

$$p(\mathbf{X}_n|\mathbf{Y}_n) = \frac{p(\mathbf{Y}_n|\mathbf{X}_n)p(\mathbf{x}_0)}{p(\mathbf{Y}_n)}. \tag{11}$$

From Eqs. (9) and (10), we can express the posterior distribution $p(\mathbf{X}_n|\mathbf{Y}_n)$ as

$$p(\mathbf{X}_n|\mathbf{Y}_n) = \frac{p(\mathbf{x}_0)\prod_{i=1}^{n} p(\mathbf{y}_i|\mathbf{x}_i)p(\mathbf{x}_i|\mathbf{x}_{i-1})}{p(\mathbf{Y}_n)}, \tag{12}$$

where $p(\mathbf{x}_0)$ is the prior density and we assume it to be a uniform density in this work, i.e., the chance of the existence of the modal frequencies is assumed to be equal over the search interval. The observation $\mathbf{y}_n$ is independent of the states at all other times and we assume that the observation data up to step n are also independent. Bayesian framework recursively estimates the marginal PDF $p(\mathbf{x}_n|\mathbf{Y}_n)$ from the previous marginal PDF $p(\mathbf{x}_{n-1}|\mathbf{Y}_n)$. By assuming that the marginal PDF $p(\mathbf{x}_{n-1}|\mathbf{Y}_{n-1})$ is available, the prediction of the PDF $p(\mathbf{x}_n|\mathbf{Y}_{n-1})$ can be computed from transitional PDF $p(\mathbf{x}_n|\mathbf{x}_{n-1})$ as suggested by state equation of Eq. (7). We can then rewrite Eq. (12) as:

$$p(\mathbf{X}_n|\mathbf{Y}_n) = \frac{p(\mathbf{y}_n|\mathbf{x}_n)p(\mathbf{x}_n|\mathbf{x}_{n-1})p(\mathbf{X}_{n-1}|\mathbf{Y}_{n-1})}{p(\mathbf{y}_n|\mathbf{Y}_{n-1})}, \tag{13}$$

where

$$\begin{aligned} p(\mathbf{y}_n|\mathbf{Y}_{n-1}) = \int\int & p(\mathbf{y}_n|\mathbf{x}_n)p(\mathbf{x}_n|\mathbf{x}_{n-1}) \\ & \times p(\mathbf{X}_{n-1}|\mathbf{Y}_{n-1})\mathrm{d}\mathbf{x}_{n-1}\mathrm{d}\mathbf{x}_n. \end{aligned} \tag{14}$$

Moreover, the PDF $p(\mathbf{x}_n|\mathbf{Y}_{n-1})$ can be expressed as the so called Chapman-Kolmogorov equation:

$$\begin{aligned} p(\mathbf{x}_n|\mathbf{Y}_{n-1}) &= \int p(\mathbf{x}_n|\mathbf{x}_{n-1},\mathbf{Y}_{n-1})p(\mathbf{x}_{n-1}|\mathbf{Y}_{n-1})\mathrm{d}\mathbf{x}_{n-1} \\ &= \int p(\mathbf{x}_n|\mathbf{x}_{n-1})p(\mathbf{x}_{n-1}|\mathbf{Y}_{n-1})\mathrm{d}\mathbf{x}_{n-1}. \end{aligned} \tag{15}$$

The new estimate of the states at time step n is:

$$p(\mathbf{x}_n|\mathbf{Y}_n) = \frac{p(\mathbf{y}_n|\mathbf{x}_n)p(\mathbf{x}_n|\mathbf{Y}_{n-1})}{p(\mathbf{y}_n|\mathbf{Y}_{n-1})}. \tag{16}$$

Assume that the observation data $\mathbf{Y}_n$ is available, the likelihood of the state vector $\mathbf{x}_n$ is obtained from the density $p(\mathbf{y}_n|\mathbf{x}_n)$. Since the posterior PDF of the states is available according to the sequential update discussed above, the statistical inference can then be performed using this probability distribution. The expected value of a function of the state can be calculated from

$$\begin{aligned} \widehat{F}(\mathbf{x}_n) &= \mathbf{E}_{p(\mathbf{x}_n|\mathbf{Y}_n)}[F(\mathbf{x}_n)|\mathbf{Y}_n] \\ &= \int F(\mathbf{x}_n)p(\mathbf{x}_n|\mathbf{Y}_n)\mathrm{d}\mathbf{x}_n. \end{aligned} \tag{17}$$

3.3. Particle filtering

Working in a sequential filtering framework, we implement PF for identifying the trajectories of the modal frequencies of the ocean acoustics signal. It must be clear that the KF families cannot be applied to our problem because the relationship between the observed data and the states is highly nonlinear.

For each time step, the PF approximates a probability density of $p(\mathbf{x}_n|\mathbf{y}_n)$ by constructing by a set of random samples with their associated weights as

$$p(\mathbf{x}_n|\mathbf{y}_n) \approx \sum_{i=1}^{N} w_n^i \delta(\mathbf{x}_n - \mathbf{x}_n^i) \tag{18}$$

and

$$w_n^i \propto \frac{p(\mathbf{X}_n^i|\mathbf{Y}_n)}{q(\mathbf{X}_n^i|\mathbf{Y}_n)}, \tag{19}$$

where δ is the Dirac delta function, N is the number of particles used in the approximation, and the quantity $q(\mathbf{X}_n^i|\mathbf{Y}_n)$ is the importance density. The accuracy of the filter, i.e., the performance of the approximated distribution to the true continuous density increases as the increasing of N [25, 11]. In other words, $\sum_{i=1}^{N} w_n^i \delta(\mathbf{x}_n - \mathbf{x}_n^i) \to p(\mathbf{x}_n|\mathbf{y}_n)$ as $N \to \infty$. Since we assume that our filtering follows the first order Markov process, the results from the previous

time step $n-1$ and the importance density can be chosen in such a way that the minimization of the IS errors is achieved, we therefore obtain the importance weight for each particle as (for full derivation details, please consult [11])

$$w_n^i = p(\mathbf{y}_n|\mathbf{x}_n^i)w_{n-1}^i. \tag{20}$$

The degradation of the sequential IS (SIS) performance stems from the problem that the variance of the importance weights always increases monotonically over time. After running a filtering process for a few iterations, only few particles tend to occupy high weights but the rest of particles holds the weights that are close to zero. In some extreme cases, just only one particle is a survival and it holds a unit weight. This means that the diversity of the particle distribution is not achieved and this results in a failure of the posterior probability distribution representation using this framework. This problem is called degeneracy. There are improvement algorithms proposed to overcome degeneracy problem, the wildly used method is called resampling scheme. The trick is to eliminate small importance weight particles and, on the other hand, those of the large weights are regenerated. The amount of regeneration depends on the importance weights of the parent particles. We call the process that combines SIS and resampling as sequential importance resampling (SIR). The resampling process is typically performed when the effective number of particles N^{eff} falls below a threshold as discussed in [12, 26]. The effective number of particles is determined as

$$N^{eff} = \frac{1}{\sum_{i=1}^{N}(w_n^i)^2}. \tag{21}$$

Even that the resampling reduces the effects of degeneracy, two new problems occur [11]. First, resampling step introduces the limitation of the ability to parallelize the SIS algorithm because all weights have to be summed during normalization. Second, the assumption of statistical independence is no longer valid after resampling. A problem that may arise after resampling is the loss of particle diversity due to all of the particles are identical, breaking down

to a noninformative distribution. Therefore, convergence issues are generated along the process if resampling takes serious loss of particle diversity. This is well-known as sample impoverishment which is commonly exhibited in PF applications. Recently, there are developments of PFs [11, 13, 27] that have been designed to resolve these problems.

4. Particle filtering implementation

In this work, the dimension of the state is unknown, therefore we need to estimate number of frequencies present at each time step, resulting in the requirement of additional state variable. The transition probability matrix is used to dictate the probabilities of order changes; that is, frequency trajectories may leave or enter at each time step [28] . If at time step $n-1$, the signal is composed of m_{n-1} modes (number of central frequencies). Then it becomes m_n in the next time step n with probability $p(m_n = j|m_{n-1} = i) = \pi_{ij}$. It should be noted that the constraint $\sum_j \pi_{ij} = 1$ must be satisfied.

According to Eq. (6), we obtain the measurement equation that relates the observation data $\mathbf{y}_n$ and frequency particles x_{nj} for the STFT method as follows:

$$\mathbf{y}_n = \sum_{j=1}^{m_n} a_{nj}[sinc(f - x_{nj})]^2 + \mathbf{w}_n. \tag{22}$$

Note that $\mathbf{y}_n$ is the FT of the acoustic time series: our approach relies on modeling the signal in the frequency domain at consecutive time slices.

Although we desire to estimate the frequencies of the signal, constructing the likelihood of the observation data requires a construction of replica of the signal. We, therefore not only estimate the frequency, but also need to estimate its corresponding amplitude as well. Since the amplitudes a_n are unknown, we create a new state vector containing these unknown quantities and treat it similarly to the unknown frequencies x_{nj}. Moreover, we also estimate the noise variance since we normally treat it to be an unknown parameter. To summarize, the state transition equations are given by:

$$\mathbf{f}_n = \mathbf{f}_{n-1} + \mathbf{v}_{1,n-1}, \tag{23}$$

$$\mathbf{a}_n = \mathbf{a}_{n-1} + \mathbf{v}_{2,n-1}, \tag{24}$$

and

$$\sigma_n^2 = \sigma_{n-1}^2 + \mathbf{v}_{3,n-1}. \tag{25}$$

Therefore, frequency particle and amplitude particle can be sampled from the following densities:

$$\mathbf{f}_n^i \sim \mathcal{N}(\mathbf{f}_{n-1}^i, \sigma_{v_1,n-1}^2), \tag{26}$$

$$\mathbf{a}_n^i \sim \mathcal{N}(\mathbf{a}_{n-1}^i, \sigma_{v_2,n-1}^2), \tag{27}$$

and the measurement noise variance particle can be drawn from the density:

$$\sigma_{w,n}^{2,i} \sim \mathcal{N}(\sigma_{w,n-1}^{2,i}, \varsigma_{v_3,n-1}^2), \tag{28}$$

where $\sigma_{v_1,n-1}^2$ and $\sigma_{v_2,n-1}^2$ are the frequency and amplitude state perturbation variances, while $\varsigma_{v_3,n-1}^2$ is the variance of the state perturbation of measurement noise variance. After sampling is employed, the likelihood can be computed via the measurement equation.

The implementation of the method for frequency estimation using particle filtering is from what was developed and presented in previous section. The χ^2 behavior of the data implies a likelihood function that will be used for weight/probablity calculation for individual particle. The χ^2 behavior of the FT that shapes the form of the likelihood is explained as follows. According to Eq. (5), the real and imaginary parts of the FFT are normally distributed with non-zero '*means*'. These '*means*' are the corresponding FTs of the signal. Follow the statistical independent property, the sum of the squares of both real and imaginary parts follows non-central χ^2 distribution with two degrees of freedom. The sum of the squares of the means of the real and imaginary parts is the non-central parameter.

The above analysis is just for a single point in the frequency domain. For the complete length of the Fourier transform for a slice of the spectrogram, the

non-central parameter is a vector of length L, which is actually the replica of the squared spectrum of the signal. The χ^2 parameters can be declared as follows: the noncentral parameter is the replica of the signal in our problem, and the degrees of freedom is two as discussed earlier. The coefficient of proportionality is based on the fact that both real and imaginary parts of the STFT are Gaussian random variables with common variance $\sigma^2/2$ [29]. Therefore, the coefficient of proportionality is $\sigma^2/2$. Let $\mathbf{x}_n$ is a state vector containing $\mathbf{f}_n$, $\mathbf{a}_n$, and m_n, from the discussion in Section II, the likelihood function can be given by:

$$l(\mathbf{y}_n|\mathbf{x}_n) \propto \frac{1}{L^{m_n}} exp\Big(\frac{-(\mathbf{y}_n + \sum_{j=1}^{m_n} a_{nj}[sinc(f - x_{nj})]^2)}{\sigma_{w,n}^2}\Big) \\ I_0\left[\frac{\sqrt{< \mathbf{y}_n, \sum_{j=1}^{m_n} a_{nj}[sinc(f - x_{nj})]^2 >}}{\sigma_{w,n}^2/2}\right]. \tag{29}$$

where $< \bullet, \bullet >$ stands for a dot product operator. Please be noted that the term $\frac{1}{L^{m_n}}$ is a prior density acting as penalizing term that impacts the value of the likelihood. For small value of m_n, this term has a value associated with a higher probability than that for larger value of m_n.

We can merge all the steps from SIS and resamping step to construct the SIR algorithm which is the essential of particle filtering approach used in this work. The SIR algorithm is outlined as follows.

- **Initialization** Since the PDFs of parameters at $n = 0$ are not known. Therefore, to construct the joint PDF of all unknown parameters, the prior densities for the parameters to be estimated need to be initialized at the beginning of the filtering process. The initial particles are sampled from these prior PDFs. Statistical properties of the priors depend on the knowledge about the data and state variables. In this work, prior densities are drawn from the uniform distributions depending on the entire support space for each parameter of the distributions. Using Bayes theorem, the likelihood must be multiplied by the priors of all unknown parameters in order to create the joint PDF of the parameters.

- **Prediction** This stage starts with a set of equal weight particles from the

previous time. The frequency, amplitude, and measurement noise variance particles from the precedent step are propagated via normal densities prescribed by the transition densities of Eqs. (26)- (28), respectively.

- **Updating** As previously described that the SIS is utilized to the PF at the prediction step and it needs a transition prior to act as its importance sampling density. Now, the updating starts with a set of equal weight particles, $w_{n-1}^{i} = 1/N$. From the measurement equation and the noise in the data acquisition process, the weight of each particle is computed using the data (spectrogram slice) just arrived.

- **Resample** This stage is introduced to remedy the sampling degeneracy. A new set of particle $\left\{\mathbf{x}_n^j, w_n^j = 1/N\right\}_{i=1}^{N}$ are sampled from an approximated density $p(\mathbf{x}_n|\mathbf{Y}_n)$ computed at the updating stage. Resampling creates new particles according to the weights of their parent particles w_n^i, generating more particles when the parents have high weights; and the parents with low weights, they will be eliminated. After resampling, all particles occupy the same weight.

The block diagram to illustrate the PF framework is shown in Fig.1. To decide what frequency is the one that we are seeking for, we select the most frequent value as a point estimates of elements of frequency state vector, namely, for a frequency state vector $\mathbf{f}_n$ of a modal frequency j at time n is computed as

$$\widehat{f}_{jn} = MAP_i(f_{ijn}), \quad j = 1,\ 2,\ \ldots,\ m_n. \tag{30}$$

where $MAP_i(f_{ijn})$ represents the mode most frequent value of f_{ijn} for mode j at time step n among all particle i.

5. Simulation Results

In this work, a frequency content between 200-600 Hz generated from a source is propagating in the ocean and is observed at a hydrophone. The signal was generated according to the environment that is similar to that of the Gulf

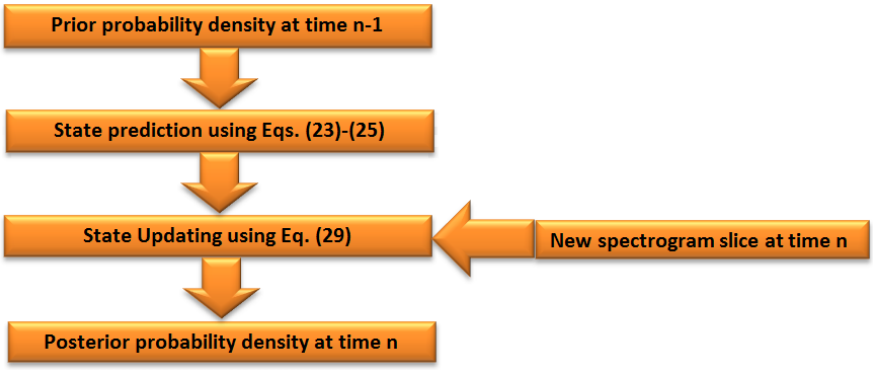

Figure 1: Block diagram of the framework.

of Mexico experiment [30], the sampling rate was 2000 Hz. The ocean acoustics time-series is shown in Fig. 2. The spectrogram of the signal as obtained from the STFT is displayed in Fig. 3.

As seen in Fig. 3 that the pattern of the dispersion curves of the signal is obviously seen after 0.3 s, therefore, we process the signal after this time. In addition, our tracking process assumption is that we are tracking the separated modal frequencies of the signal, the mentioned starting time is reasonable in this case since the pattern shows that the modes are quite well separated after this time segment. For simulation results in this work, the signal in Fig. 3 is used for the tracking process but the white Gaussian noise was added to the acoustic time-series before the STFT and spectrogram calculation. The MAP frequency trajectory estimates obtained for the PDFs as provided by the PF are illustrated in Fig. 4 with black dots and they are superimposed on a segment of the spectrogram.

To illustrate the validity of the model and the performance of the filter, we show in Fig. 5 the spectrogram slice of the signal at a particular time using a solid line; and displayed using red stars, a MAP replica of the signal obtained from the filter. We can see that the squared STFT magnitude are coinciding with MAP replica spectrum; this shows how the mathematical and statistical models made in this work are successfully combined to estimate the frequency

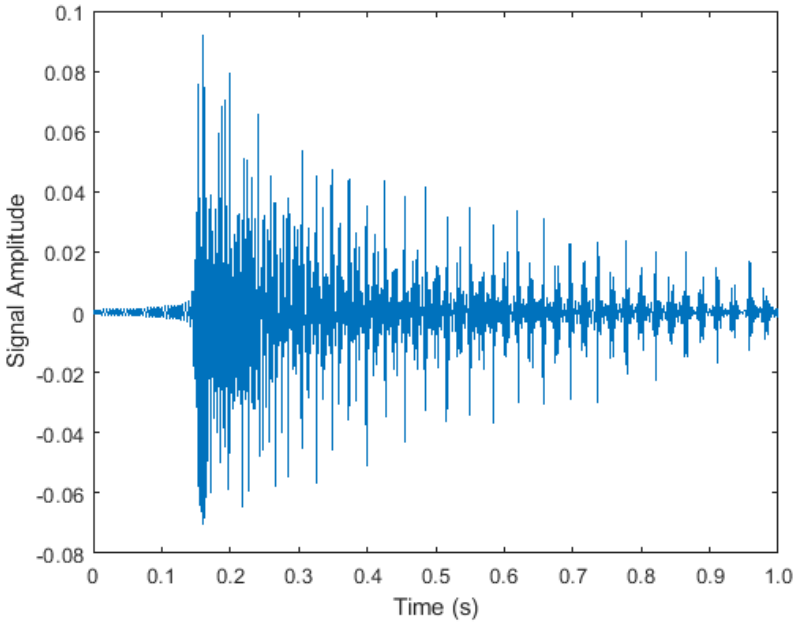

Figure 2: The synthetic ocean acoustics time-series.

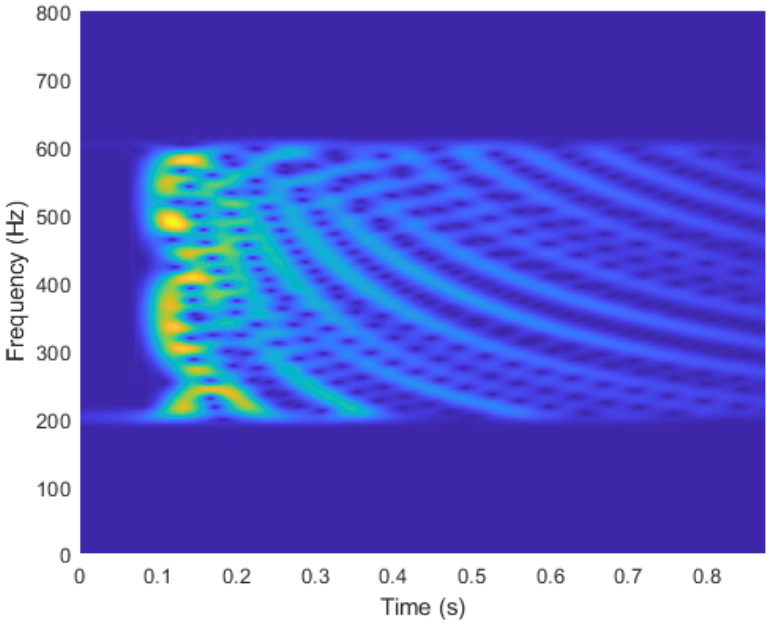

Figure 3: The spectrogram of synthetic ocean acoustics time-series.

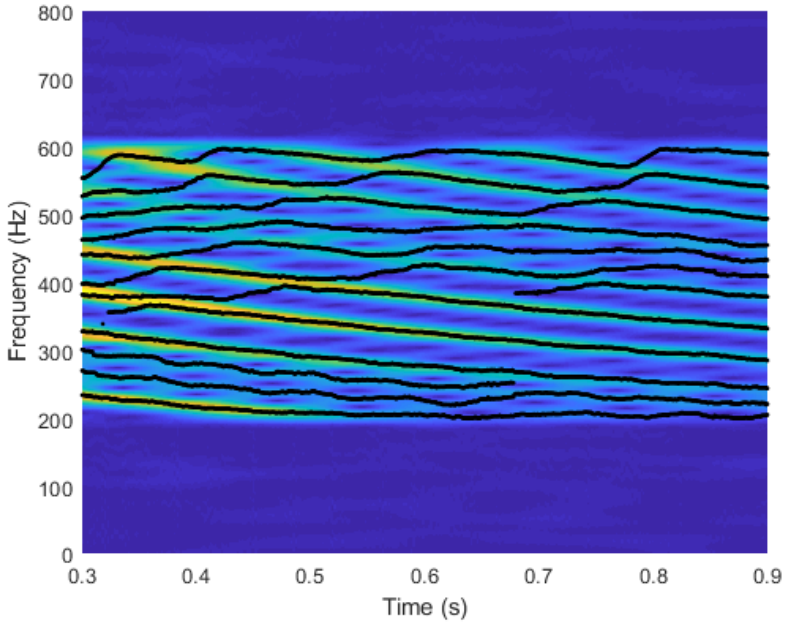

Figure 4: A segment of the spectrogram of synthetic ocean acoustics time-series to be processed.

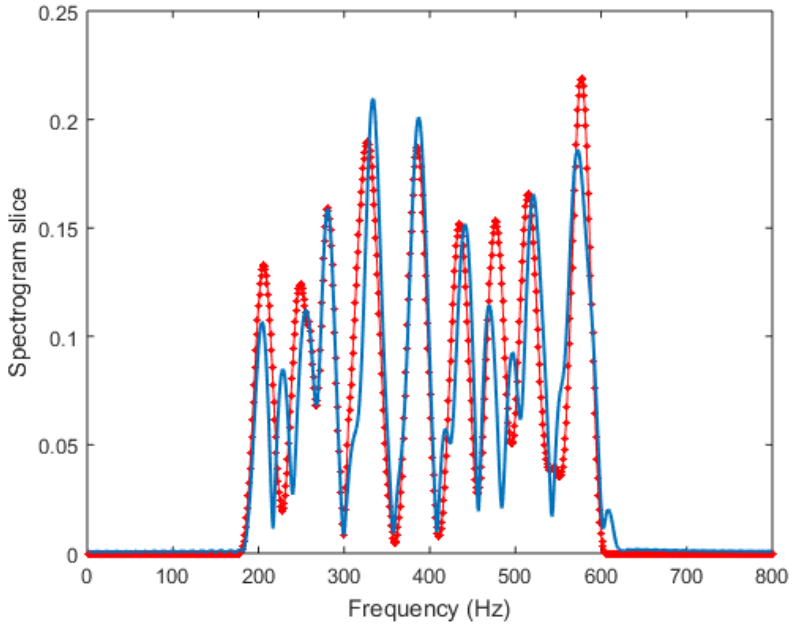

Figure 5: A spectrogram slice of the synthetic ocean acoustics time-series at a particular time (solid line) and the replica spectrum constructed using the results from the PF superimposed (red stars).

of the ocean acoustics signal.

We further investigate the robustness of the proposed model to noise by adding higher level of noise into the original signal. It should be noted that, in our work, we cannot define a single signal to noise ratio (SNR) value since the signal becomes weaker as time progresses due to the attenuation of signal with time. Two noisy realizations for different SNR levels are shown in Fig. 6, where the signal in later case was contaminated by a higher noise level as we can see from Fig. 6(b) that the spectrogram is noisier, resulting in more uncertainty in the dispersive pattern. The frequency estimates as obtained by the PF are shown in Figs 7-8. The quality of the tracking results from the filter for both cases are quite similar even the noise level in the measured signal is higher in the later one. This could be an evidence of the noise robustness of the filter

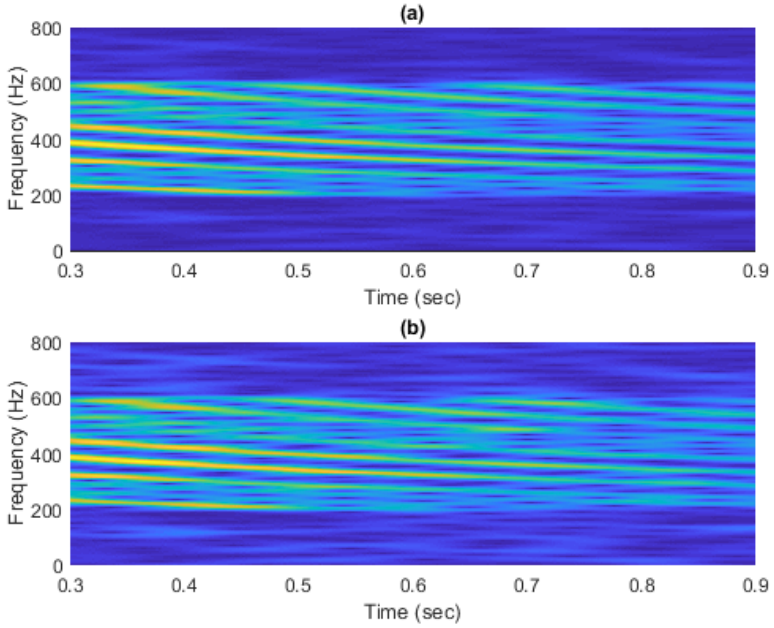

Figure 6: Two noisy realization spectrograms of the synthetic ocean acoustics time-series for two different noise levels.

which is a result of the proposed accurate statistical characteristic of the TF representation of the signal.

We provide a tracking result from a severe case where the signal is corrupted by extreme amount of noise, the spectrogram is shown in Fig. 9. The MAP frequency trajectory estimates obtained from the PF are revealed in Fig. 10. Although some modes are missing in the tracking results, the frequency estimates are fairly satisfied, and the estimated dispersion is adequate for further processing since a few modes are nicely traced by the filter and these are sufficient for the inversion for sediment sound speed profile and other geoacoustics properties [7, 8].

Root Mean Squared Error (RMSE) results from the PF implementation are shown in Fig. 11, with stars, diamonds and circles indicating the RMS errors for the average SNRs 15, 10, and 5 dB, respectively. To compare the performance

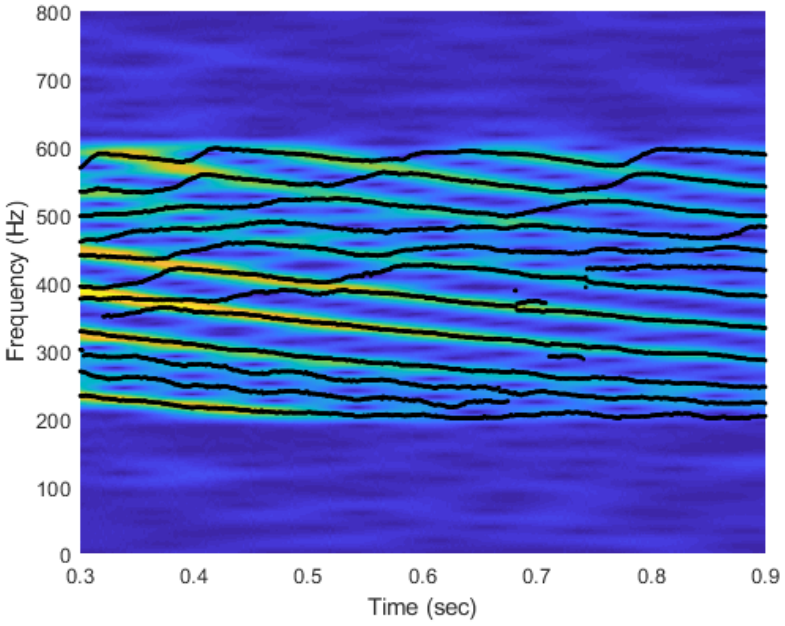

Figure 7: Tracking results as provided by the PF; the average SNR is 19.3 dB.

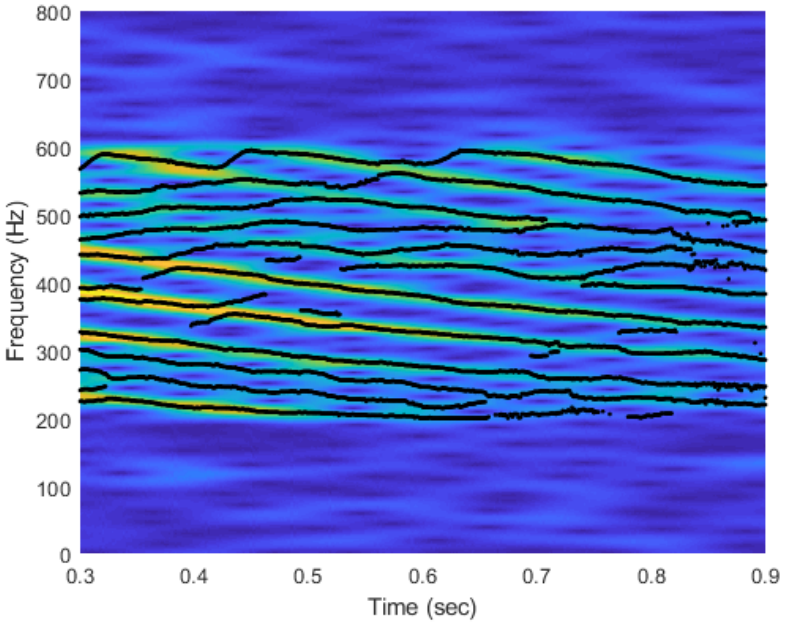

Figure 8: Tracking results as provided by the PF; the average SNR is 14.6 dB.

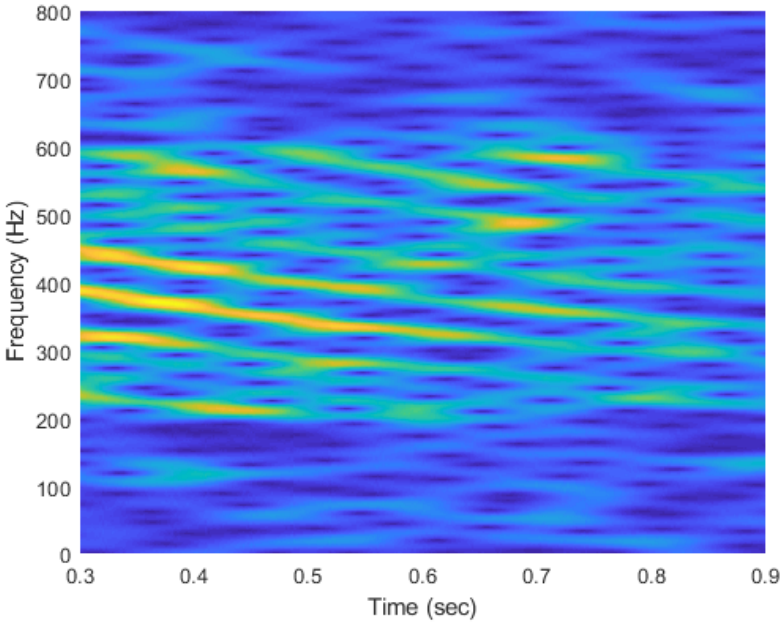

Figure 9: Spectrogram of extreme noisy ocean acoustics time-series; the average SNR is 5 dB.

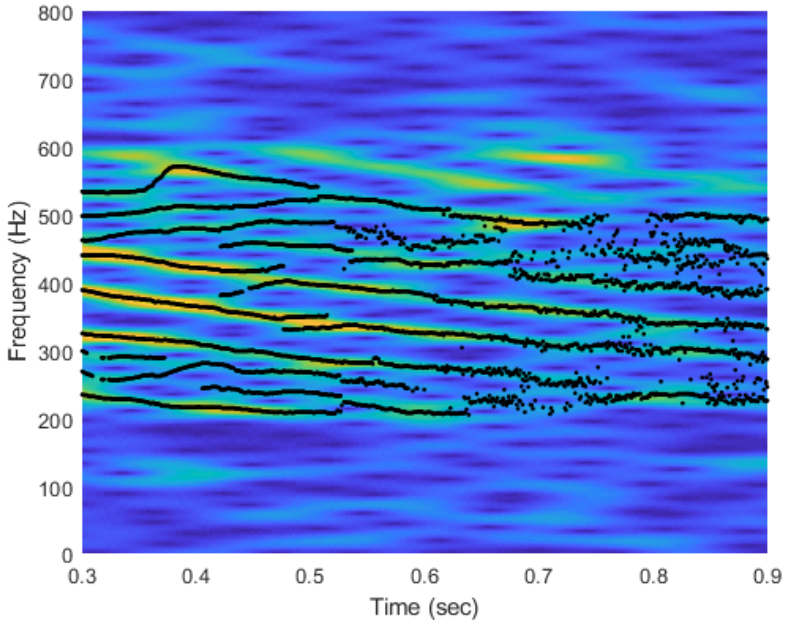

Figure 10: Frequency tracks as estimated by the PF for the extreme noisy ocean acoustics time-series; the average SNR is 5 dB.

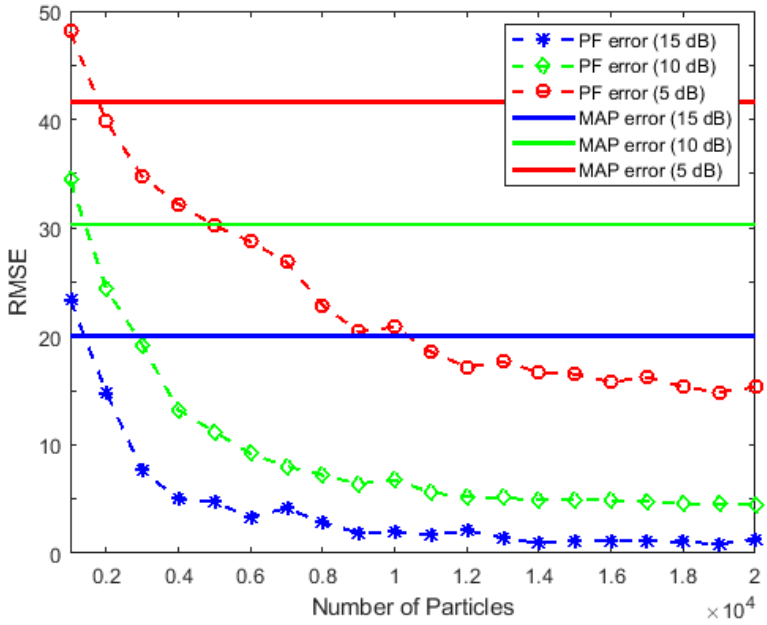

Figure 11: Comparison of PF estimation for different noise levels. Maximum likelihood estimates are superimposed.

of the filter, we perform conventional Maximum a Posteriori (MAP) estimation which is equivalent to the Maximum Likelihood (ML) estimation since uniform priors are chosen in our work. It is not surprising that for a small number of particles, the proposed method delivers high RMSE than that of the MAP estimation. This is because of a limited number of particles in the processor cannot capture a stochastic behavior of the signal. However, the errors for all cases significantly decrease as the increase of the number of particles. More importantly, the PF errors become dramatically lower than the corresponding conventional MAP errors, illustrating the superiority of the proposed method to the MAP estimation.

6. Conclusions

Mathematical description of modal frequency of ocean acoustics and an accurate statistical model are integrated to fabricate the particle filtering framework for frequency estimation of the ocean acoustics time-series. A time-frequency analysis was performed via the STFT in order to construct the accurate stochastic characteristic of the signal in the frequency domain. The likelihood function is in the form of the non-central chi-squared distribution with two degrees of freedom and this plays the crucial role in weight calculation of the particle. Based on the derived likelihood function, a multiple order particle filtering, a filter that is capable of capturing the time-varying property of the unknown number of modes of the signal, was developed for the estimation of the modal frequencies along with their corresponding amplitudes of the ocean acoustics signal. The results show that filter performs excellent tracking compared to the conventional MAP estimate. We also tested the noise robustness capability of the filter by providing the tracking results in different noise levels, and the results illustrated its performance under different noise levels. Finally, we provide a performance comparison of the proposed method with a conventional MAP estimator via the RMS errors. As expected, PF errors are significantly lower than that from the conventional MAP estimator for almost every cases, especially when higher number of particles was used.

Acknowledgements

This work was supported by the Thailand Research Fund (TRF) and the Office of the Higher Education Commission (OHEC) under the grant MRG6080152. The authors would like to thank School of Information Technology, Mae Fah Luang University for facilities support. Also, the authors would like to acknowledge the advice and support of Professor Zoi-Heleni Michalopoulou at the Department of Mathematical Sciences, New Jersey Institute of Technology, NJ, USA.

References

[1] A. A. Syed, Q. Sun, H. Foroosh, Frequency estimation of sinusoids from nonuniform samples, Signal Processing 129 (2016) 67 – 81.

[2] N. Aunsri, Z.-H. Michalopoulou, Sequential filtering for dispersion tracking and sediment sound speed inversion, J. Acoust. Soc. Am. 136 (5) (2014) 2665–2674.

[3] S. Tomar, P. Sumathi, Amplitude and frequency estimation of exponentially decaying sinusoids, IEEE Transactions on Instrumentation and Measurement 67 (1) (2018) 229–237. doi:10.1109/TIM.2017.2755998.

[4] T. Chen, L. Liu, L. Guo, Joint carrier frequency and doa estimation using a modified ula based mwc discrete compressed sampling receiver, IET Radar, Sonar Navigation 12 (8) (2018) 873–881. doi:10.1049/iet-rsn.2017.0436.

[5] E. E. Tsakonas, N. D. Sidiropoulos, A. Swami, Optimal particle filters for tracking a time-varying harmonic or chirp signal, IEEE Transactions on Signal Processing 56 (10) (2008) 4598–4610.

[6] C. Yardim, Z.-H. Michalopoulou, P. Gerstoft, An overview of sequential Bayesian filtering in ocean acoustics, IEEE J. Oceanic Eng. 36 (1) (2011) 73–91. doi:10.1109/JOE.2010.2098810.

[7] Z.-H. Michalopoulou, A. Pole, Sediment sound speed inversion with time-frequency analysis and modal arrival time probability density functions, The Journal of the Acoustical Society of America 140 (1) (2016) EL131–EL136.

[8] Z.-H. Michalopoulou, N. Aunsri, Environmental inversion using dispersion tracking in a shallow water environment, The Journal of the Acoustical Society of America 143 (3) (2018) EL188–EL193.

[9] R. E. Kalman, A new approach to linear filtering and prediction problems, Transactions of the ASME - Journal of Basic Engineering 82 (series B) (1960) 35–45.

[10] M. Arulampalam, S. Maskell, N. Gordon, T. Clapp, A tutorial on particle filters for online nonlinear/non-Gaussian Bayesian tracking, IEEE Trans. Signal Process. 50 (2002) 174–188.

[11] B. Ristic, S. Arulampalam, N. Gordon, Beyond the Kalman Filter: Particle Filters for Tracking Applications, Artech House, Boston, MA, 2004.

[12] A. Doucet, S. Godsill, C. Andrieu, On sequential Monte Carlo sampling methods for Bayesian filtering, Statistics and Computing 10 (3) (2000) 197–208.

[13] F. Gustafsson, F. Gunnarsson, N. Bergman, U. Forssell, J. Jansson, R. Karlsson, P. J. Nordlund, Particle filters for positioning, navigation, and tracking, IEEE Trans. Signal Process. 50 (2002) 425–437.

[14] F. Yang, L. Zheng, Y. Luo, A novel particle filter based on hybrid deterministic and random sampling, IEEE Access 6 (2018) 67536–67542.

[15] L. Pei, D. Liu, D. Zou, R. L. F. Choy, Y. Chen, Z. He, Optimal heading estimation based multidimensional particle filter for pedestrian indoor positioning, IEEE Access 6 (2018) 49705–49720.

[16] T. C. Yang, A method for measuring the frequency dispersion for broadband pulses propagated to long ranges, The Journal of the Acoustical Society of America 76 (1) (1984) 253–261.

[17] I. Zorych, Z.-H. Michalopoulou, Particle filtering for dispersion curve tracking in ocean acoustics, J. Acoust. Soc. Am. 124 (2) (2008) EL45–EL50.

[18] Z.-H. Michalopoulou, A Bayesian approach to modal decomposition in ocean acoustics, J. Acoust. Soc. Am. 126 (5) (2009) EL147–EL152.

[19] N. Aunsri, S. Hemrungrote, A Bayesian approach for frequency estimation using TV AR model for ocean acoustics time-series, in: Signal and Information Processing Association Annual Summit and Conference (APSIPA), 2014 Asia-Pacific, 2014, pp. 1–4. doi:10.1109/APSIPA.2014.7041813.

[20] G. Potty, J. Miller, P. Dahl, C. Lazauski, Geoacoustic inversion results from the ASIAEX East China Sea Experiment, J. Acoust. Soc. Am. 29 (4) (2004) 1000–1010.

[21] S. D. Rajan, K. M. Becker, Inversion for range-dependent sediment compressional-wave-speed profiles from modal dispersion data, IEEE Journal of Oceanic Engineering 35 (1) (2010) 43–58.

[22] H. Dong, S. E. Dosso, Bayesian inversion of interface-wave dispersion for seabed shear-wave speed profiles, IEEE Journal of Oceanic Engineering 36 (1) (2011) 1–11.

[23] C. Li, S. E. Dosso, H. Dong, D. Yu, L. Liu, Bayesian inversion of multimode interface-wave dispersion from ambient noise, IEEE Journal of Oceanic Engineering 37 (3) (2012) 407–416.

[24] R. V. Hogg, J. W. McKean, A. T. Craig, Introduction to Mahematical Statistics, 6th Edition, Pearson Prentice Hall, 2005.

[25] J. V. Candy, Bayesian Signal Processing: Classical, Modern and Particle Filtering Methods, John Wiley & Sons, New Jersey, 2009.

[26] A. Kong, J. S. Liu, W. H. Wong, Sequential imputations and Bayesian missing data problems, J. Amer. Statist. Assoc. 89 (425) (1994) 278–288.

[27] P. Malarvezhi, R. Kumar, Particle filter with novel resampling algorithm: A diversity enhanced particle filter, Wireless Personal Communications. 84 (4) (2015) 3171–3177.

[28] J. R. Larocque, J. P. Reilly, W. Ng, Particle filters for tracking an unknown number of sources, IEEE Trans. Signal Processing 50 (12) (2002) 2926–2937.

[29] C. Hory, N. Martin, A. Chehikian, Spectrogram segmentation by means of statistical features for non-stationary signal interpretaion, IEEE Trans. Signal Processing 50 (12) (2002) 2915–2925.

[30] Z.-H. Michalopoulou, M. B. Porter, J. P. Ianniello, Broadband source localization in the Gulf of Mexico, J. Comput. Acoust. 4 (1996) 361–370.

Particle Filtering with Adaptive Resampling Scheme for Modal Frequency Identification and Dispersion Curves Estimation in Ocean Acoustics

Nattapol Aunsri[a,b,*], Kosin Chamnongthai[c]

[a] *School of Information Technology, Mae Fah Luang University, Chiang Rai, Thailand*
[b] *Brain Science and Engineering Innovation Research Group, Mae Fah Luang University, Chiang Rai, Thailand*
[c] *Faculty of Engineering, King Mongkuts University of Technology Thonburi, Bangkok, Thailand*

Abstract

The goal of this work is to accurately estimate the modal frequencies and dispersion curves from a measured ocean acoustics signal. A particle filtering approach, a class of sequential Monte Carlo methods, is developed for modal frequency identification and dispersion curves estimation from a time-frequency representation of ocean acoustics signal. The adaptive resampling algorithm for enhancing the quality of a set of particles after likelihood calculation is implemented to improve the accuracy of the modal estimates as well as the dispersion curves of the signal. Results demonstrate the advantages in implementing the adaptive resampling into the conventional sequential importance sampling particle filter (SIS-PF) instead of using the sequential importance resampling (SIR) scheme. The noise robustness of the proposed method is demonstrated through examples where the realizations of different Signal-to-Noise Ratio (SNR) levels were used to test the performance of the adaptive resampling method. The results display the evidences that the adaptive resampling particle filter (AR-PF) is superior to the SIR-PF. Via root mean square error (RMSE), the AR-PF delivers smaller errors than those obtained by the SIR-PF for all SNR levels, emphasizing the benefit in incorporating the adaptive resampling into the PF

*Corresponding author
Email address: nattapol.aun@mfu.ac.th (Nattapol Aunsri)

for modal frequency identification and dispersion curves estimation of ocean acoustics signal.

Keywords: Modal frequency, frequency identification, dispersion curve, adaptive resampling, particle filter, ocean acoustics.

1. Introduction

The task of signal estimation and detection is one of the most important areas in signal processing. The problem of frequency estimation has been very challenging for decades. In ocean acoustics, the signals that propagate in the medium carry information about the underwater environments. Extracting information from these signals allows us to obtain the medium characteristics and, hence, the system design for environmental study, climate monitoring, and defense applications can be achieved efficiently. The frequency content embedded in the ocean acoustics time-series is one of the quantities that has been extensively utilized for the ocean acoustics inversion since it occupies the ability to exhibit the dispersion characteristic of the ocean acoustics signals. To accomplish this task, we worked on the frequency domain via the short time Fourier transforms (STFTs) to identify the modal frequencies of the ocean acoustics signal. This is done by constructing the replicas of the original signal and then formulating the likelihoods to perform Bayesian inference on the modal frequencies [1, 2].

An appropriate processor framework to handle the noise in such a way that the impact on the embedded information of interest is minimized can be obtained from the ability in dealing with the characterization of the signal and that of the noise. This characterization is to capture the stochastic model that relates statistical properties of the information and noise effectively. The difficulties, however, can be regarded as the uncertainty of noise identification. In other words, when the statistical properties of noise are not easily determined, consequently, the characteristic of the noise may not be justified precisely. As

for the view of filtering, the accuracy of the estimated parameters of interest cannot be satisfied. Simple Bayesian filtering methods may fail to give satisfactory results. Not only does the noise characterization has the capability of the filtering, most physical systems in practice are classified as nonlinear systems, thus dictating the complexity of the mathematical models used for describing the observed data and the interested parameters. These complications have brought engineers and scientists to focus on a sophisticated filtering approach that can deal with these problems effectively.

A Particle filtering framework, a class of sequential Monte Carlo method, is concerned with the estimation of the underlying posterior probability distribution of a random data of interest for performing statistical inferences, allowing the extraction of the desired information from noisy measurement data. This kind of filtering framework has started from the Kalman Filter (KF) [3]. It is the very first well-known filter in sequential Bayesian filtering framework and it delivers an optimal estimator for the minimum mean squared error goal. The assumption for the implementation of this filter is that the evolution of the unknown parameters is classified in the cases of Gaussian and additive perturbations, the additive Gaussian noise model present in the observed data, and a linear function describing the measurements and state vector parameters.

Many practical systems in real world problems are nonlinear/non-Gaussian and non-additive noise systems, therefore, a simple filtering framework cannot work with these systems properly. Consequently, the generalizations of the standard KF filter are required to handle such kind of problems. In literature, variants of the KFs were proposed and implemented for solving those problems including extended Kalman filter (EKF) [4, 5, 6], unscented Kalman filters (UKFs) [7], and ensemble Kalman filter (EnKF) [8]. Unfortunately, a large number of problems with highly nonlinear models and complex noise processes are not easy to deal with, and they require a computational or numerical approach for the formulation of the desired posterior PDFs and the inferences on the state parameters. Particle filtering is a powerful framework to deal with nonlinear filtering developed for such scenarios using stochastic computational

techniques for nonlinear/non-Gaussian systems, which comes into the consideration. Some problems in ocean acoustics that the particle filtering approach was used are reported in the literature [1, 9, 10, 11, 12, 13, 14]. In addition, it was also used in acoustic source tracking application which can be found from the work in [15].

Conventional particle filter is implemented based on the sequential importance resampling (SIR) algorithm. This formulation usually initiates the sampling impoverishment problem, leading to the situation that the particles suffer from the loss of their diversity. This stems from the fact that the particle filtering method formulates new samples from a set of discrete random numbers for a representation of the continuous probability distribution. For the extreme case, when SIR recursively performs, only one particle is used to represent a whole parameter space, thus resulting in a failure of the process. There are developments of enhancing algorithm in order to remedy this problem as found in the studies done by [16, 17, 18]. We extended the work in [19] to this study to improve the performance of the PF for the identification of the modal frequencies and dispersion curves of the ocean acoustics signals.

The remainder of this paper is structured as follows. Section 2 provides a short review of particle filtering framework and describes the adaptive resampling scheme. Section 3 presents a mathematical ocean acoustics modelling via the time-frequency space of the ocean acoustics signals that were propagated in the medium. We discuss in Section 4 how the PF formulation based on the constructed ocean acoustics model can be constructed to identify the modal frequencies and estimate the dispersion curves. In Section 5, we present the results of the modal estimates from particle filters; ones from the conventional resampling scheme and ones from adaptive resampling method. Section 6 is devoted to the dispersion tracking. We show in this section the evidences that the adaptive resampling method offers better tracking results than the conventional resampling. Conclusions follow in Section 7.

2. Particle Filtering with Adaptive Resampling Scheme

2.1. Sequential Filtering Framework and Particle filter

Working in a sequential filtering framework, we implemented PFs for identifying the trajectories of the modal frequencies of the ocean acoustics signal with time. It must be clearly noted here that the KF families cannot be applied to our problem because the relationship between the observed data and the state parameters (modal frequencies) is nonlinear. To utilize the PF framework, let $\mathbf{X}_k = [\mathbf{x}_1, \mathbf{x}_2, \ldots, \mathbf{x}_k]$ be the sequence of the unknown state vectors and $\mathbf{Y}_k = [\mathbf{y}_1, \mathbf{y}_2, \ldots, \mathbf{y}_k]$ be the set of the observations measured at the first k time steps. The goal of the method is to gather the posterior PDF of the unknown state parameters when the observed data is available at time step k, $p(\mathbf{X}_k|\mathbf{Y}_k)$, and it can be given as:

$$p(\mathbf{X}_k|\mathbf{Y}_k) = \frac{p(\mathbf{Y}_k|\mathbf{X}_k)p(\mathbf{X}_0)}{p(\mathbf{Y}_k)}, \tag{1}$$

where $p(\mathbf{X}_0)$ is the prior density and we assume it to be a uniform density in this work, i.e., the chance of the existence of the modal frequencies is assumed to be equal over the search interval. The observation $\mathbf{y}_k$ is independent of the states at all other times and we assume that the observation data up to step k are also independent. To justify the possible states when the data is observed, we constructed the likelihood function based on the assumption explained above as $p(\mathbf{Y}_k|\mathbf{X}_k) = \prod_{i=1}^{k} p(\mathbf{y}_i|\mathbf{X}_k)$. In addition, the first order Markov process is considered, incorporating the prior density allows us to rewrite Eq.(1) as:

$$p(\mathbf{X}_k|\mathbf{Y}_k) = \frac{p(\mathbf{x}_0)\prod_{i=1}^{k} p(\mathbf{y}_i|\mathbf{x}_i)p(\mathbf{x}_i|\mathbf{x}_{i-1})}{p(\mathbf{Y}_k)}. \tag{2}$$

The construction of the state space model is typically based on two equations as follows:

$$\mathbf{X}_k = \mathbf{f}_{k-1}(\mathbf{X}_{k-1}, \mathbf{v}_{k-1}), \tag{3}$$

and

$$\mathbf{Y}_k = \mathbf{g}_k(\mathbf{X}_k, \mathbf{w}_k). \tag{4}$$

The first one is the state equation that describes how the states evolve with time. The transition of the states from the consecutive time is followed the nonlinear function $\mathbf{f}_{k-1}$ under the first order Markov process as given in Eq. (3). The second equation, Eq.(4), is called the observation equation that describes the relation between the observation data and the state vector through a nonlinear function $\mathbf{g}_k$. Both $\mathbf{f}_k$ and $\mathbf{g}_k$ are known in this work which will be discussed later. The state and observation noise quantities are declared as $\mathbf{v}_k$ and $\mathbf{w}_k$, respectively.

For particle filtering, at each time step, the approximated probability density $p(\mathbf{x}_k|\mathbf{y}_k)$ is built by the probability mass function (PMF) using a set of random samples with their associated weights as

$$p(\mathbf{x}_k|\mathbf{y}_k) \approx \sum_{i=1}^{N} w_k^i \delta(\mathbf{x}_k - \mathbf{x}_k^i) \tag{5}$$

and

$$w_k^i \propto \frac{p(\mathbf{X}_k^i|\mathbf{Y}_k)}{q(\mathbf{X}_k^i|\mathbf{Y}_k)}, \tag{6}$$

where δ is the Dirac delta function, and N is the number of particles used in the approximation. The accuracy of the filter, i.e., the performance of the approximated distribution to the continuous density, increases as the increasing of N [20, 21]. In other words, $\sum_{i=1}^{N} w_k^i \delta(\mathbf{x}_k - \mathbf{x}_k^i) \rightarrow p(\mathbf{x}_k|\mathbf{y}_k)$ as $N \rightarrow \infty$. The quantity $q(\mathbf{X}_k^i|\mathbf{Y}_k)$ is the importance density. Since we assume that our process follows the first order Markov process, the results from the previous time step $k-1$ and the importance density can be chosen whereas the minimization of the IS errors is achieved, we therefore obtain the importance weight for each particle as (for full derivation details, please consult [21])

$$w_k^i = p(\mathbf{y}_k|\mathbf{x}_k^i) w_{k-1}^i. \tag{7}$$

One way the SIS performance can be sabotaged is by seeing that the variance of the importance weights always increases monotonically over time. After running a filtering process for a few iterations, only few particles tend to occupy high weights but close to zero for the rest. In some extreme cases, just

only one particle is a survival and it holds a unit weight. This means that the diversity of particle distribution is not achieved and this results in the failure of the posterior probability distribution representation by using this framework. This problem is called degeneracy. There has been number of improvements from the proposed algorithms to overcome the degeneracy problem; the wildly use method is called a resampling process, an extra step that is performed after particle weight calculation. The trick of the resampling is eliminating small importance weight particles and, on the other hand, those of the large weights are regenerated. The amount of regeneration depends on the importance weights of the parent particles. We call the process that combines SIS and resampling as sequential importance resampling (SIR) [22]. The resampling step is typically performed when the effective number of particles N^{eff} falls below a threshold as discussed in [23, 24, 25]. The effective number of particles is determined as

$$N^{eff} = \frac{1}{\sum_{i=1}^{N}(w_k^i)^2}. \tag{8}$$

2.2. Adaptive Resampling

Even with the resampling step reducing the effects of degeneracy, new problems still occurs [21]. First, resampling step introduces the limitation of the ability to parallelize the SIS algorithm because all weights have to be summed during normalization. Second, the assumption of statistical independence is no longer valid after resampling. Therefore, convergence issues are generated along the process if resampling takes a serious loss of particle validity. For some cases, a problem that may arise after resampling is the loss of particle diversity due to all of the particles being identical as a result from a replication of those particles with high importance weights, breaking down to a noninformative distribution. This is well-known as sample impoverishment which is commonly exhibited when the noise level in the observed data is low. Recently, there are some developments of PFs [17, 21, 26, 27] that have been designed to resolve these problems.

In this work we incorporated the *adaptive resampling* scheme for eliminating the loss of particle diversity problem. This is one of the main concerns of the conventional SIR problems. The scheme was introduced in a seismic event tracking application [16] and it was successfully applied to the PF for frequency estimation using a time-varying autoregressive model [19]. New particles for the next state are constructed based on the weights of their parent particles. Number of the offspring particles, $m_k^i = \lceil N w_k^i \rceil + M$, is calculated and then the process generates the offspring particles from their parents $\mathcal{N}(x_k^i, \lambda_k^i)$. M is an integer chosen empirically. Note that $\lceil \bullet \rceil$ creates the roundup to the nearest integer. Amount of new particles also depends on the weights of their parents and the quantity λ_k^i, called fission factor, that is used to control the offsprings construction. The fission factor of the ith particle can be computed by [16]

$$\lambda_k^i = \Big[1 + exp\Big(\frac{w_k^i - \overline{w}_k}{\max\limits_i \; w_k^i - \overline{w}_k}\Big)\Big]^{-1}, \tag{9}$$

where $\overline{w}_k$ represents the mean of the weights at time step k. Then we create new particles based on the parent particles and the corresponding fission factor as

$$x_k^j \sim \mathcal{N}(x_k^i, \lambda_k^i), \tag{10}$$

where x_k^j and x_k^i are the offspring the parent particles, respectively.

Eq. (9) works as follows: if a parent particle occupies low weight, the higher fission degree is obtained, dictating the process to create higher quality particles. On the other hand, if the parent particle has high weight, the lower fission degree acts as a protector to conserve the high quality parent particle. In summary, the adaptive resampling process creates a new better set of particles based on the importance weights of their parent particles, and then propagates this new set into the next time step.

3. Modal Frequency Approach in Time-Frequency Representation of Ocean Acoustics Model

The evolution of the frequency content of an acoustic signal with time plays a key role as a "*footprint*" of the propagation medium. This is typically the case with broadband signals with frequencies of a few hundred Hz propagating from long distances in underwater environments. The frequency content with time exhibits the variation pattern as a result of dispersion characteristics of the waveguide, allowing the estimation of modal arrival times and amplitudes for various modes and frequencies within each mode.

The ocean acoustics model in the time-frequency space can be considered as a broadband acoustic signal received at a hydrophone. The acoustic signal received at a hydrophone in the ocean can be expressed as

$$p(r,z,z_r,t) = \frac{1}{2\pi}\sum_n \int_{-\infty}^{+\infty} \mu(\omega^{'}) G_n(r,z,z_r,\omega^{'}) exp\{i(\omega^{'}t - k_n r - \frac{\pi}{4})\} d\omega^{'}. \quad (11)$$

where r represents the distance between source and receiver, z and z_r are the source and receiver depths, respectively, k_n stands for the modal wave number, μ is the source spectrum, $\omega = 2\pi f$, where f is frequency in Hz and

$$G_n(r,z,z_r,\omega) = \frac{i\sqrt{\pi}}{\rho(z_r)\sqrt{2k_n r}} \Psi_n(z)\Psi_n(z_r), \quad (12)$$

where Ψ_n are orthogonal, normalized, depth-dependent functions, and $\rho(z_r)$ is the medium density. To simplify the analysis, we consider now only one mode. The frequency spectrum of a finite time segment of the signal is given by [28, 29]:

$$P_n(\omega,t) = \int_{t-\Delta t}^{t+\Delta t} p_n(r,z,z_r,t) e^{-i\omega\tau} d\tau, \quad (13)$$

whereas the segment starts and ends at $t - \Delta t$ and $t + \Delta t$, respectively. Substituting the nth term of Eq. (11) into Eq. (13) and performing integration, we then obtain

$$P_n(\omega,t) = \frac{e^{-i\omega t}}{\pi} \int_{\infty}^{\infty} \mu(\omega^{'}) G_n(r,z,z_r,\omega^{'}) \frac{\sin(\omega^{'} - \omega)\Delta t}{\omega^{'} - \omega} exp\{i(\omega^{'}t - k_n r - \frac{\pi}{4})\} d\omega^{'}. \quad (14)$$

We can approximate the above quantity by using stationary phase approximation technique as explained in [29], then the squared frequency spectrum of a finite time segment of the signal can be expressed as

$$|P_n(\omega,t)|^2 = \frac{\pi}{|k_n''|^2}|\mu(\omega_n)G_n(r,z,z_r,\omega_n)|^2\Big|\frac{\sin(\omega-\omega_n)\Delta t}{\omega-\omega_n}\Big|^2, \tag{15}$$

for $|\omega-\omega_n| < \frac{\pi}{\Delta t}$.

It can be clearly seen that the spectrum expressed in Eq. (15) has a peak at ω_n which is called a *modal frequency*. This observation allows us to formulate a PF framework for tracking the instantaneous power spectral peaks to identify the modal frequencies of the acoustic signal, which will be discussed in the next section.

4. Particle Filtering Formulation for Modal Frequency Identification

To construct the PF equations, we here use f_n for instantaneous modal frequency instead of ω_n. From the above analysis, we can express the observation equation of Eq. (4) as follows:

$$\mathbf{y}_k = \sum_{j=1}^{M_k} a_{kj}[sinc(f-f_{kj})]^2 + \mathbf{w}_k. \tag{16}$$

The quantity f_{kj} is a value containing the modal frequency of mode j at time step k, and M_k is the order or number of modal frequencies (modes) at time step k. The observed data $\mathbf{y}_k$ is the squared magnitude of the Fourier transform of the acoustics time series, and this model is considered in the frequency domain. For each time step (spectrogram slice), the center of a *sinc* is a position of modal frequency and it evolves with time. By connecting the modal frequencies at all spectrogram slice, it creates full trajectories of the frequencies, providing the estimation of a dispersive pattern of the ocean acoustics signal. The measurement noise $\mathbf{w}_k$ is assumed here to be an additive, zero mean, and normally distributed, that is, $\mathbf{w}_k \sim \mathcal{N}(\mathbf{0},\sigma_k^2)$. It should be noted that even the assumption of the noise is Gaussian type but the system is highly nonlinear since the state and the observed data are related via a nonlinear function. Therefore,

the PF is considered to be a framework for modal frequency and dispersion curves tracking in this work.

Number of modal frequencies is varied with time, therefore we also need to estimate the number of the modal frequencies for each time slice. To do so the multiple order particle filter (MMPF) is required [30]. In addition, we also assumed in this work that the amplitude of each modal frequency and the noise variance are not known. Therefore, number of modal frequencies along with the noise variance must also be estimated at every time slices; the strategies to deal with this can be found in [1, 31, 32].

For each time step, the predicting frequency at the current step is obtained from the frequency at the previous time and a small perturbation, $\mathbf{v}_{k-1}$. The state equation containing those parameters to be estimated is given by

$$\mathbf{x}_k = \mathbf{x}_{k-1} + \mathbf{v}_{k-1}, \tag{17}$$

here $\mathbf{x}_k$ is a vector containing modal frequencies.

For each iteration, once the importance weights of particles are computed based on the observation equation of Eq. (16) which forms the Gaussian error model, the full joint posterior PDF for modal frequencies, modal amplitudes, number of modes, and observation noise variance is [1],

$$p(\mathbf{x_k}, \mathbf{a_k}, \mathbf{M_k}, \sigma_k^2 | \mathbf{y}_k) \propto \frac{1}{\sigma_k^2} \frac{1}{(2\pi\sigma_k^2)^{R/2}} \frac{1}{L^{M_k}} exp\{-\frac{1}{2\sigma_k^2} \|\mathbf{y}_k - \sum_{j=1}^{M_k} a_{kj}[sinc(f - x_{kj})]^2\|^2\}. \tag{18}$$

where R is the length of the analysis window of the Fourier transform, $\mathbf{a_k}$ is a vector containing modal amplitudes that correspond to the modal frequencies at time step k, and M_k is the number of modal frequencies at time step k. A prior $1/L^{M_k}$ acts as a penalization factor that protects the process from favoring a large order. At this point, the adaptive resampling scheme is then performed in order to obtain a new efficient set of particles for the next time slice.

The joint posterior PDFs obtained from both sampling methods are identical by means of the form of equation. However, the approximated PDFs constructed from both methods are different since they are formulated from different sets of

particles. Since a set of particles after resampling using adaptive reasampling method is better than the SIR method, the approximated PDF from adaptive resampling PF (AR-PF) also represents joint PDFs that are closer to the true ones. Simulation results to illustrate this are provided in Section 6.

5. Modal Identification

To test the performance of the AR-PF, we employed the SIR-PF and AR-PF to the data generated for a realistic underwater medium. Fig. 1 displays a noise-free spectrogram of an ocean acoustics signal calculated from a length of the time-segment 180 via a short-time Fourier transform with hamming window. A slice of the spectrogram at time 200 ms is shown in Fig. 2. We can see that there are a few modes that appear at this time slice. It should be noted that we can have up to six modes but the possibility for this scenario is very low. To justify the number of modes, the filter allows itself to track model order and the decision is based on the weights of particles. We assume that the signal contains at least one modal component and may not exceed six modes. Particle filter initialization is constructed with a uniform prior for the searching frequency interval of 200-600 Hz, therefore we initiated the frequency particles with $\mathbf{x} \sim \mathcal{U}[200, 600]$, where $\mathbf{x} \sim \mathcal{U}[a, b]$ is the uniform distribution PDF with parameters a and b. Also, the noise variance particles are initiated according to work reported in [1].

Next we show the modal estimates from the SIR-PF and AR-PF where the signal is clean, as seen in Fig. 3. The number or particles used in this experiment was 500 for both filters. The results shown in Fig. 3 are the estimated spectrums as obtained by SIR-PF that is shown with red colour, and by AR-PR as displayed with green colour. The modal frequencies (spectral peaks) are calculated from the highest posterior probability, i.e., the modal frequencies are identified via the *maximum a posterior* (MAP) estimator, i.e., the most frequent value of the tracking parameter is chosen. From the results, the estimated spectrums from both filters coincide nicely with the squared FT magnitude of the acoustic

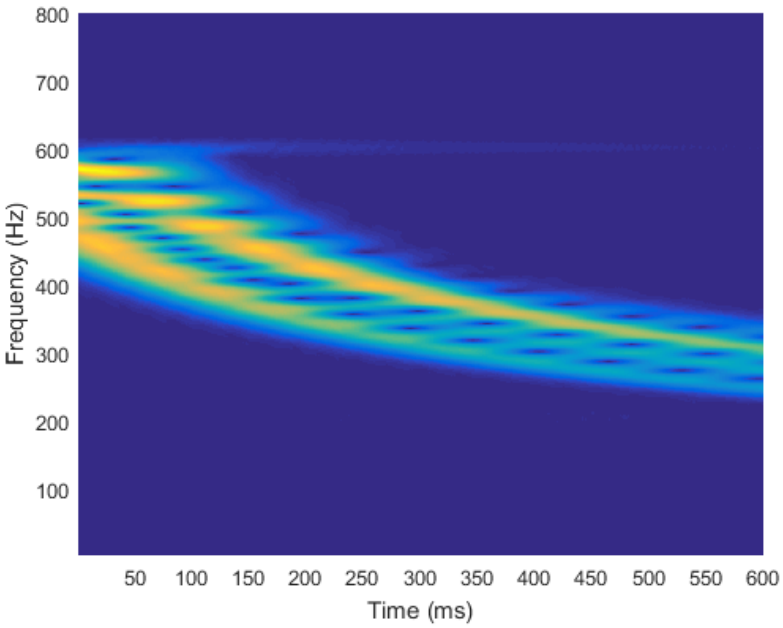

Figure 1: Spectrogram of an ocean acoustics signal.

data. This is not surprising that the SIR-PF can capture almost all of the useful information embedded in the data since the noise level is extremely small. For this case AR-PF may not be necessary.

We further illustrate the tracking results when the noise level becomes higher. Noise is assumed to contaminate the signal in the frequency domain and we added the same amount for all time slices. Since the spectrogram becomes weaker as time progresses, a single signal-to-noise ratio (SNR) cannot be defined but is decreasing as time evolves.

We demonstrated, with number of particles of 1000 for both filters, in Fig. 4 that the performance of the AR-PF becomes superior than the SIR-PF when the noise level is increased. The SIR-PF can estimate the modal frequencies in the spectrogram only with those modes that occupy high amplitudes. For the frequencies with low amplitudes, SIR-PF fails to do so but the AR-PF. A zoomed in version of Fig. 4 is provided to demonstrates the AR-PF. This

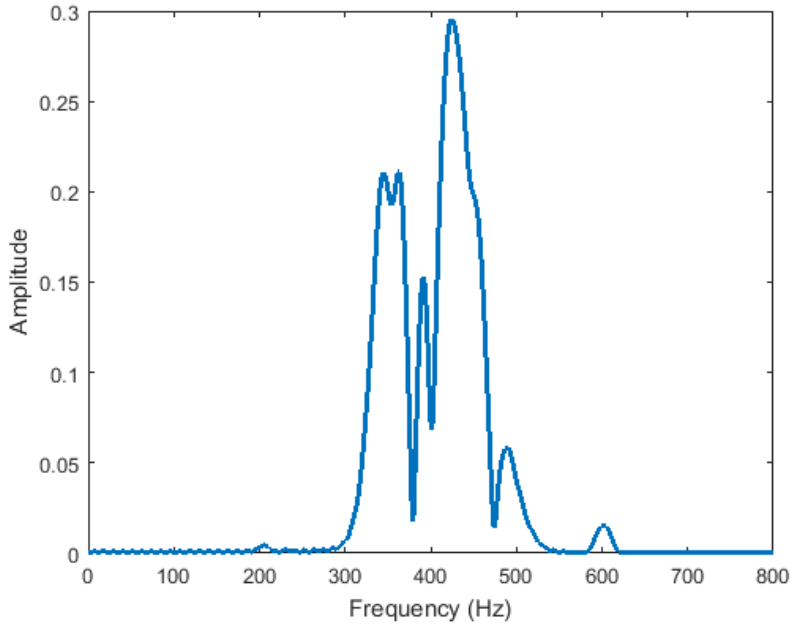

Figure 2: A slice of the spectrogram at time 200 ms.

evidence is presented in Fig. 5 which obviously presents that a modal frequency of 458 Hz can be captured by the AR-PF while the SIR-PF cannot track it. The AR-PF, therefore, exhibits an excellent match between the estimated spectrum and the observed noisy data.

Finally, we demonstrated the robustness of the AR-PF where the acoustic signal was contaminated by a high level of noise, i.e., the SNR is low. Again, the number of particles used for this test was 5000. The illustrating example of the modal identification at time slide 250 ms is shown in Fig. 6. In Fig. 6(a), we show the original signal and its noisy realization, while the estimates from SIR-PF and AR-PF, and plot of original signal are presented in 6(b). The estimates from SIR-PF are displayed using red colour, the estimates from AR-PF are indicated by the green colour, and the black line is the original signal. The estimated spectrum as obtained from the AR-PF clearly outperforms that from the SIR-PF. For this case, we obviously observed that the SIR-PF loses

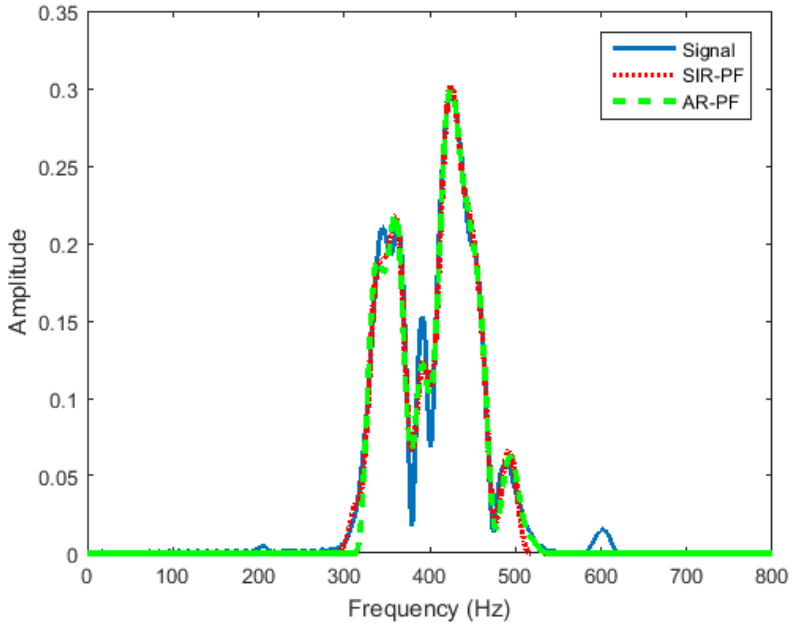

Figure 3: A slice of the spectrogram at time 200 ms (solid line) with the modal spectrum constructed using the MAP estimates for the SIR-PF and AR-PF superimposed.

its capability to track the modal frequencies effectively since most peaks of the estimates from the SIR-PF do not match with those of the original ones. On the other hand, peaks and modal amplitudes are almost similar to the original signal, therefore, AR-PF offers an estimated spectrum that is closed to the original signal. Another observation is that the SIR-PF also misses a modal frequency at 455 Hz, but not with the AR-PF. This demonstration is to emphasize the robustness capability of the AR-PF.

6. Dispersion Tracking

We now perform the full sequential Bayesian filtering framework to obtain dispersion curves of the ocean acoustics signal. According to the acoustic model of the propagated signal under the dispersive media discussed in Section 3, we utilized the particle filtering along with the adaptive resampling scheme to

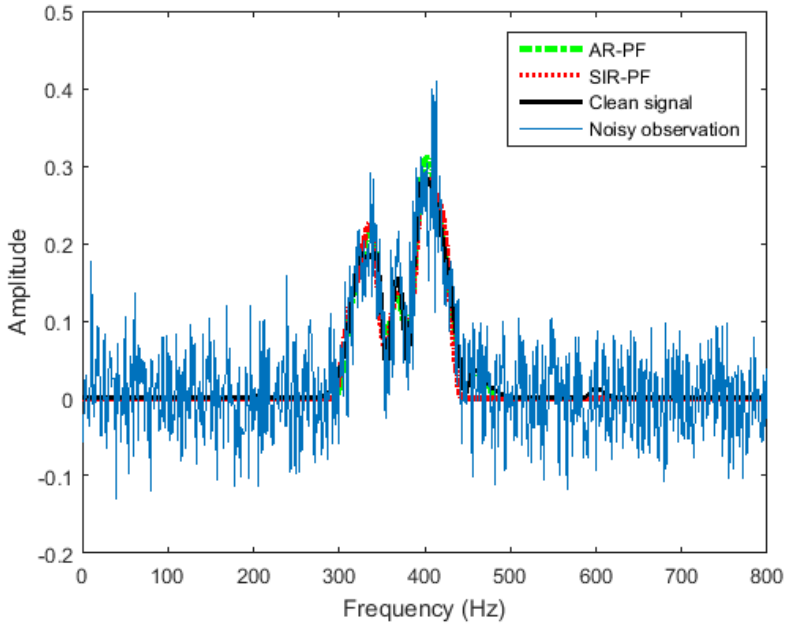

Figure 4: A slice of the spectrogram at time 250 ms (solid line) with the modal spectrum constructed using the MAP estimates for the SIR-PF and AR-PF superimposed.

extract the modal frequencies of the acoustic signal. These frequencies form the dispersion characteristic of the ocean acoustics property via the dispersion curves that were obtained from the PF.

We showed in Fig. 7 the spectrogram of the noisy ocean acoustics signal. It should be noted that the signal is weaker as time increases, therefore the SNR cannot be defined as a single SNR for the whole signal but it is decreasing as time evolves. We set the number of particles for this experiment to 2000 for both filters. The tracking results from the SIR-PF and AR-PF are shown in Figs. 8-9. For the first 350 ms, the tracks from the SIR-PF and AR-PF are not significantly different. However, the tracks from AR-PF are better than those from the SIR-PF as clearly seen from the present of more uncertainty in the tracks from SIR-PF, meaning that the ability to handle the noise of the SIR-PF is inferior to that of the AR-PF. Moreover, at time 450-475 ms, we observed

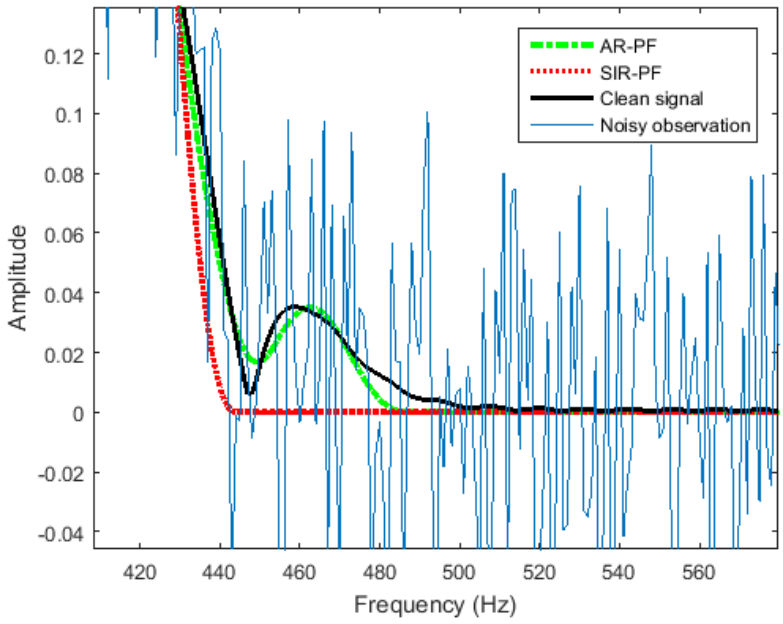

Figure 5: Illustration of the ability of AR-PF to capture a mode with modal frequency of 458 Hz.

that the estimates from AR-PF do not deliver ambiguity but SIR-PF, as seen at the top most tracks.

To get a better justification of the performance of the filters, we compute the RMS error (RMSE) defined by the L_2 norm averaged over K spectrogram slides:

$$RMSE = \sqrt{\frac{1}{K}\sum_{k=1}^{K} ||\mathbf{f}_k^{'} - \hat{\mathbf{f}}^{'}_k||^2} \tag{19}$$

where $\mathbf{f}_k^{'}$ is the vector of true values of the normalized frequencies and $\hat{\mathbf{f}}^{'}_k$ is the vector containing the normalized frequency estimates at time step k. The RMSE values from both filters are shown in Table 1. Please be noted that the SNR for each case is the average SNR over all slices since the SNR for each slice varies with time as mentioned earlier. From the Table, for any SNR levels, the

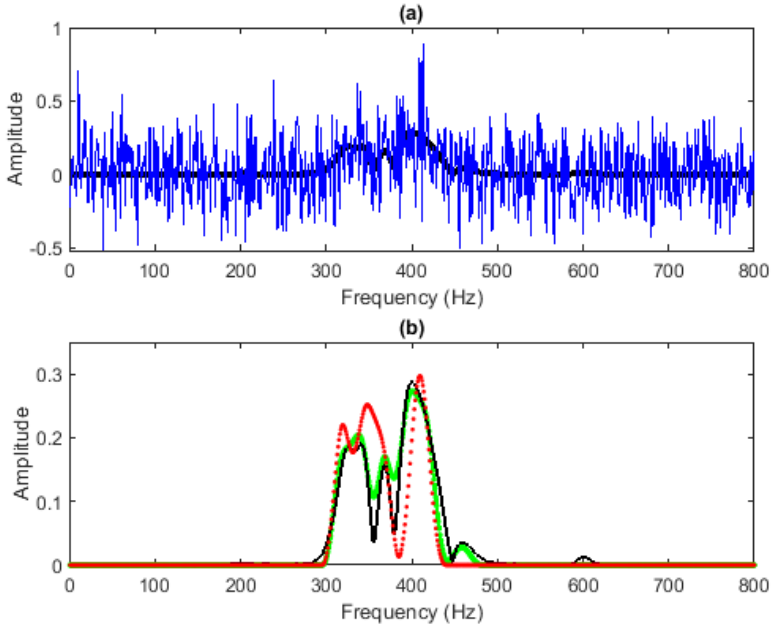

Figure 6: Original and estimated spectrums at time 250 ms from AR-PF and SIR-PF for low SNR: (a) original signal (black) and its noisy realization (blue); (b) original signal (black), estimated spectrum as obtained by the SIR-PF (red), and estimated spectrum as obtained by the AR-PF (green).

AR-PF provides lower RMSEs than the SIR-PF. Moreover, the quality of the estimation by the AR-PF is much better when the SNR levels become lower as seen from much higher RMSEs for the SIR-PF compared to RMSEs for AR-PF.

Next, we present the robustness of the proposed filter by considering two different SNRs, the SNRs vs time for the two noise levels are displayed in Fig. 10. For the SNR level of Fig. 10(a), in Fig. 11 we demonstrated how the proposed filter is robust to the noise. It can be obviously seen that the quality of the frequency estimates from the AR-PF is much better than those from the SIR-PF, resulting in an excellent tracking as the dispersion curves can be followed nicer by using AR-PF. We observed from the tracks from the SIR-PF that the appearance of noisy tracks is more obvious as the decreasing of the SNR. More evidence to show the robustness of the proposed filter is also

Table 1: Prediction performance of PF via RMSE with different SNR levels.

Average SNR (dB)	**RMSE**$_{(SIR-PF)}$	**RMSE**$_{(AR-PF)}$
3	0.2122	0.1565
-3	0.2982	0.1855
-7	0.3653	0.2321
-10	0.4592	0.2959

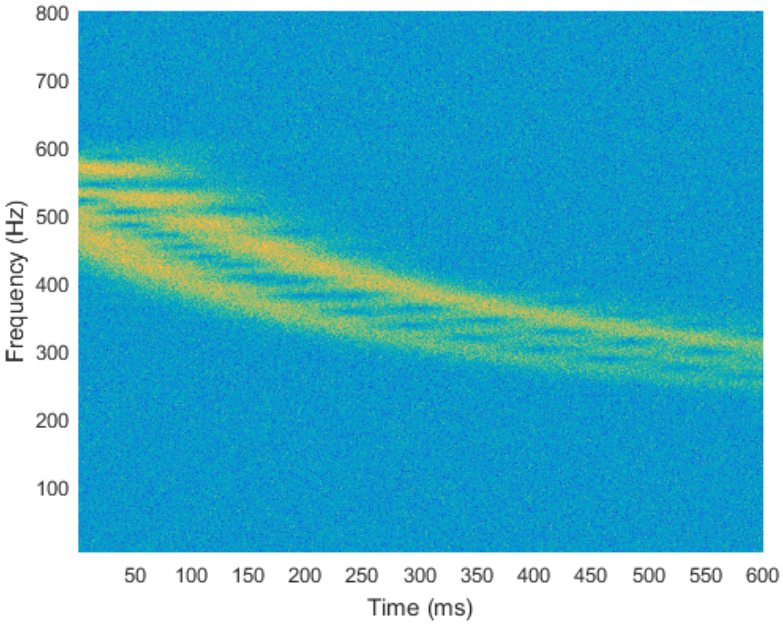

Figure 7: Spectrogram of a noisy ocean acoustics signal.

revealed in the tracks from AR-PF shown in Fig. 12, where the noise level for this test is given in Fig. 10(b). The frequency estimates that were obtained from the AR-PF is superior to those obtained from the SIR-PF, the tracks after 250 ms from the AR-PF is much better since more modes can be tracked very well while the SIR-PF losses its capability to do so.

We showed in Fig. 13(a) the frequency estimates from the SIR-PF, while

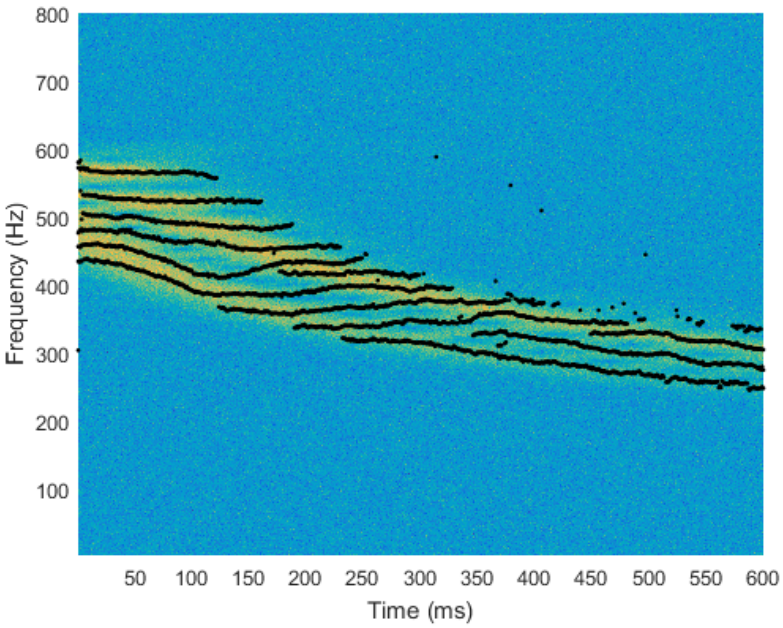

Figure 8: Frequency tracks of a noisy ocean acoustics signal as estimated by the SIR-PF.

in Fig. 13(b) the frequency estimates from the AR-PF, the average SNR level in this case was -7 dB. The quality of the frequency trajectories from AR-PF is maintained better than the ones obtained from the SIR-PF, especially when the signal becomes weaker, i.e. for noisier situations. Therefore the AR-PF offers a better estimated dispersion curves than the SIR-PF. To investigate the capability in capturing the modal frequencies PDFs of the ocean acoustics signal of both filters, Fig. 14 demonstrates the frequency PDFs at time 200 ms obtained from the filters. At time 200 ms, the signal contains 3 modes: the true values of modal frequencies are 358, 389, and 396 Hz. It is obviously seen that the AR-PF delivers high likelihood regions to the true values and it can detect all modes, but the SIR-PF can detect only two modes. Moreover, the AR-PF provides lower uncertainty in frequency estimation, resulting in a better tracking performance.

Finally, we comprehensively validated the adaptive resampling algorithm by

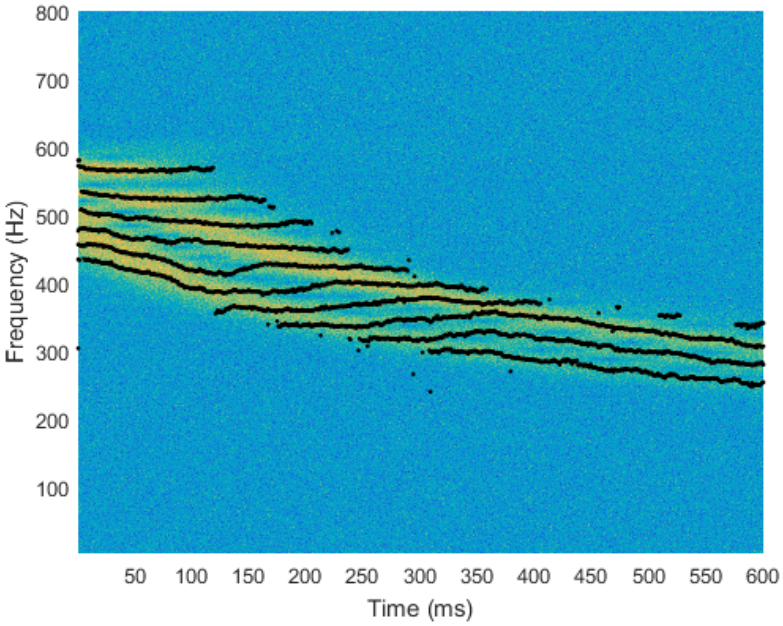

Figure 9: Frequency tracks of a noisy ocean acoustics signal as estimated by the AR-PF.

varying the number of particles and average noise levels. Shown in Fig. 15 is the Monte Carlo RMSE (MCRMSE) over all spectrogram slides $K = 600$ and N_r noisy realizations, the MCRMSE is defined by

$$MCRMSE = \sqrt{\frac{1}{KN_r}\sum_{k=1}^{K}||\mathbf{f}_k^{'} - \hat{\mathbf{f}}^{'}_k||^2} \tag{20}$$

where $\mathbf{f}_k^{'}$ and $\hat{\mathbf{f}}^{'}_k$ are as defined previously, two-hundred realizations were run for a Monte Carlo performance evaluation, $N_r = 200$.

MCRMSEs are plotted against the number of particles, line with squares and line triangles to represent the MCRMSEs for AR-PF and SIP-PF, respectively. In the figure, blue lines with marks indicate the errors for average SNR of 3 dB; red lines with marks indicate the errors for average SNR of 3 dB; and magenta lines with marks indicate the errors for average SNR of -7 dB. With the number of particles increasing, the errors are significantly reduced as a result

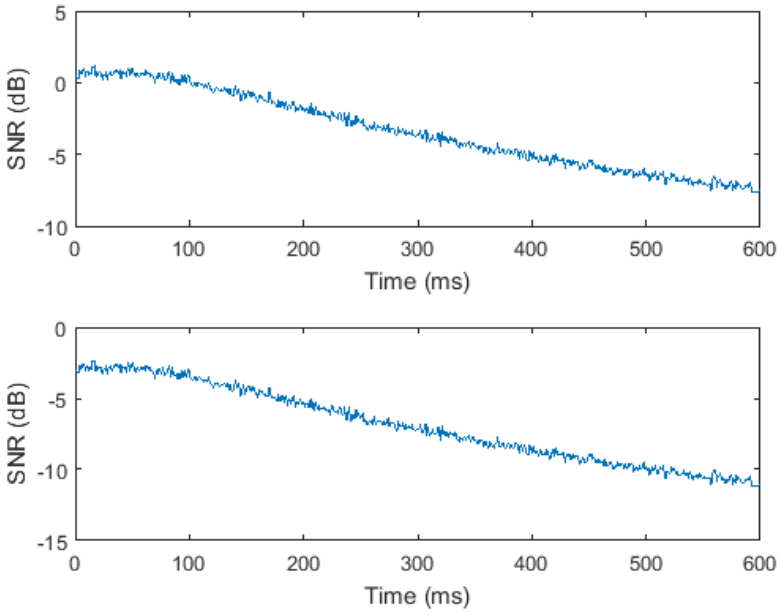

Figure 10: The SNR of a noisy ocean acoustics signal for two different noise levels as a function of time.

from the approximated PDFs that are closer to the true ones, demonstrating the advantage in using large number particles. In addition, for any SNR levels, PF provides smaller errors for both resampling methods, but the errors from the AR-PF are significantly smaller than the errors from SIR-PF, illustrating the benefit of implementing the adaptive resampling instead of the conventional resampling method. These results confirm that the AR-PF can handle the ocean acoustics signal with a low SNR efficiently.

7. Conclusions

Mathematical and statistical models are integrated to construct the particle filtering framework along with an efficient adaptive resampling scheme for the identification of the modal frequencies and dispersion curves tracking in the ocean acoustics signal. The broadband acoustic signal propagating in the

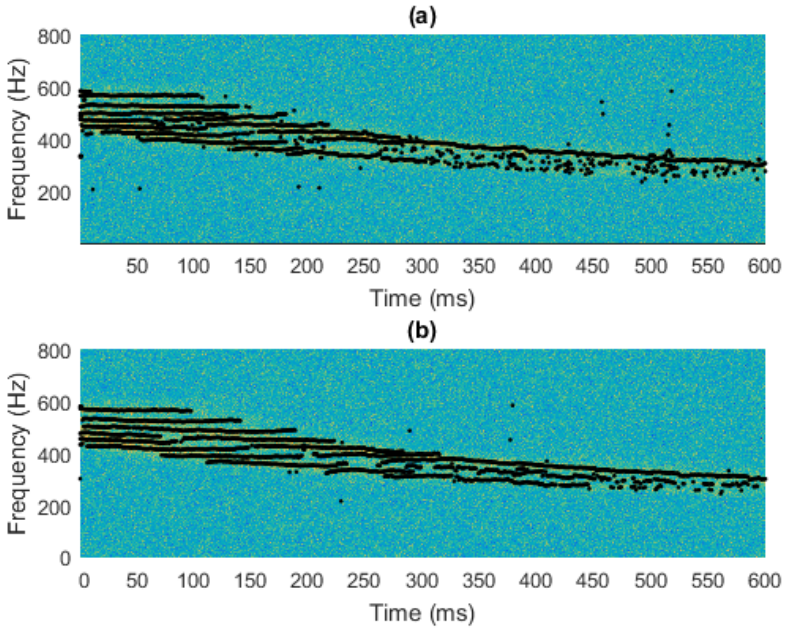

Figure 11: Frequency tracks of a noisy ocean acoustics signal with SNR of Fig. 10(a) as estimated by: (a) SIR-PF and (b) AR-PF.

medium is considered in the time-frequency representation of the signal via the STFTs. Each modal frequency is modelled as the squared *sinc* waveform centered at the modal frequency and each time slice allows multiple modes to appear. The adaptive resampling scheme offers a new better set of particles that will be used for the next time step, allowing the modal frequencies and dispersion curves to be extracted more efficiently. The simulation results show that the AR-PF performs much better than the SIR-PF for all SNR levels. The modal frequencies and dispersion curves are successfully tracked using the developed method and the estimates with AR-PF are substantially better than the conventional SIR-PF, especially for low SNR. Finally, we illustrated via the Monte carlo RMSE vs the number of particles that the tracking performance of the AR-PF was found to be noticeably superior, obtaining much lower errors for all SNR levels.

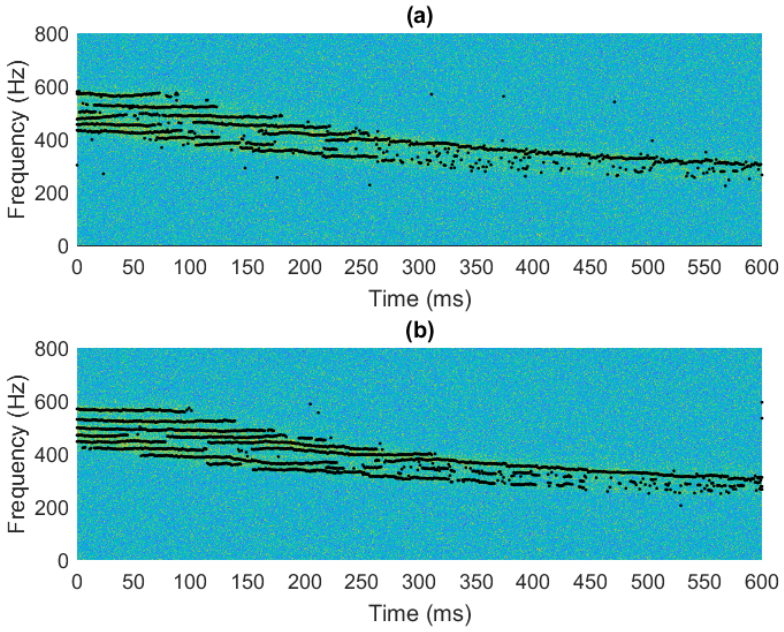

Figure 12: Frequency tracks of a noisy ocean acoustics signal with SNR of Fig. 10(b) as estimated by: (a) SIR-PF and (b) AR-PF.

Acknowledgements

This work was supported by the Thailand Research Fund (TRF) and the Office of the Higher Education Commission (OHEC) under the grant MRG6080152. The authors would like to thank School of Information Technology, Mae Fah Luang University for facilities support. Also, the authors would like to acknowledge the advice and support of Professor Zoi-Heleni Michalopoulou at the Department of Mathematical Sciences, New Jersey Institute of Technology, NJ, USA.

References

[1] N. Aunsri, Z.-H. Michalopoulou, Sequential filtering for dispersion tracking and sediment sound speed inversion, J. Acoust. Soc. Am. 136 (5) (2014) 2665–2674.

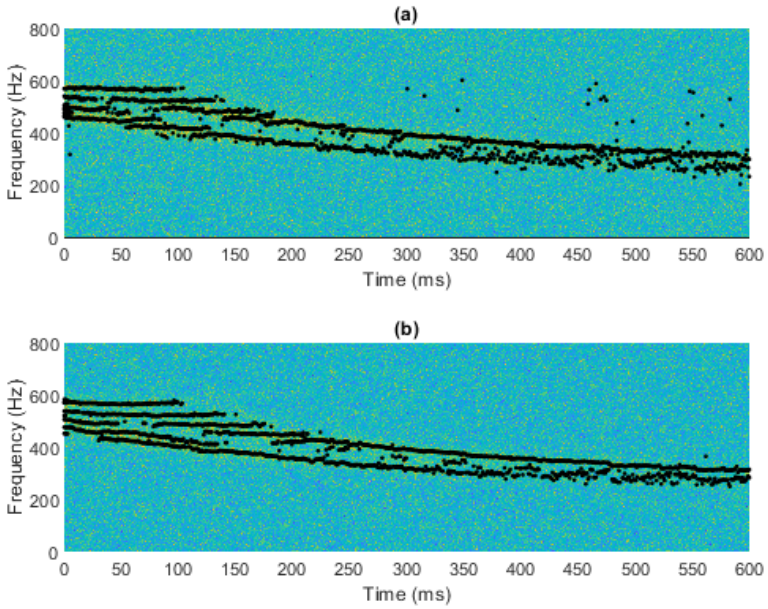

Figure 13: Tracking for two filters: (a) SIR-PF and (b) AR-PF. The numbers of particles was 10,000.

[2] N. Aunsri, A Bayesian filtering approach with time-frequency representation for corrupted dual tone multi frequency identification, Engineering Letters 24 (4) (2016) 370–377.

[3] R. E. Kalman, A new approach to linear filtering and prediction problems, Transactions of the ASME - Journal of Basic Engineering 82 (series B) (1960) 35–45.

[4] J. V. Candy, E. J. Sullivan, Model-based processor design for a shallow water ocean acoustic experiment, J. Acoust. Soc. Am. 95 (4) (1994) 2038–2051.

[5] J. V. Candy, D. H. Chambers, Model-based dispersive wave processing: A recursive Bayesian solution, J. Acoust. Soc. Am. 105 (6) (1999) 3364–3374.

[6] O. Carrière, J.-P. Hermand, J.-C. Le Gac, M. Rixen, Full-field tomography

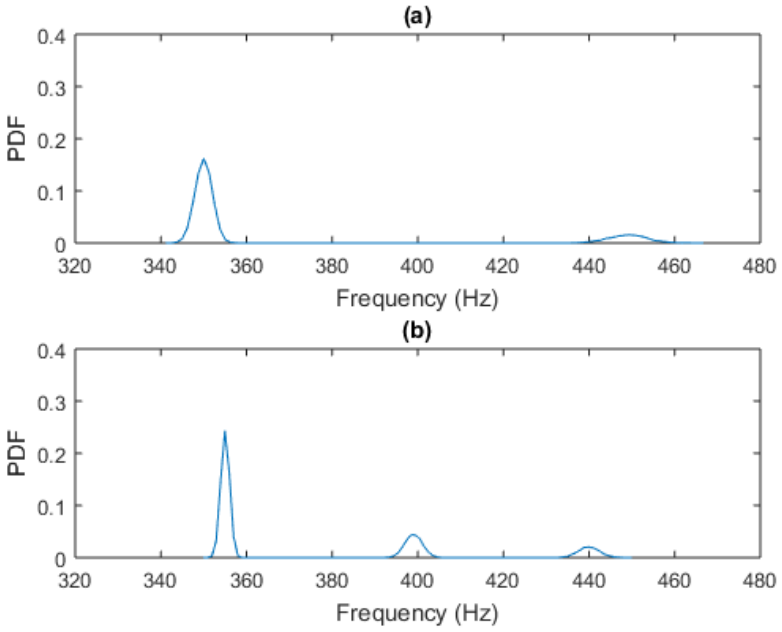

Figure 14: The frequency probability density functions for the signal at time 200 ms. (a) The frequency PDFs as obtained by SIR-PF and (b) the frequency PDFs as obtained by AR-PF.

and Kalman tracking of the range-dependent sound speed field in a coastal water environment, J. Mar. Syst. 78 (4) (2009) S382–S392.

[7] C. Yardim, P. Gerstoft, W. S. Hodgkiss, Sensitivity analysis and performance estimation of refractivity from clutter techniques, Radio Science 44 (2009) RS1008.

[8] O. Carrière, J.-P. Hermand, J. V. Candy, Inversion for time-evolving sound-speed field in a shallow ocean by ensemble Kalman filtering, IEEE J. Oceanic Eng. 34 (4) (2009) 586–602.

[9] J. V. Candy, Environmentally adaptive processing for shallow ocean applications: A sequential bayesian approach, The Journal of the Acoustical Society of America 138 (3) (2015) 1268–1281. arXiv:https://doi.org/

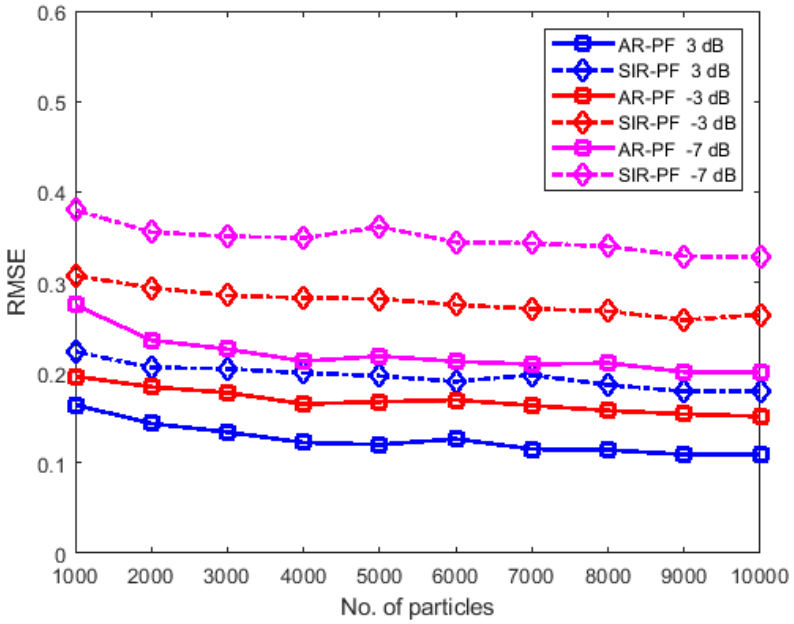

Figure 15: Comparison of PF estimation performance at average SNRs of 3, -3, and -7 dB: RMS errors are plotted vs the number of particles.

10.1121/1.4928140, doi:10.1121/1.4928140.
URL https://doi.org/10.1121/1.4928140

[10] N. Aunsri, S. Hemrungrote, A Bayesian approach for frequency estimation using TV AR model for ocean acoustics time-series, in: Proceedings. Asia-Pacific Signal and Information Processing Association Annual Summit and Conference (APSIPA), 2014, pp. 1–4.

[11] Z.-H. Michalopoulou, N. Aunsri, Environmental inversion using dispersion tracking in a shallow water environment, J. Acoust. Soc. Am. 143 (3) (2018) EL188–EL193. doi:10.1121/1.5026245.

[12] C. Yardim, Z.-H. Michalopoulou, P. Gerstoft, An overview of sequential Bayesian filtering in ocean acoustics, IEEE J. Oceanic Eng. 36 (1) (2011) 73–91. doi:10.1109/JOE.2010.2098810.

[13] R. Duan, K. Yang, F. Wu, Y. Ma, Particle filter for multipath time delay tracking from correlation functions in deep water, The Journal of the Acoustical Society of America 144 (1) (2018) 397–411. arXiv:https://doi.org/10.1121/1.5047671, doi:10.1121/1.5047671.
URL https://doi.org/10.1121/1.5047671

[14] Z. Yang, H. Zhao, W. Xu, Bayesian passive acoustic tracking of a cooperative moving source in shallow water, IET Radar, Sonar Navigation 8 (3) (2014) 202–208. doi:10.1049/iet-rsn.2012.0338.

[15] K. A. Steen, J. H. McClellan, O. Green, H. Karstoft, Acoustic source tracking in long baseline microphone arrays, Applied Acoustics 87 (2015) 38 – 45. doi:https://doi.org/10.1016/j.apacoust.2014.06.002.
URL http://www.sciencedirect.com/science/article/pii/S0003682X14001534

[16] X. Han, H. Lin, Y. Li, H. Ma, X. Zhao, Adaptive fission particle filter for seismic random noise attenuation, IEEE Geoscience and Remote Sensing Letters 12 (9) (2015) 1918–1922.

[17] P. Malarvezhi, R. Kumar, Particle filter with novel resampling algorithm: A diversity enhanced particle filter, Wireless Personal Communications. 84 (4) (2015) 3171–3177.

[18] C. Musso, N. Oudjane, F. LeGland, "Improving regularised particle filters" , in A. Doucet, N. de Freitas, and N. Gordon, Sequential Monte Carlo Methods in Practice, Springer, New Jersey, 2001.

[19] N. Aunsri, A TVAR particle filter with adaptive resampling for frequency estimation, in: 2016 International Symposium on Intelligent Signal Processing and Communication Systems (ISPACS), 2016, pp. 1–5. doi:10.1109/ISPACS.2016.7824772.

[20] J. V. Candy, Bayesian Signal Processing: Classical, Modern and Particle Filtering Methods, John Wiley & Sons, New Jersey, 2009.

[21] B. Ristic, S. Arulampalam, N. Gordon, Beyond the Kalman Filter: Particle Filters for Tracking Applications, Artech House, Boston, MA, 2004.

[22] A. F. M. Smith, A. E. Gelfand, Bayesian statistics without tears: A sampling-resampling perspective, Amer. Statistician 46 (1992) 84–88.

[23] N. J. Gordon, D. J. Salmond, A. F. M. Smith, Novel approach to nonlinear/non-Gaussian Bayesian state estimation, IEE Proc. F, Radar and Signal Processing 140 (2) (1993) 107–113.

[24] A. Doucet, S. Godsill, C. Andrieu, On sequential Monte Carlo sampling methods for Bayesian filtering, Statistics and Computing 10 (3) (2000) 197–208.

[25] A. Kong, J. S. Liu, W. H. Wong, Sequential imputations and Bayesian missing data problems, J. Amer. Statist. Assoc. 89 (425) (1994) 278–288.

[26] O. Cappé, S. Godsill, E. Moulines, An overview of existing methods and recent advances in sequential Monte Carlo, Proc. IEEE 95 (5) (2007) 899–924.

[27] F. Gustafsson, F. Gunnarsson, N. Bergman, U. Forssell, J. Jansson, R. Karlsson, P. J. Nordlund, Particle filters for positioning, navigation, and tracking, IEEE Trans. Signal Process. 50 (2002) 425–437.

[28] Z.-H. Michalopoulou, A Bayesian approach to modal decomposition in ocean acoustics, J. Acoust. Soc. Am. 126 (5) (2009) EL147–EL152.

[29] T. C. Yang, A method for measuring the frequency dispersion for broadband pulses propagated to long ranges, The Journal of the Acoustical Society of America 76 (1) (1984) 253–261.

[30] J. R. Larocque, J. P. Reilly, W. Ng, Particle filters for tracking an unknown number of sources, IEEE Trans. Signal Processing 50 (12) (2002) 2926–2937.

[31] C. Andrieu, M. Davy, A. Doucet, Improved auxiliary particle filtering: applications to time-varying spectral analysis, in: 11th IEEE Signal Processing Workshop on Statistical Signal Processing, 2001, pp. 309–312.

[32] Z.-H. Michalopoulou, R. Jain, Particle filtering for arrival time tracking in space and source localization, J Acoust. Soc. Am. 132 (5) (2012) 3041–3052. doi:10.1121/1.4756954.

REFERENCES

[1] C. Andrieu and A. Doucet. Joint Bayesian model selection and estimation of noisy sinusoids via reversible jump MCMC. *IEEE Trans. Signal Processing*, 47(10):2667 –2676, Oct 1999.

[2] M. Arulampalam, S. Maskell, N. Gordon, and T. Clapp. A tutorial on particle filters for online nonlinear/non-Gaussian Bayesian tracking. *IEEE Trans. Signal Process.*, 50:174–188, 2002.

[3] N. Aunsri. A TVAR particle filter with adaptive resampling for frequency estimation. In *2016 International Symposium on Intelligent Signal Processing and Communication Systems (ISPACS)*, pages 1–5, Oct 2016.

[4] N. Aunsri. Effect of window functions on the sequential bayesian filtering based frequency estimation. In *The 21st International Symposium on Wireless Personal Multimedia Communications (WPMC- 2018),*, pages 411–415, 2018.

[5] N. Aunsri and S. Hemrungrote. A Bayesian approach for frequency estimation using TV AR model for ocean acoustics time-series. In *Signal and Information Processing Association Annual Summit and Conference (APSIPA), 2014 Asia-Pacific*, pages 1–4, Dec 2014.

[6] N. Aunsri and Z.-H. Michalopoulou. Sequential filtering for dispersion tracking and sediment sound speed inversion. *J. Acoust. Soc. Am.*, 136(5):2665–2674, 2014.

[7] G. E. P. Box and G. C. Tiao. *Bayesian Inference in Statistical Analysis*. Addison–Wesley, New York, 1992.

[8] J. V. Candy. *Bayesian Signal Processing: Classical, Modern and Particle Filtering Methods*. John Wiley & Sons, New Jersey, 2009.

[9] O. Cappé, S. Godsill, and E. Moulines. An overview of existing methods and recent advances in sequential Monte Carlo. *Proc. IEEE*, 95(5):899–924, 2007.

[10] T. Chen, L. Liu, and L. Guo. Joint carrier frequency and doa estimation using a modified ula based mwc discrete compressed sampling receiver. *IET Radar, Sonar Navigation*, 12(8):873–881, 2018.

[11] H. Dong and S. E. Dosso. Bayesian inversion of interface-wave dispersion for seabed shear-wave speed profiles. *IEEE Journal of Oceanic Engineering*, 36(1):1–11, 2011.

[12] A. Doucet, S. Godsill, and C. Andrieu. On sequential Monte Carlo sampling methods for Bayesian filtering. *Statistics and Computing*, 10(3):197–208, 2000.

[13] F. Gustafsson, F. Gunnarsson, N. Bergman, U. Forssell, J. Jansson, R. Karlsson, and P. J. Nordlund. Particle filters for positioning, navigation, and tracking. *IEEE Trans. Signal Process.*, 50:425–437, 2002.

[14] X. Han, H. Lin, Y. Li, H. Ma, and X. Zhao. Adaptive fission particle filter for seismic random noise attenuation. *IEEE Geoscience and Remote Sensing Letters*, 12(9):1918–1922, Nov. 2015.

[15] R. V. Hogg, J. W. McKean, and A. T. Craig. *Introduction to Mahematical Statistics*. Pearson Prentice Hall, 6th edition, 2005.

[16] C. Hory, N. Martin, and A. Chehikian. Spectrogram segmentation by means of statistical features for non-stationary signal interpretaion. *IEEE Trans. Signal Processing*, 50(12):2915–2925, 2002.

[17] R. E. Kalman. A new approach to linear filtering and prediction problems. *Transactions of the ASME - Journal of Basic Engineering*, 82 (series B):35–45, 1960.

[18] A Kong, J. S. Liu, and W H Wong. Sequential imputations and Bayesian missing data problems. *J. Amer. Statist. Assoc.*, 89(425):278–288, 1994.

[19] J. R. Larocque, J. P. Reilly, and W. Ng. Particle filters for tracking an unknown number of sources. *IEEE Trans. Signal Processing*, 50 (12):2926–2937, 2002.

[20] C. Li, S. E. Dosso, H. Dong, D. Yu, and L. Liu. Bayesian inversion of multi-mode interface-wave dispersion from ambient noise. *IEEE Journal of Oceanic Engineering*, 37(3):407–416, 2012.

[21] P. Malarvezhi and R. Kumar. Particle filter with novel resampling algorithm: A diversity enhanced particle filter. *Wireless Personal Communications.*, 84(4):3171–3177, 2015.

[22] Z.-H. Michalopoulou. A Bayesian approach to modal decomposition in ocean acoustics. *J. Acoust. Soc. Am.*, 126(5):EL147–EL152, 2009.

[23] Z.-H. Michalopoulou, M. B. Porter, and J. P. Ianniello. Broadband source localization in the Gulf of Mexico. *J. Comput. Acoust.*, 4:361370, 1996.

[24] Zoi-Heleni Michalopoulou and Nattapol Aunsri. Environmental inversion using dispersion tracking in a shallow water environment. *The Journal of the Acoustical Society of America*, 143(3):EL188–EL193, 2018.

[25] Zoi-Heleni Michalopoulou and Andrew Pole. Sediment sound speed inversion with time-frequency analysis and modal arrival time probability density functions. *The Journal of the Acoustical Society of America*, 140(1):EL131–EL136, 2016.

[26] L. Pei, D. Liu, D. Zou, R. Lee Fook Choy, Y. Chen, and Z. He. Optimal heading estimation based multidimensional particle filter for pedestrian indoor positioning. *IEEE Access*, 6:49705–49720, 2018.

[27] G. Potty, J.H. Miller, P. Dahl, and C.J. Lazauski. Geoacoustic inversion results from the ASIAEX East China Sea Experiment. *J. Acoust. Soc. Am.*, 29 (4):1000–1010, 2004.

[28] S. D. Rajan and K. M. Becker. Inversion for range-dependent sediment compressional-wave-speed profiles from modal dispersion data. *IEEE Journal of Oceanic Engineering*, 35(1):43–58, 2010.

[29] B. Ristic, S. Arulampalam, and N. Gordon. *Beyond the Kalman Filter: Particle Filters for Tracking Applications*. Artech House, Boston, MA, 2004.

[30] Alam Abbas Syed, Qiyu Sun, and Hassan Foroosh. Frequency estimation of sinusoids from nonuniform samples. *Signal Processing*, 129:67 – 81, 2016.

[31] P. Taveeapiradeecharoen, K. Chamnongthai, and N. Aunsri. Bayesian compressed vector autoregression for financial time-series analysis and forecasting. *IEEE Access*, 7:16777–16786, 2019.

[32] S. Tomar and P. Sumathi. Amplitude and frequency estimation of exponentially decaying sinusoids. *IEEE Transactions on Instrumentation and Measurement*, 67(1):229–237, Jan 2018.

[33] E. E. Tsakonas, N. D. Sidiropoulos, and A. Swami. Optimal particle filters for tracking a time-varying harmonic or chirp signal. *IEEE Transactions on Signal Processing*, 56(10):4598–4610, 2008.

[34] F. Yang, L. Zheng, and Y. Luo. A novel particle filter based on hybrid deterministic and random sampling. *IEEE Access*, 6:67536–67542, 2018.

[35] T. C. Yang. A method for measuring the frequency dispersion for broadband pulses propagated to long ranges. *The Journal of the Acoustical Society of America*, 76(1):253–261, 1984.

[36] I. Zorych and Z.-H. Michalopoulou. Particle filtering for dispersion curve tracking in ocean acoustics. *J. Acoust. Soc. Am.*, 124(2):EL45–EL50, 2008.